

1-1-1982

An Inferred Crustal velocity structure of Eastern Pennsylvania-Northern New Jersey from Inversion of Wide-Angle Reflections.

Roy J. Redmond

Follow this and additional works at: <http://preserve.lehigh.edu/etd>

 Part of the [Geology Commons](#)

Recommended Citation

Redmond, Roy J., "An Inferred Crustal velocity structure of Eastern Pennsylvania-Northern New Jersey from Inversion of Wide-Angle Reflections." (1982). *Theses and Dissertations*. Paper 2013.

This Thesis is brought to you for free and open access by Lehigh Preserve. It has been accepted for inclusion in Theses and Dissertations by an authorized administrator of Lehigh Preserve. For more information, please contact preserve@lehigh.edu.

An Inferred Crustal Velocity Structure of
Eastern Pennsylvania-Northern New Jersey
from Inversion of Wide-Angle Reflections

by

Roy J. Redmond

A Thesis Presented to the Graduate Committee
of Lehigh University in Candidacy for the
Degree of Master of Science

in

Department of Geological Sciences

Lehigh University

1982

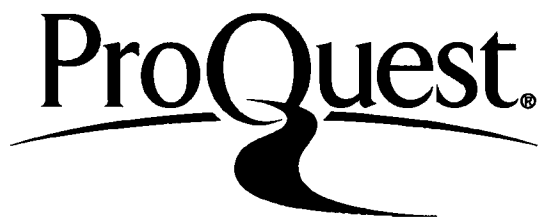
ProQuest Number: EP76286

All rights reserved

INFORMATION TO ALL USERS

The quality of this reproduction is dependent upon the quality of the copy submitted.

In the unlikely event that the author did not send a complete manuscript and there are missing pages, these will be noted. Also, if material had to be removed, a note will indicate the deletion.



ProQuest EP76286

Published by ProQuest LLC (2015). Copyright of the Dissertation is held by the Author.

All rights reserved.

This work is protected against unauthorized copying under Title 17, United States Code
Microform Edition © ProQuest LLC.

ProQuest LLC.
789 East Eisenhower Parkway
P.O. Box 1346
Ann Arbor, MI 48106 - 1346

Certificate of Approval

This thesis is accepted and approved in partial fulfillment of the requirements for the degree of Master of Science.

Sept 4, 1982
(date)

Professor in Charge

Chairman of Department

Acknowledgments

I would like to thank my advisor, Dr. Kenneth P. Kodana, for his advice and encouragement on this project. I would also like to thank my other thesis committee members, Dr. Shelton S. Alexander, Penn State University, and Dr. P. B. Myers, Lehigh University.

I appreciate the time and effort spent with me by my partner in this research project, Robert Hawman, Princeton University.

I would like to thank my whole family, especially my parents, who continually supported me on this endeavor. I would also like to thank someone very special, Judy Cuzzo, who made my graduate life tolerable.

This study was supported under U. S. Geological Survey Contract 14-08-001-18262 through Penn State University.

I would like to dedicate this work to the memory of the 10 Irish hunger strikers of 1981, Bobby Sands, Francis Hughes, Raymond McCreech, Patsy O'Hara, Joe McDonnell, Martin Hurson, Kevin Lynch, Kieran Doherty, Tom McIlwee, and Mickey Devine, who fought and died for the freedom of Ireland. May the cause they believed in soon be realized.

Table of Contents

Certificate of Approval	ii
Acknowledgments	iii
ABSTRACT	1
1. INTRODUCTION	2
1.1 Northeastern Stress and Seismicity	2
1.2 Previous Work	4
1.3 Objectives	8
1.4 Regional Geology of Study Area	9
1.5 Crustal Geology	15
2. METHODS	19
2.1 Wide-Angle Reflections	19
2.2 Fieldwork	21
2.3 Data Acquisition	30
2.4 Data Processing	38
3. INVERSE THEORY	51
3.1 Inversion Technique	51
3.2 Theoretical Modelling	61
3.3 Data Inversion	66
4. DISCUSSION	72
4.1 Data Quality	72
4.2 Modelling	74
4.3 Results	74
4.4 Suggestions for Future Work	76
REFERENCES	77
I. Appendix 1: Final Processed Data	83
II. Appendix 2: Theoretical Models	90
VITA	97

List of Figures

- Figure 1-1:** Large scale geologic map of the Great Valley in Pennsylvania and New Jersey. Heavy dashed line indicates location of profile. 10
- Figure 1-2:** Isopach map of the sedimentary rocks in the present-day Appalachian basin. Heavy dashed line indicates location of profile. 14
- Figure 1-3:** Bouguer gravity anomaly map of the Great Valley (in milligals). Heavy dashed line indicates location of profile. 16
- Figure 2-1:** Relative amplitude energy variation with angle of incidence for reflected waves. 20
- Figure 2-2:** $T(X)$ curve showing the direct wave, and the refracted and reflected waves of the first reflector. 22
- Figure 2-3:** Geology of the recording site illustrating Paulinskill Lake and the adjacent railroad track. Hatched lines represent thrust faults. 24
- Figure 2-4:** Quarry locations used in this study. B, E, and M dots indicate recorded blast locations. Other dots indicate quarries used to test the triggering device. 26
- Figure 2-5:** Section of the smoked recording noise survey. Instrument settings were: filter (0-10 Hz), gain (90 dB), and maximum deflection (10 mm). 27
- Figure 2-6:** Location of recording site along Paulinskill Lake (waves). Dots indicate individual geophone group locations. 29
- Figure 2-7:** Common-receiver seismic array. S indicates sources, Z is the depth of the reflector. 32
- Figure 2-8:** Geophone response at an 8 Hz natural frequency. h indicates the percentage of damping. 33
- Figure 2-9:** Geophone setup for timing blasts. The quarry geophone sends a FM carrier signal via the phoneline to the recording computer. 34
- Figure 2-10:** Example of temporal sampling. The sampling rate used was 0.00576 seconds. 36

Figure 2-11:	Example of spatial sampling. The waveform must be sampled twice per wavelength to avoid aliasing.	37
Figure 2-12:	Amplifier cutoff filter responses for the frequency filters used in this study.	39
Figure 2-13:	Demultiplexed data in the time domain before filtering. No waveforms except for the first channel can be observed. Time increases down and to the right.	41
Figure 2-14:	Illustration of a taper function removing the end effects of a field record.	42
Figure 2-15:	Fourier Transform into the frequency domain of the demultiplexed data. Notice the noise at 60 Hz except for the first channel quarry geophone.	44
Figure 2-16:	Data filtered from 0 Hz to 45,55 Hz in the time domain. The 60 Hz noise has been removed and waveforms can now be observed. Time increases down and to the right.	46
Figure 2-17:	Fourier Transform into the frequency domain of the filtered data. With the removal of 60 Hz noise, the dominant frequencies appear below 20 Hz.	47
Figure 2-18:	Data filtered from 0 Hz to 14,16 Hz in the time domain. Wave amplitudes have increased due to the removal of high frequency noise. Time increases down and to the right.	48
Figure 2-19:	Data filtered from 6,8 Hz to 14,16 Hz in the time domain. This trapezoidal band-pass filter gives the desired frequency range. Time increases down and to the right.	49
Figure 3-1:	Slant stacking over a reflected wave in increments of dp . dt is also varied.	54
Figure 3-2:	Interpretation of a two-layered crust in a $t(p)$ section. X_c is the critical distance for the first refraction, and the slope of the curve approaches minus infinity as it reaches its refraction point.	55
Figure 3-3:	Behavior of reflected wave in a $t(p)$ section when a LVZ is encountered. The LVZ thickness is determined by $dt/2p$.	60
Figure 3-4:	Data points from all blasts plotted on a $t(p)$ section.	68
Figure 3-5:	Data points with limiting bounds (light	69

	dash) and best-fit ellipse (heavy dash).	
Figure 4-1:	Final processed data of MLRB 1, 11/13/81. The records have been shifted forward 0.3168 seconds to breakpulse. The expected P-arrivals occur between 24.4566 to 30.3874 seconds.	84
Figure 4-2:	Final processed data of MLRB 2, 11/13/81. The records have been shifted forward 4.6656 seconds to breakpulse. The expected P-arrivals occur between 24.4566 to 30.3874 seconds.	85
Figure 4-3:	Final processed data of EIW, 11/19/81. The records have been shifted forward 0.7949 seconds to breakpulse. The expected P-arrivals occur between 12.2933 to 19.7844 seconds.	86
Figure 4-4:	Final processed data of BPST, 12/9/81. The records have been shifted backward 2.2982 seconds to breakpulse. The expected P-arrivals occur between 19.7150 to 25.9641 seconds.	87
Figure 4-5:	Final processed data of MLRB 1, 12/11/81. The records have been shifted backward 0.5472 seconds to breakpulse. The expected P-arrivals occur between 24.4566 to 30.3874 seconds.	88
Figure 4-6:	Final processed data of MLRB 2, 12/11/81. The records have been shifted forward 0.9389 seconds to breakpulse. The expected P-arrivals occur between 24.4566 to 30.3874 seconds.	89
Figure 4-7:	Model 1: T(X) section of two horizontal layers in a 35 km thick crust.	91
Figure 4-8:	Model 1: t(p) section of two horizontal layers in a 35 km thick crust.	92
Figure 4-9:	Model 2: T(X) section of three horizontal layers in a 40 km thick crust.	93
Figure 4-10:	Model 2: t(p) section of three horizontal layers in a 40 km thick crust.	94
Figure 4-11:	Model 3: T(X) section of a 10 km continuous velocity function overlain by a 25 km horizontal layer.	95
Figure 4-12:	Model 3: t(p) section of a 10 km	96

continuous velocity function overlain
by a 25 km horizontal layer.

List of Tables

Table 1-1:	Cambrrian and Ordovician stratigraphic sequences in the Great Valley.	12
Table 2-1:	Quarries used in this study. Those with codes were used as source blasts, others were used to test the triggering device.	25
Table 2-2:	Parameter information of the recorded blasts. f indicates filter setting, g indicates gain setting.	30
Table 3-1:	Comparison of previous crustal structure studies to this study's results.	71

ABSTRACT

A wide-angle reflection profiling experiment was conducted in the northeast trending Great Valley of Pennsylvania and New Jersey to determine the crustal velocity structure of the region. Six timed quarry blasts were recorded at three offsets of 73.76 km, 118.29 km, and 146.74 km. The blasts were timed exactly by an 8 Hz geophone located at the quarry. The seismic array was located at an abandoned railroad track parallel to Paulinskill Lake, Sussex County, New Jersey. It consisted of 11 geophone groups spaced every 213 meters. Since the reduced data contained a low S/N ratio, the data were treated subjectively by time windowing the expected P-wave arrivals and measuring the travel time and normal moveout for coherent phase signals across the traces. These data were plotted on a $t(p)$ (intercept time-ray parameter) curve and an ellipse was fit to them by hand. The data suggest that the crust is approximately 41.2 km thick and has a near surface compressional wave velocity of 5.8 km/s. No layering within the crust could be inferred. This crustal velocity model is consistent with previous studies in this area.

1. INTRODUCTION

1.1 Northeastern Stress and Seismicity

Recent interest in northeastern United States seismicity has caused an increase in crustal structure studies. The seismicity of this area, which is situated centrally on the North American plate, can not be associated with a tectonically active plate boundary. However, large recent and historic earthquakes have occurred.

The region along the Atlantic coast, situated east of the Appalachian fold belt, is now undergoing maximum horizontal compressional stress in a W-WNW direction [Yang and Aggarwal, 1981]. This is indicated by high angle reverse focal mechanisms of earthquakes [Yang and Aggarwal, 1981, Zoback and Zoback, 1981]. There are two suggested sources of intraplate stress for the Atlantic coast. It is believed ridge push, normal to offshore magnetic lineations, is the main source of regional compressive stress [Yang and Aggarwal, 1981]. This stress pattern must be post-Mesozoic in origin [Sbar and Sykes, 1973], since it is perpendicular to the initial rift creating the present Atlantic Ocean. Another possible stress source is that the tectonics east of the Appalachians are controlled by backsliding at the steepest portions of the Appalachian detachment [Seeber

and Armbruster, 1981]. Tensional features are also observed in the northeastern U.S., such as those observed in the fault plane solutions of the 1969 Lake Hopatcong, N.J. earthquake [Sbar et al., 1970] and the 1973 Delaware-N.J. earthquake [Sbar et al., 1975]. These stresses may be the result of either remnant stresses [Sbar and Sykes, 1973] or backsliding along a detachment [Seeber and Armbruster, 1981], and not indicative of the regional stress as a whole. The Appalachian fold belt, reflecting a broad zone of stress transition, separates the different stress regimes of the Atlantic coast and the midwest [Zoback and Zoback, 1981]. The maximum horizontal compressional stress direction west of the Appalachians is in an E-ENE direction [Yang and Aggarwal, 1981, Zoback and Zoback, 1981, Sbar and Sykes, 1973].

Seismic activity occurs where maximum compressive stress is associated perpendicularly to lithospheric zones of weakness. These zones are localized along pre-existing faults or post-orogenic fault areas [Yang and Aggarwal, 1981, Sbar and Sykes, 1977]. They have not been healed by metamorphism or igneous activity, and are thought to be capable of reactivation [Yang and Aggarwal, 1981]. The general region in which this study is located, southern New York, northern New Jersey, and

eastern Pennsylvania, has moderate northeast-trending seismic activity [Sbar and Sykes, 1977] along pre-existing faults such as the Ramapo fault. The capability of locating earthquakes and determining focal mechanisms in this area has improved over the past 10 years with an increase of fixed stations in the Northeastern Seismic Network. The majority of events in this area are single events, as opposed to swarms and foreshock-aftershock sequences. This would indicate a relatively homogeneous crust and a constant stress field [Mogi, 1963].

Tectonically, the northeastern U.S. has been subject to similar stress forces from late Mesozoic to the present. The fault activity has been characterized by long periods of quiescence [Zoback and Zoback, 1981], and small cumulative offsets due to vertical jostling of crustal blocks rather than unidirectional motion [Root and Hoskins, 1977]. There is a great need for an accurate crustal velocity model in the northeastern U.S. to improve the delineation of seismically active areas using fixed station data.

1.2 Previous Work

There are three areas in the U.S., the midwest, the southeast, and east central, where the crustal structure is similar to the structure of the study region. Their

crustal velocity models could serve as constraints to the crustal velocity structure for the study area.

The intraplate midcontinent of the U.S. has been the site of major historical earthquakes. The New Madrid, Missouri earthquakes (1811-1812) had unusually large felt areas and caused much damage [Yang and Aggarwal, 1981]. Therefore, the midcontinent has been studied extensively. Techniques have included refraction surveys and teleseismic P-wave spectra transfer functions at fixed stations. Stewart (1968) and McEvelly (1964) each determined a three layer crustal model using refraction data with thicknesses of 40 km and 38 km, respectively. Using transfer functions, Kurita (1973) constructed a two layer, 39 km thick crustal model; Fernandez and Careaga (1968) determined a one layer, 42 km thick model.

In the southeastern U.S., crustal velocity structure studies have been conducted to better understand the geologic setting of the noted historical earthquake at Charleston, South Carolina (1886). Near-vertical reflection profiling, transverse to the Appalachian fold belt, has shown that the allochthonous Blue Ridge has been thrust westward over a thick sequence of underlying Cambro-Ordovician sediments [Harris et al., 1981, Cook et al., 1979]. These studies did not determine crustal thicknesses. In crustal refraction surveys, Kean and

Long (1980) determined a one layer, 33 km thick crust, whereas Carts and Bollinger (1981) suggest a one layer, 40 km thick crust for the southern Appalachian valley and ridge. Compiled refraction data for the eastern U.S. suggests a two layer, 42 km thick crust (Braile and Smith, 1975). On a larger regional scale, studies for the eastern U.S. using surface wave phase and group velocity inversions from midcontinent earthquakes yielded a heterogeneous crust approximately 43 km thick (Mitchell and Herrmann, 1979).

In eastern Pennsylvania and northern New Jersey, the area investigated by this study, Katz's (1955) crustal refraction model has been the foundation of all subsequent crustal velocity studies. Katz determined a 34.4 km thick homogeneous crust for Pennsylvania. Other early studies include inversion of Rayleigh wave phase velocities using a tripartite array and teleseisms as sources (Oliver et al., 1961). This latter study covered the PA.-N.Y. area, determining a three layer, 37 km crust. However, Oliver et al. (1961) admit that the data was incomplete since the derived structure is an average over long distances where elastic parameters vary. Dorman and Ewing (1962) used inversion of surface wave dispersion in the PA.-N.Y. area to construct a one layer, 38.6 km crustal model.

More recent studies have used P-wave travel-time residuals from nuclear explosions and teleseisms. Fletcher et al. (1978) observed a correlation between positive travel-time residuals which follow the northeast-trending Appalachian geosyncline, and a negative (-40 mgal) Bouguer gravity anomaly which stretches from Virginia to eastern Pennsylvania. Taylor and Toksoz (1979) used travel-time residuals from teleseisms to compute a single layer, 37 km crust. A study of teleseismic P-SV wave conversions at the crust-mantle interface, recorded on radial components, suggests a single layer, 41 km crust [Langston and Isaacs, 1981]. A study of wide-angle reflections and refractions from quarry blasts suggest a two layered, 37 km thick crust in south-central Pennsylvania [Sienko, 1982].

A near-vertical reflection profile was interpreted by Harris and Bayer (1979) to indicate approximately 10 km of Paleozoic sediments overlying the Precambrian basement, and separated from it by a master decollement. No crustal model was inferred.

More work needs to be done to better delineate the crustal velocity structure in the northeastern U.S. Near-vertical reflection profiling yields good results for near surface structure, but does not allow

construction of crustal models. There has been no crustal refraction work since Katz (1955). Katz's study was conducted before regional gravity trends believed to delineate crustal blocks (Diment et al., 1979, King and Zeitz, 1978) were recognized, therefore his profile cuts across these inferred blocks. It would be important to design an experiment which is located within one crustal block.

1.3 Objectives

The major objective of this study is to construct an accurate crustal model for eastern Pennsylvania and northwest New Jersey based on wide-angle reflection data.

Advances in exploration seismology and processing techniques permit an updated crustal model for this region. The technique for determining crustal structure will be to invert wide-angle reflection data into the $t(p)$ (intercept time-ray parameter) domain. The following parameters should be determined:

- 1) Thickness and velocity of the sedimentary layer.
- 2) Thickness and velocity of an intermediate layer.
- 3) Possible existence of the Conrad discontinuity in the study area.
- 4) Thickness and velocity of the layer between the Conrad and Moho discontinuities.

5) Depth to Moho (thickness of crust).

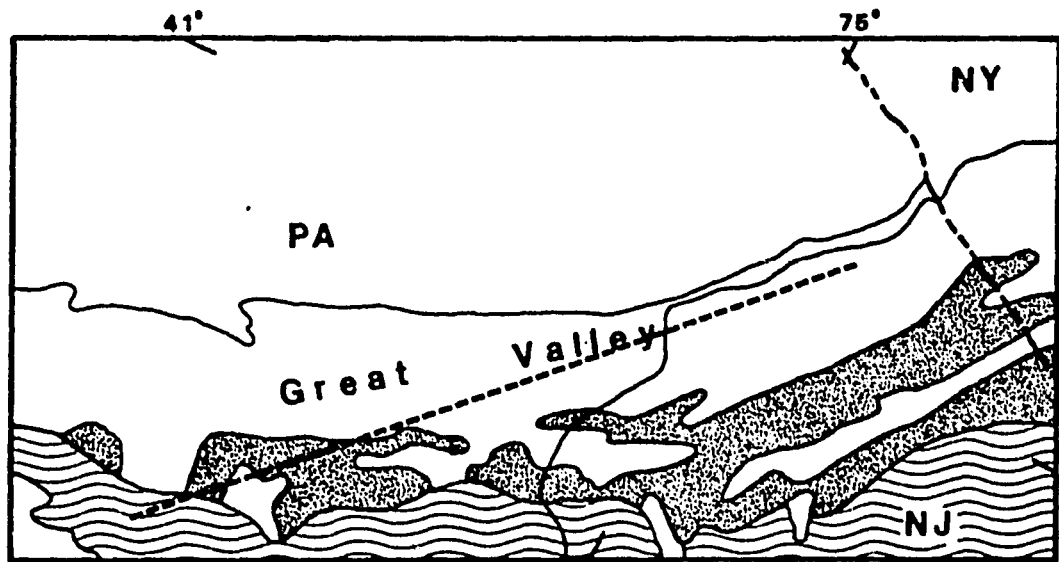
Synthetic data can then be calculated for the inverted model to illustrate the difference between field record data and a theoretical, best-fitting data set.

The new crustal model will lead to better delineation of the seismicity in the seismically active areas. Two such areas, the Ramapo fault in southern New York, northern New Jersey, and Willow Grove, Pennsylvania, southeast and along strike of the Ramapo fault, may actually be part of some pre-existing fault. Fixed station data may delineate a connection between these two seismic areas by establishing more accurate regional earthquake epicenter locations along strike of the Ramapo fault.

1.4 Regional Geology of Study Area

The Great Valley province, located in Pennsylvania and New Jersey, was chosen as the site of our fieldwork (Fig. 1-1). The northeast trending Great Valley of the Appalachian basin is a great arcuate salient composed of a thick sequence of highly folded and faulted Cambrian and Ordovician rocks [Rankin, 1976, Gwinn, 1964].

These Cambrian to Middle Ordovician sedimentary rocks are composed of an orthoquartzite-carbonate facies, deposited eastward on a shallow shelf. From Middle to



0 50 km.




-  Triassic, Newark Basin
-  Lower Paleozoic, sedimentary
-  Precambrian, Reading Prong

Figure 1-1: Large scale geologic map of the Great Valley in Pennsylvania and New Jersey. Heavy dashed line indicates location of profile.

Late Ordovician, a basin reversal occurred resulting in a graywacke-shale, flysch deposit [Drake, 1979] represented by the Martinsburg Formation. Table 1-1 lists the stratigraphic rock units of the Great Valley. The thickness and rock facies indicate a miogeosynclinal deposit where the rate of subsidence approximately equalled the rate of deposition. This was followed by deep water deposition of the Martinsburg Formation.

Subsequent to and during the late stages of Ordovician deposition, the Appalachian basin was uplifted and deformed [Colton, 1970]. Low-angle thrust faulting and broad folding developed throughout the latter half of the Paleozoic and Early Mesozoic. Drake (1978) explains the complicated structural relations in the Great Valley by nappe theory. He states that the nappes developed during the Taconic orogeny, towards the end of the Martinsburg deposition. The Taconic orogeny is well documented by the angular unconformity between Ordovician and Silurian rocks [Colton, 1970]. The faulting and folding of these nappes subsequently took place during the Alleghenian orogeny (Middle Permian) [Drake, 1978].

Paleozoic orogenic processes resulted in a master decollement and tectonic thickening. The east dipping master decollement developed continuously through the Paleozoic orogenies, separating the Cambro-Ordovician

Table 1-1: Cambrian and Ordovician stratigraphic sequences in the Great Valley.

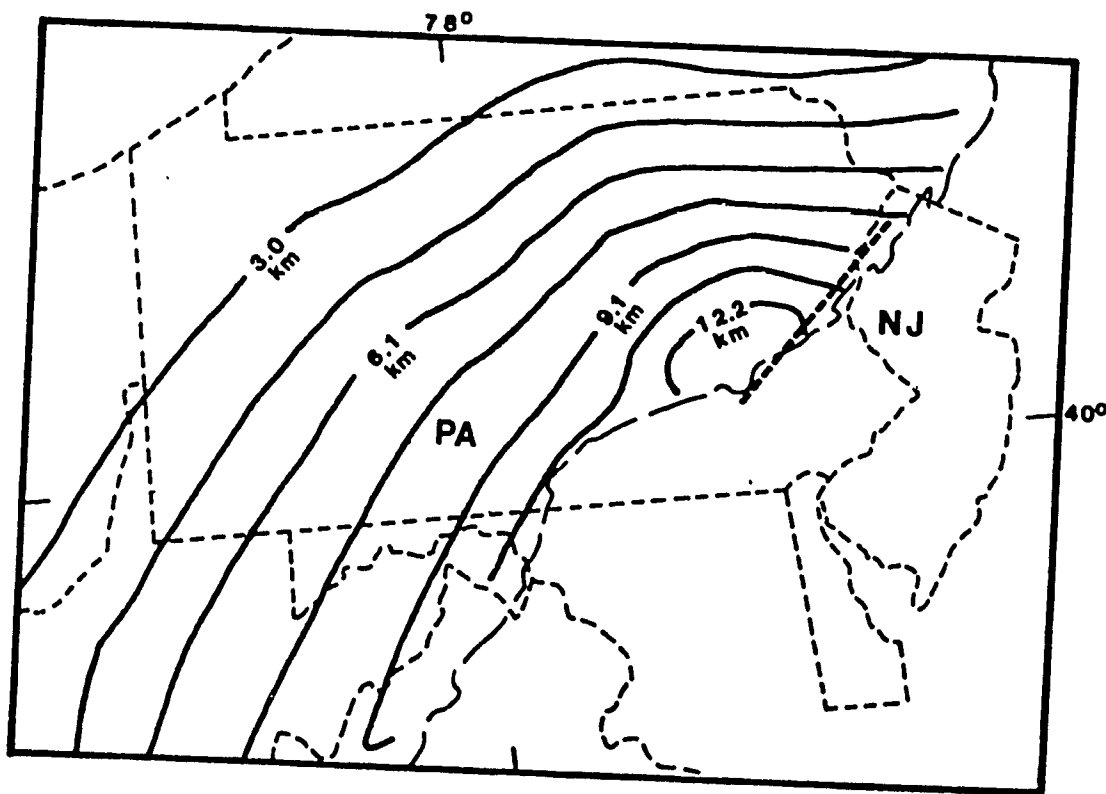
FORMATION	DESCRIPTION
Martinsburg Formation (Middle to Upper Ordovician)	Medium- to dark-gray slate that alternates with beds of light- to medium-gray graywacke. Thickness: 3280-4280 meters
Jacksonburg Limestone (Middle Ordovician)	Dark-gray, argillaceous limestone, and light- to medium-gray calcarenite and high-calcium limestone. Thickness: 170-460 meters
Ontelaunee Formation (Lower Ordovician)	Medium-dark gray dolomite. Thickness: 0-200 meters
Epler Formation (Lower Ordovician)	Interbedded light- to medium-gray limestone and light-gray to dark-medium-gray dolomite. Thickness: ~270 meters
Rickenbach Dolomite (Lower Ordovician)	Light-medium to medium-dark-gray dolomite. Thickness: ~220 meters
Allentown Dolomite (Upper Cambrian)	Light-gray to medium-dark-gray rhythmically bedded dolomite containing abundant algal stromatolites. Thickness: ~575 meters
Leithsville Formation (Lower to Middle Cambrian)	Interbedded light-medium-gray to dark-gray dolomite and calcitic dolomite, light-gray to tan phyllite, and dolomite sandstone. Thickness: ~350 meters
Hardyston Quartzite (Lower Cambrian)	Gray quartzite, feldspathic quartzite, arkose, quartz pebble conglomerate, and silty shale or phyllite. Thickness: ~30 meters

[Adapted from Drake (1978)]

rocks from the basement [Harris and Bayer, 1979]. The tectonic thickening resulted from imbricate thrust faulting, developing the thick sequence of rocks now observed in the Great Valley. Taylor and Toksoz (1979) believe that the imprint of the orogenic events extend into the lithosphere. However, Gwinn (1970, 1964) infers from the low-angle thrust faulting that the tectonics are thin-skinned and do not involve the basement rocks.

Many studies have been done to determine the thickness of sedimentary rocks in the Appalachian basin [Harris and Bayer, 1979, Drake, 1978, Colton, 1970]. Thickness estimates of these studies range from 8 to 17 km. Private oil company seismic lines show the basin to be 12 to 17 km below surface off the western front of the outcropping Precambrian rocks [Drake, 1978]. A seismic reflection profile of Pennsylvania suggests a sedimentary thickness of 10 km [Harris and Bayer, 1979]. Figure 1-2 is an isopach map of the present-day Appalachian basin.

One of the primary reasons for choosing this site for a crustal velocity study is the lateral homogeneity in its geology as indicated by the previous discussion. The area is also interesting geophysically because of the relation between the Great Valley and Reading Prong with a regional Bouguer gravity low [Drake, 1978] [Fig. 1-3]



0 200 km.

Figure 1-2: Isopach map of the sedimentary rocks in the present-day Appalachian basin. Heavy dashed line indicates location of profile.

and positive P-wave travel time residuals [Fletcher et al., 1978]. Aeromagnetic lineations, although not directly associated with outcropping geologic features of the Great Valley, is also northeast trending [Diment et al., 1979, King and Zeitz, 1978].

1.5 Crustal Geology

The tectonically uplifted and exposed Ivrea Zone in the Southern Alps provides an example of a theoretical geologic crustal cross-section. Here it is observed that the lower crust is felsic in nature, since granulitic rocks are exposed in the bottom zone. The granulitic rocks grade upward into migmatites, representative of the middle crust, and schists, gneisses, and granites, representative of the upper crust [Smithson and Brown, 1977, Smithson and Shive, 1977]. Velocity and density studies suggest that the upper mantle is composed of a peridotite type rock [Garland, 1979, Murrell, 1976].

Geological and geophysical data indicate that the uppermost part of the crust in the study area is composed of a thick sequence of sedimentary rocks. Crustal thickness may increase toward the Appalachian basin [James et al., 1968]. This increase is supported by positive travel-time residuals [Fletcher et al., 1978].

The transition between the sedimentary cover and the

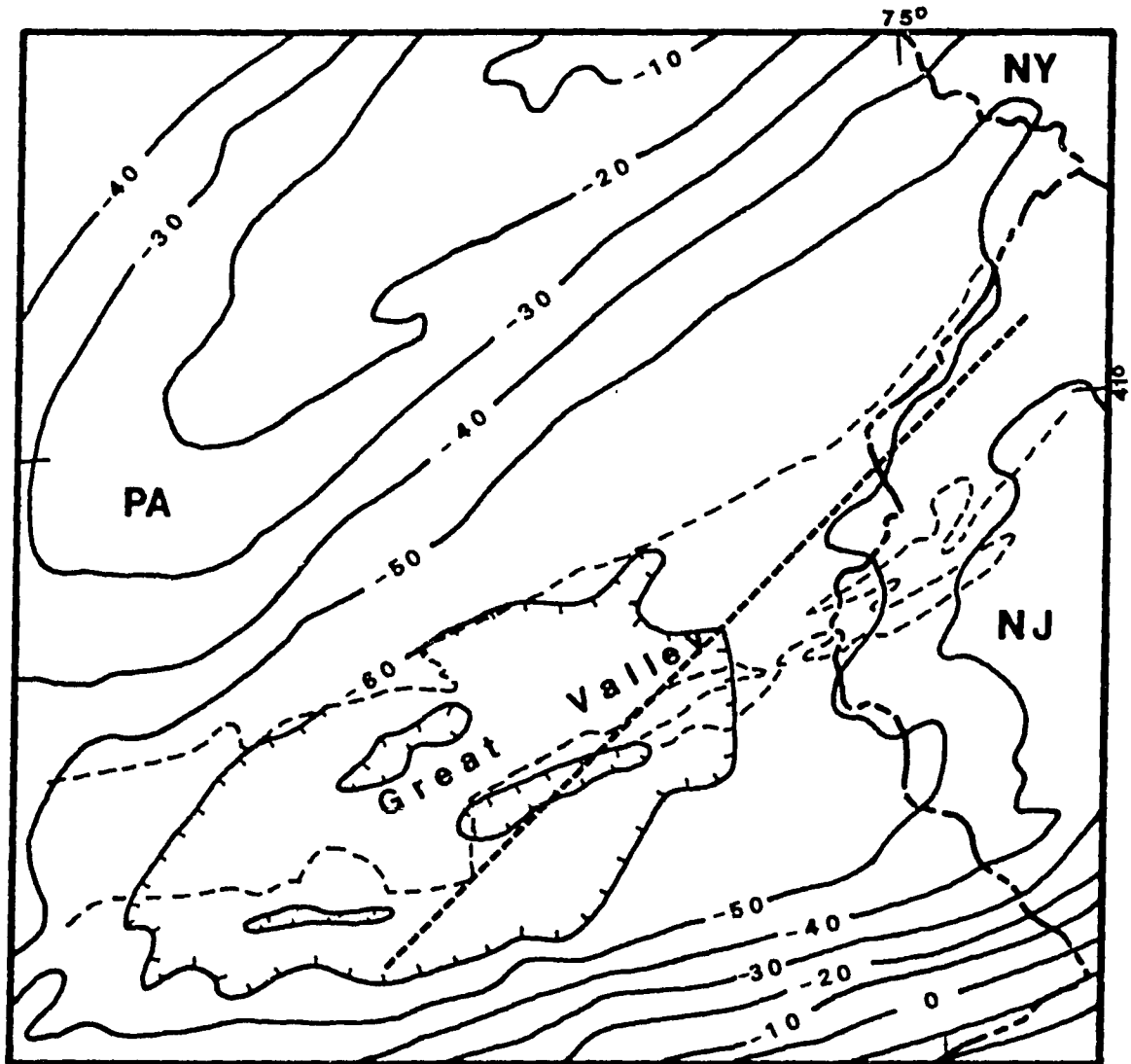


Figure 1-3: Bouguer gravity anomaly map of the Great Valley (in milligals). Heavy dashed line indicates location of profile.

basement rocks is a first order decollement zone detected in seismic profiles. The transitions, or discontinuities, between other rock lithologies within the crust are thinly laminated alternating high and low velocity zones a few kilometers in thickness [Mueller, 1977, Prodehl, 1977, Smithson and Brown, 1977, Smithson and Shive, 1977]. These velocity transitions cause the Conrad discontinuity at the top of the lower crust, and the Moho discontinuity at the crust-mantle interface. This complex layering may cause strong reflections through constructive interference of the wavefront.

Crustal low velocity zones (LVZ's) are believed to result from granitic intrusions into surrounding metamorphic rocks. These intrusions have an increased water content as either pore fluid or hydrous minerals [Garland, 1979, Mueller, 1977]. Where LVZ's occur, the depth determined by reflection profiling is between 5 to 15 km and is 2 to 10 km thick.

The existence of a crustal LVZ in the eastern U.S. is questionable. If LVZ's occur at the site of tectonic adjustments where there has been semi-continuous acidic intrusion [Landisman et al., 1971], and the Appalachian basin underwent only thin-skinned tectonics with no basement involvement [Gwinn, 1970], then a LVZ should not exist under the study area. In support of this

interpretation, a compilation of crustal studies for the eastern U.S. shows no LVZ [Braile and Smith, 1975].

2. METHODS

2.1 Wide-Angle Reflections

Exploration seismology is the study of wave propagation through the earth using known travel times and distances. Reconstruction of these wave paths yield information on subsurface geology.

In this study, we are concerned only with the wide-angle reflections of P-waves. A wide-angle reflection is a total internal reflection, occurring only at post-critical angles. The critical angle, as determined from Snell's law is

$$\sin i_c = V_1 / V_2$$

where i_c is the critical angle, V_1 is the velocity of the upper medium, and V_2 is the velocity of the lower medium. In total internal reflection, more energy is reflected because none is transmitted into the lower medium. Therefore, as the critical angle is approached, a sharp increase in reflected compressional energy is observed causing larger wave amplitudes. A systematic study of amplitude with angle of incidence shows this increase in energy [Fig. 2-1]. However, the decrease in amplitude with an increase in depth of the reflector [Meissner, 1967] tends to counter this effect.

A wide-angle reflection is shown on the T(X) (travel

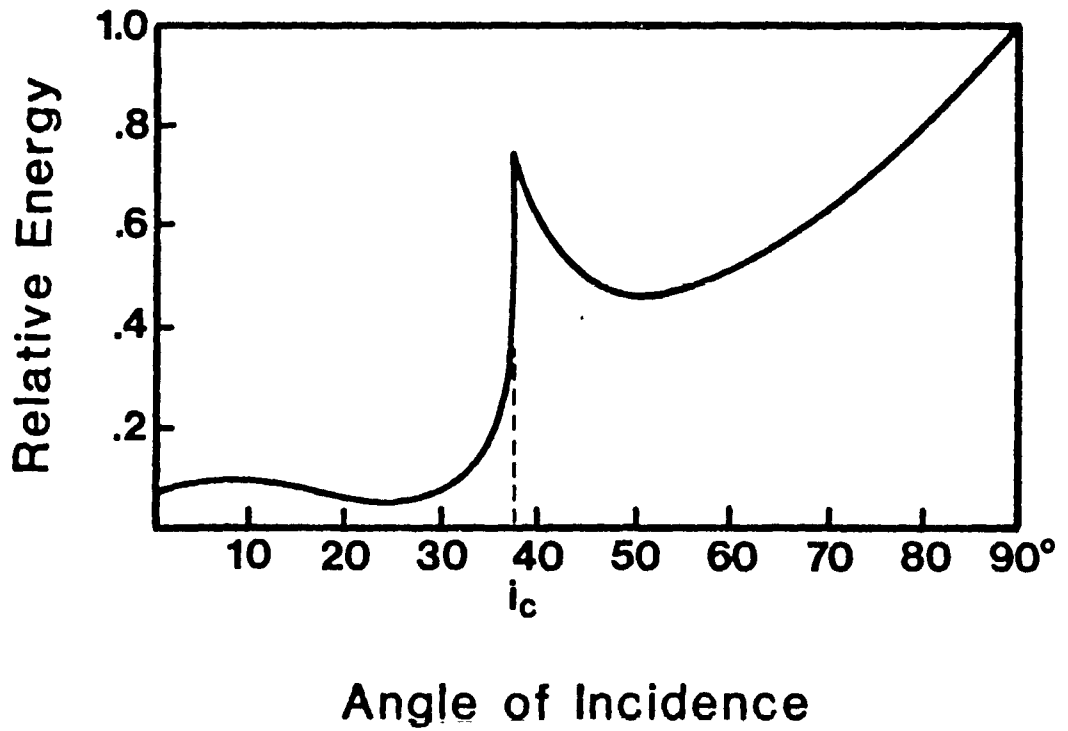


Figure 2-1: Relative amplitude energy variation with angle of incidence for reflected waves.

time-distance) section in Figure 2-2. The wave amplitude is largest at the critical distance

$$X_c = 2Z \tan i_c$$

where X_c is the critical distance, Z is the depth of the reflector, and i_c is the critical angle. The travel time equation for reflected waves is

$$T = 2/V [Z^2 + (X/2)^2]^{1/2}$$

and as seen in Figure 2-2 is hyperbolic. At great distances, the travel times for direct and reflected waves approach each other, and the wave paths merge.

2.2 Fieldwork

The field area for the seismometer array had to meet the following requirements:

- 1) allow the 2.1 km long geophone array to be aligned with the source area quarries in the Great Valley;
- 2) have minimal elevation variation along the geophone array;
- 3) be accessible to a 110 volt - 60 cycle power source and telephone connection;
- 4) be isolated from cultural noise;
- 5) be accessible by truck.

The area which best fulfilled these requirements was

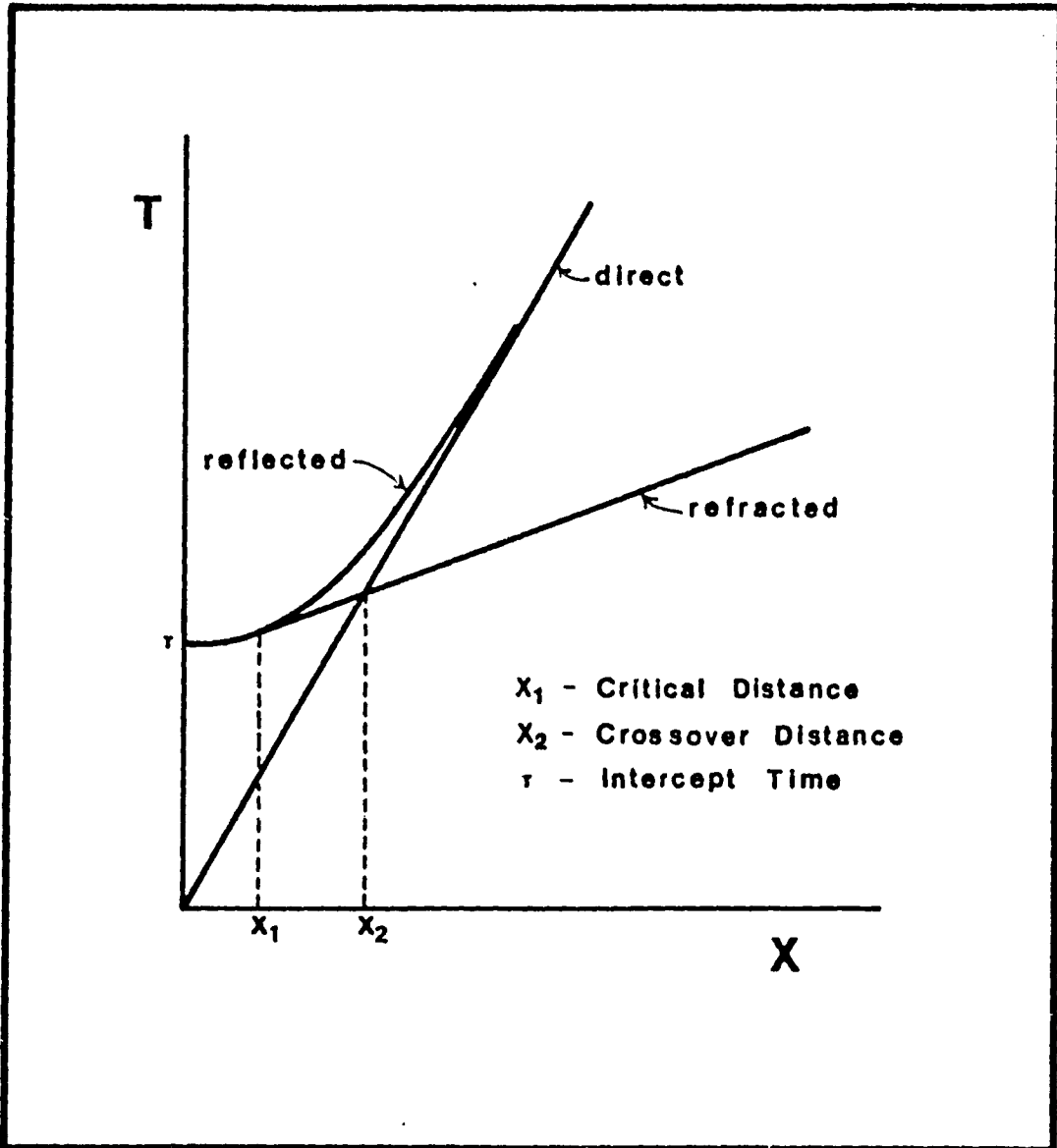
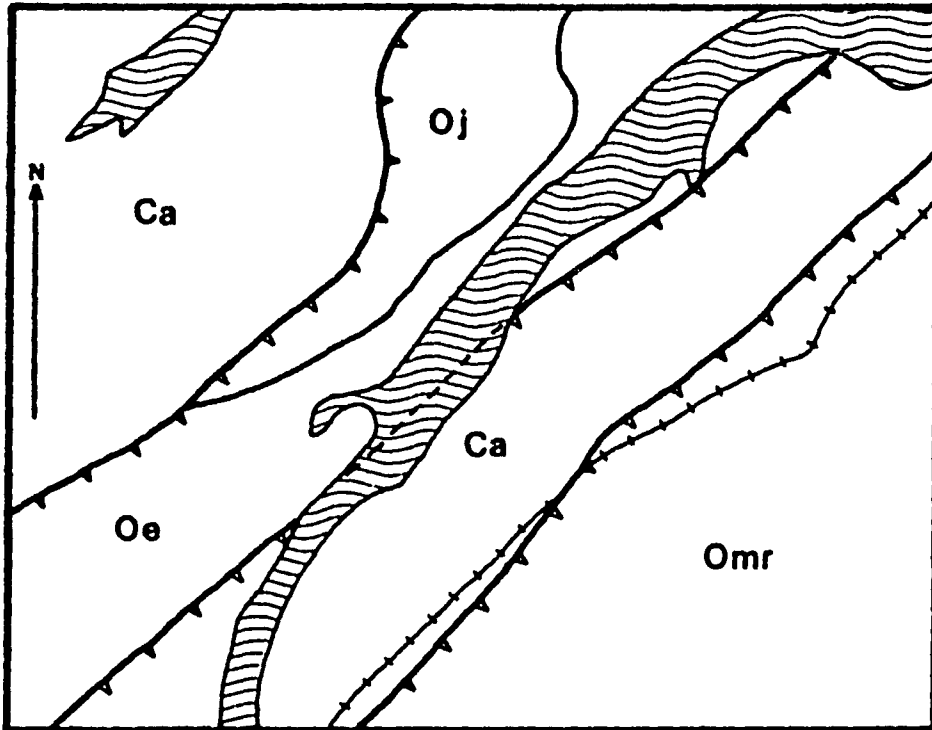


Figure 2-2: $T(X)$ curve showing the direct wave, and the refracted and reflected waves of the first reflector.

an abandoned railroad track (now owned by Newark Water Supply) situated along Paulinskill Lake, Stillwater Township, Sussex County, New Jersey, in the Great Valley of rural northwest New Jersey [Fig. 2-3]. The track trends northeast and is relatively flat. There are power and telephone connections in nearby residences.

Because the Great Valley sequence is composed of carbonate rocks, many quarries exist parallel to trend in what is referred to as the "cement belt." Table 2-1 is a list of quarries used as sources. The number of quarries gave a large range for receiving wide-angle reflections and line up on an azimuthal direction with the recording array [Fig. 2-4].

The isolation from cultural noise is necessary for recognition of a seismic event. Noise is any interference that reduces observation of the event, and can be coherent (followed across traces) or incoherent. Noise surveys were made during the late summer of 1981 at the recording site and at New Jersey's Worthington State Park, Warren County, the alternate recording site. These surveys were made on smoked paper using a 1 Hz geophone receiver. The instrument's filter and gain settings at the recording site were a low-pass frequency filter of 0-30 Hz, a gain of 90 decibals, and a maximum deflection of 10 mm. No maximum deflections indicate that the area



0 .5 1 km.

- Omr Martinsburg Formation
- Oj Jacksonburg Limestone
- Oe Epler Formation
- Ca Allentown Dolomite

Figure 2-3: Geology of the recording site illustrating Paulinskill Lake and the adjacent railroad track. Hatched lines represent thrust faults.

Table 2-1: Quarries used in this study. Those with codes were used as source blasts, others were used to test the triggering device.

QUARRY LOCATION	CODE
Berks Products South Temple, PA. Longitude: 75°55'42"; Latitude: 40°23'26"	HPST
Eastern Industries Main Office: Wescosville, PA. Whitehall, PA. Longitude: 75°31'19"; Latitude: 40°39'42" Nazareth, PA. Ormrod, PA. Kutztown, PA. Kunkletown, PA.	EIW
Martin Limestone Quarry Blue Ball, PA. Longitude: 76°03'46"; Latitude: 40°08'06"	MLBB

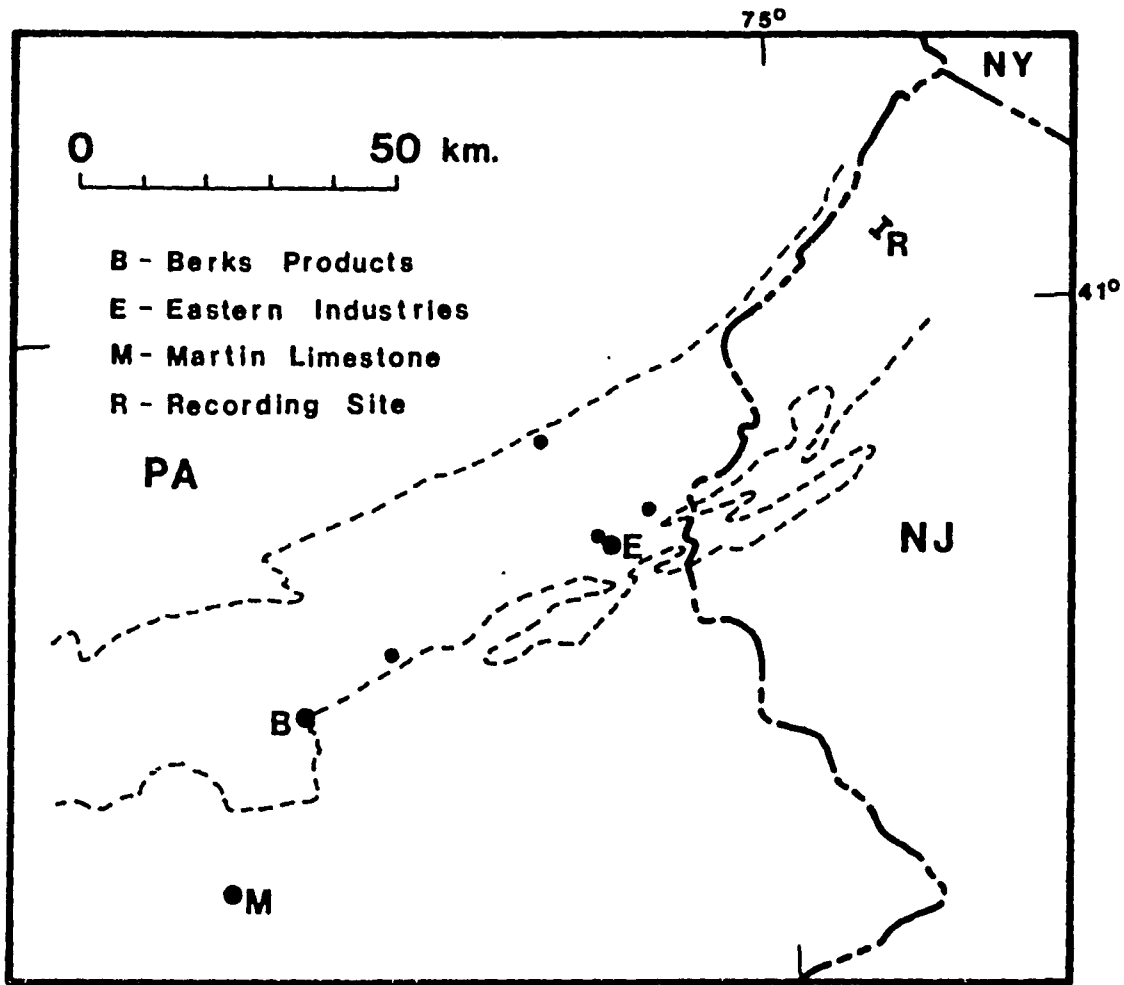


Figure 2-4: Quarry locations used in this study. B, E, and M dots indicate recorded blast locations. Other dots indicate quarries used to test the triggering device.



1 MINUTE

Figure 2-5: Section of the smoked recording noise survey.
Instrument settings were: filter (0-10 Hz), gain
(90 dB), and maximum deflection (10 mm).

is relatively quiet [Fig. 2-5].

During the months of September and October, 1981, the triggering device was tested using quarry blasts. It is deployed at the source and is recorded on the first channel of the digital system. The purpose of these tests was to adjust the gain so that the high frequency vibrations from rock crushers and trucks did not trigger the system, but the low frequency, high amplitude blast did.

During the early part of November, 1981, twenty five 106.7 meter cables were laid out alongside the railroad track with geophone groups attached to every other cable take-out. The total length of the spread was 2.67 km with a geophone spacing of 213.4 meters [Fig. 2-6]. During this period, the basement of a local residence was rented to store the computer used to record the data. This house supplied the power and telephone service to the recording instruments.

Six quarry blasts at three different localities were recorded during the months of November and December, 1981 [Fig. 2-4]. Table 2-2 is a list of these blasts, their offset distances, their size, and the recording instrument's filter and gain settings. Only six blasts were recorded due to the end of the quarries' operational season.

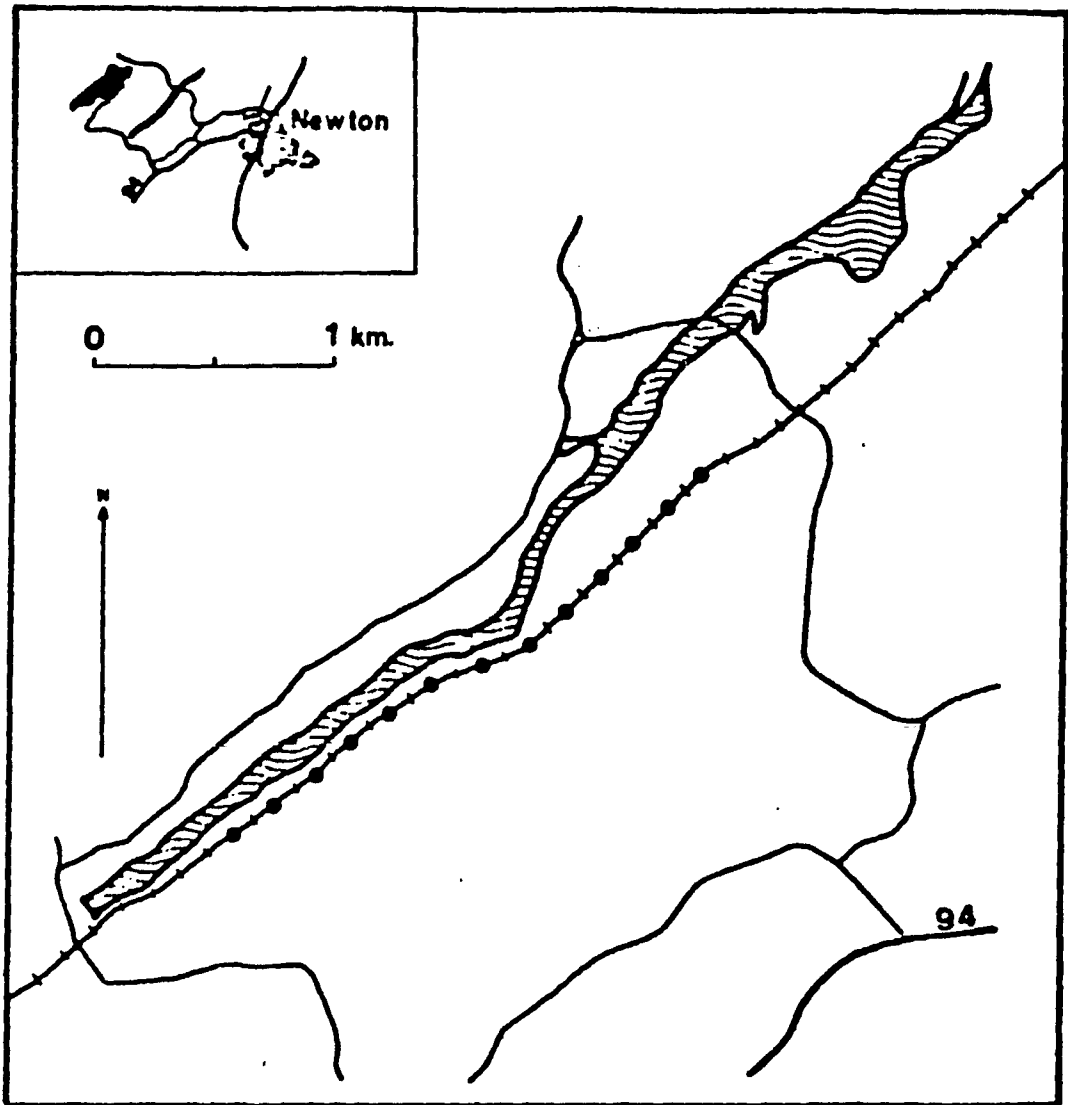


Figure 2-6: Location of recording site along Paulinskill Lake (waves). Dots indicate individual geophone group locations.

Table 2-2: Parameter information of the recorded blasts.
f indicates filter setting, g indicates gain setting.

BLAST	OFFSET	SIZE	INSTRUMENT SETTINGS
MLBB 1 11/13/81	146.74 km	2847 kg	f = 0-35 Hz g = 84 dB
MLBB 2 11/13/81	146.74 km	3651 kg	f = 0-35 Hz g = 84 dB
EIW 11/19/81	73.76 km	2869 kg	f = 0-16 Hz g = 74 dB
BPST 12/9/81	118.29 km	~1497 kg	f = 0-16 Hz g = 74 dB
MLBB 1 12/11/81	146.74 km	2808 kg	f = 0-16 Hz g = 74 dB
MLBB 2 12/11/81	146.74 km	2522 kg	f = 0-16 Hz g = 74 dB

2.3 Data Acquisition

The data were collected using a common-receiver array (Fig. 2-7). This system digitally recorded the signals utilizing a 12 channel spread of linear geophone groupings. The geophones used were the standard moving coil electromagnetic type. The magnet is attached to the frame, moving with earth motion as the coil remains

inertial. This generates a voltage proportional to the velocity of motion. The instrument is damped so that the output is not dominated by resonance at the natural frequency. The natural frequency of the geophones used was 8 Hz [Fig. 2-8]. This acts as a high pass frequency filter, limiting the response of any frequencies below 8 Hz.

The geophone located at the quarry was recorded on the first channel of the multi-channel digital equipment. This geophone recorded the breakpulse of the blast as well as serving as the triggering device of the recording system. The output of its amplifier is an FM carrier signal relayed over the telephone into the recording computer [Fig. 2-9].

The geophone groups consisted of 4 linearly spaced geophones 10 meters apart, with a separation of 213.4 meters between each group. Each group is connected in series, with the output equivalent to a single geophone at the group center. Thirteen groups were set up though only 11 could be utilized at one time.

Since aliasing of higher frequency signals could occur in the data due to temporal and spatial sampling, the output was appropriately filtered.

In temporal aliasing, the original waveforms are recoverable if they contain frequencies less than the

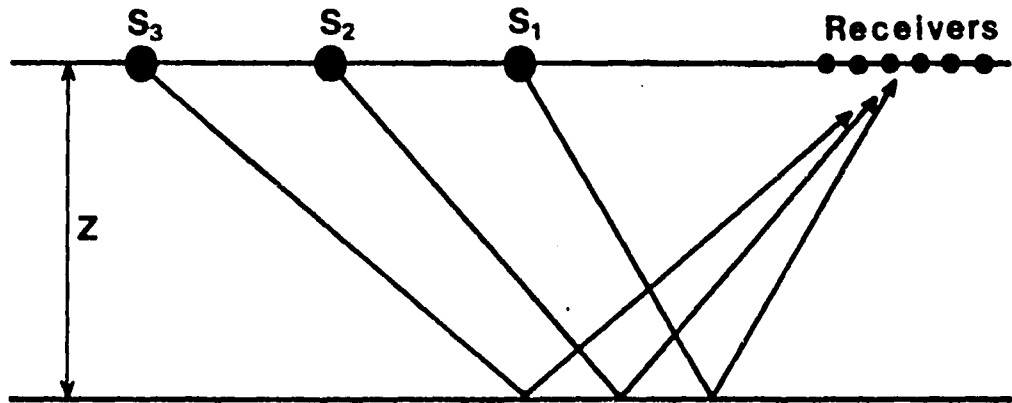


Figure 2-7: Common-receiver seismic array. S indicates sources, Z is the depth of the reflector.

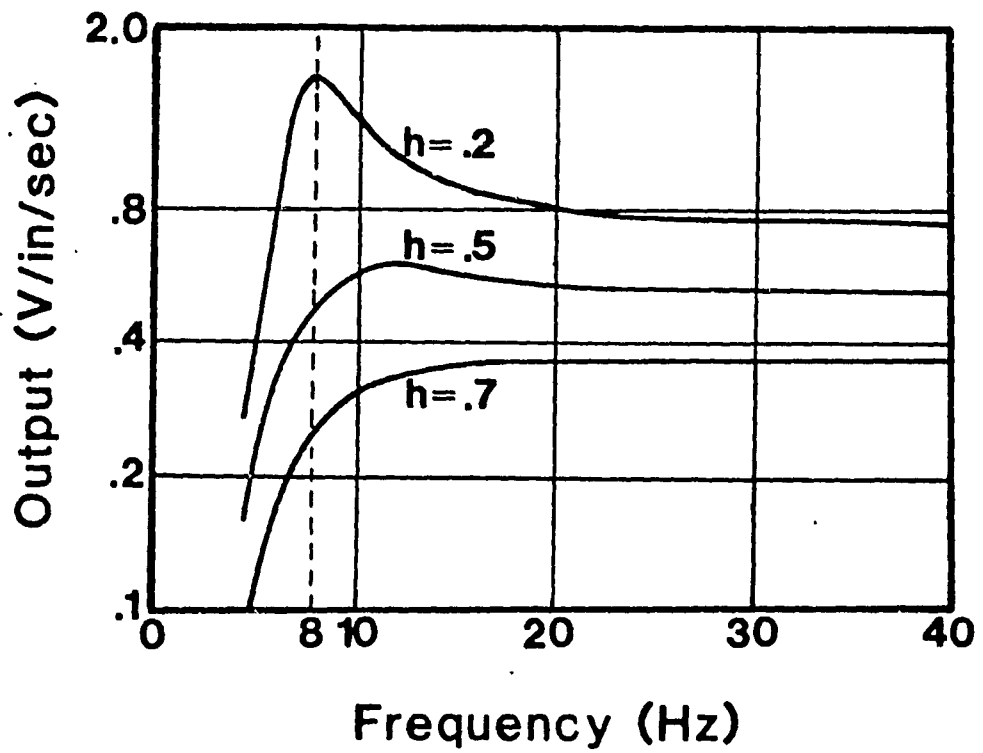


Figure 2-8: Geophone response at an 8 Hz natural frequency. h indicates the percentage of damping.

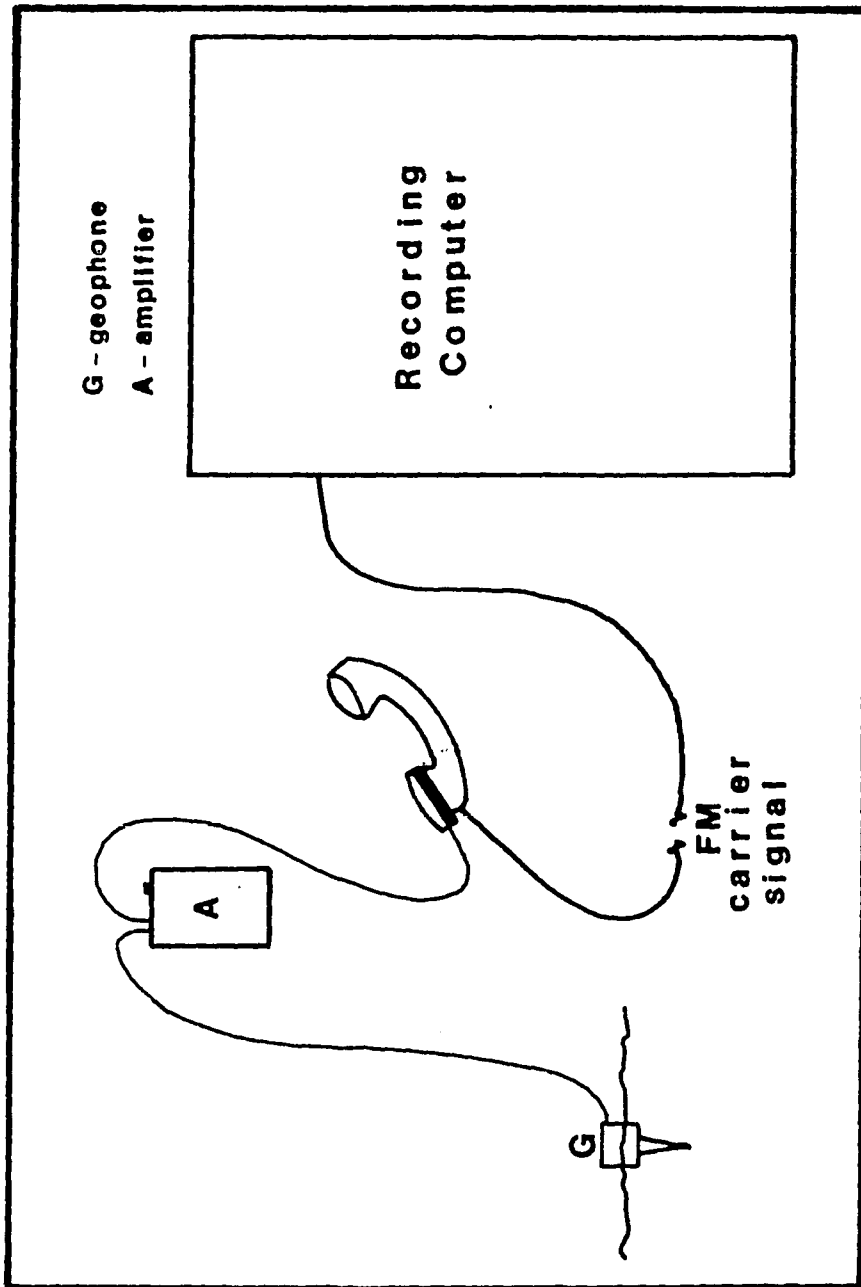


Figure 2-9: Geophone setup for timing blasts. The quarry geophone sends a FM carrier signal via the phoneline to the recording computer.

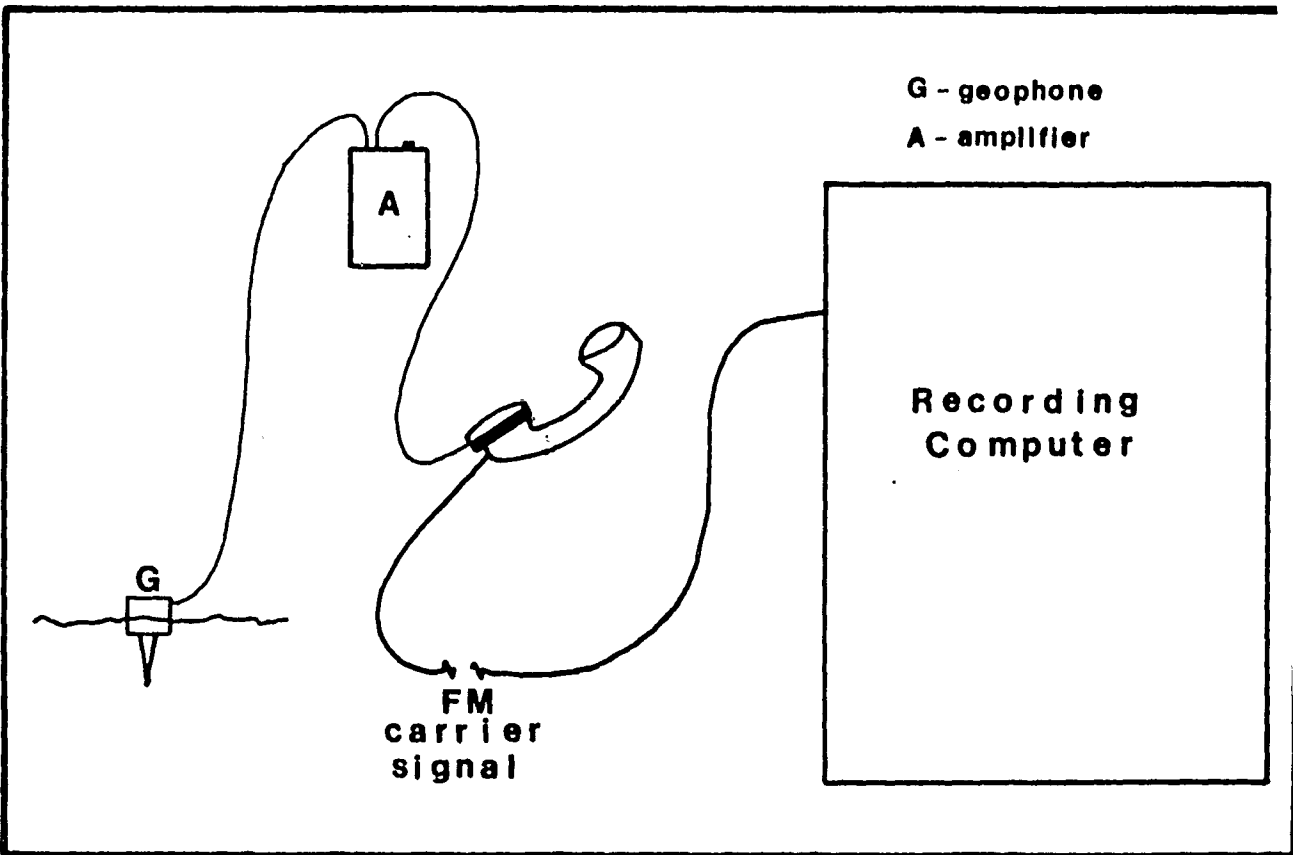


Figure 2-9: Geophone setup for timing blasts. The quarry geophone sends a FM carrier signal via the phoneline to the recording computer.

Nyquist frequency. The Nyquist frequency, half of the sampling frequency, is dependent upon the rate which the digital system samples the individual channels [Fig. 2-10]. The sampling rate of our system

$$T = 0.00576 \text{ seconds}$$

gives a Nyquist frequency of

$$f_n = 1/(2T) = 86.8 \text{ Hz.}$$

Any frequency above this was removed by filtering before being recorded.

Spatial aliasing occurs if there is less than 2 geophones per wavelength [Fig. 2-11]. The frequencies for deep reflectors are very low, on the order of 5 to 20 Hz. With a geophone spacing of 213.4 meters, the frequency of the minimum recoverable wavelength is determined by

$$f = V/(2x) = 14.06 \text{ Hz}$$

assuming a velocity of 6 km/s. It is less for even lower velocities.

After being received at the geophone the signal is amplified. The amplifier was also used to act as a low pass frequency filter to remove any frequencies above the Nyquist frequency and to filter the output to enhance the

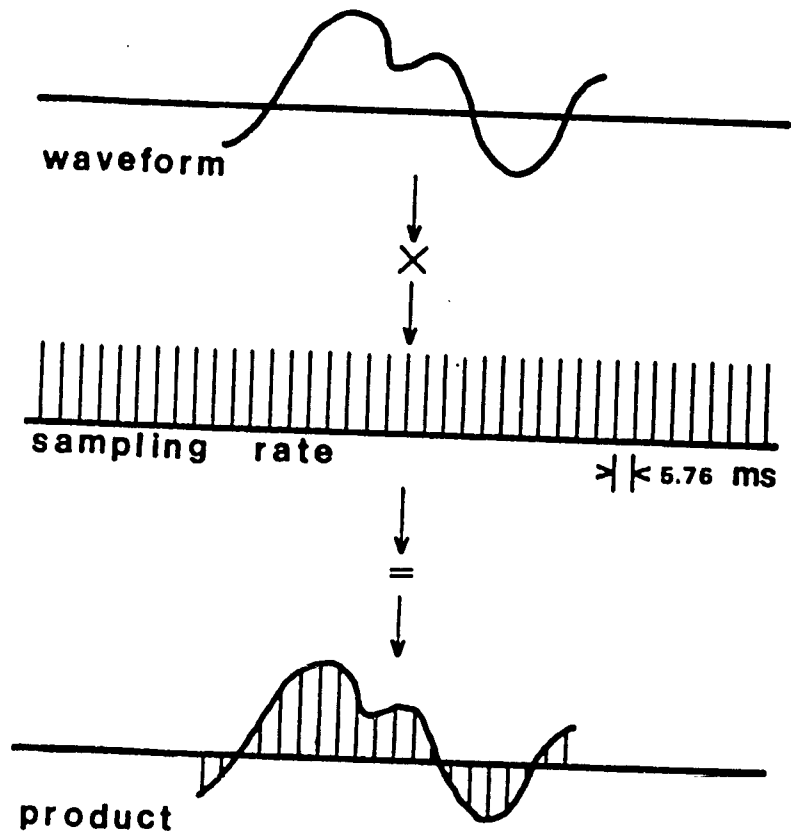


Figure 2-10: Example of temporal sampling. The sampling rate used was 0.00576 seconds.

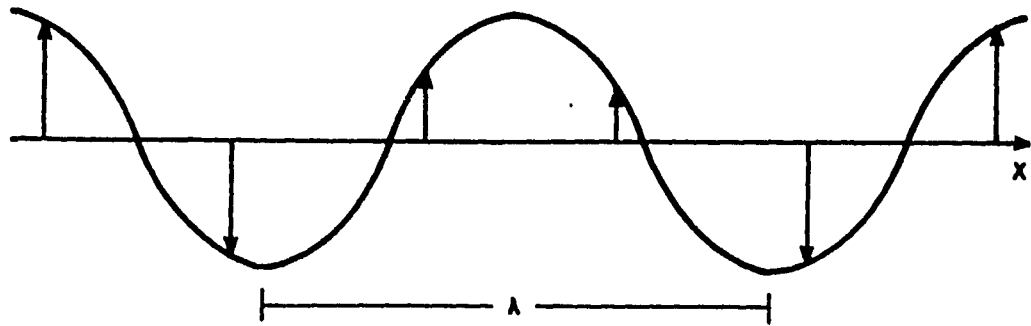


Figure 2-11: Example of spatial sampling. The waveform must be sampled twice per wavelength to avoid aliasing.

signal to noise (S/N) ratio. The high-cut frequency filter characteristics of the amplifier can be seen in Figure 2-12. Table 2-2 lists the filter and gain settings of the recorded blasts.

The digital recording system digitizes the analog output of the amplifier, and with the multiplexer, a high-speed electronic switch, reduces the 12 channels into 1. The digital system records the signal by a time series of integers which denote the geophone output values measured at the sampling rate (Fig. 2-10). The digitized data are recorded onto one half-inch digital magnetic tape. Each sample is represented by a 14 bit word giving value to the waveform, the first bit determining the positive or negative sign of the waveform.

While recording, a continuous viewing of 4 channels at one time on a cathode ray tube (CRT) allows a check on the cable continuity and the blast time.

2.4 Data Processing

The Whitehall quarry blast, recorded on November 19, 1981, will serve as a step-by-step example of the data processing used in this experiment. The reasons for examining this blast are that the offset is small and the blast large, thereby yielding the strongest signals.

Processing the data begins with demultiplexing the

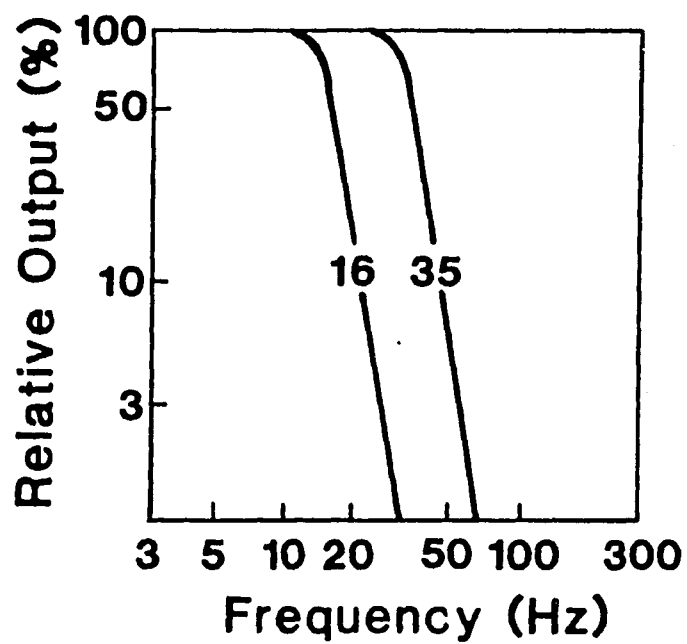


Figure 2-12: Amplifier cutoff filter responses for the frequency filters used in this study.

multiplexed signals from one channel into their original 12 traces [Fig. 2-13]. These data are given an integer value and then stored as words in separate traces. Each word multiplied by the sampling rate (0.00576 seconds) equals the time length of the trace.

After demultiplexing, the data are converted from integer form to fixed point numbers. The output now consists of 4 words per sample, one new record equaling 4 times the old record. This conversion is necessary for later processing.

A taper function is applied to both ends of the 1024 word records, since truncation in the time domain leads to oscillations in the frequency domain [Gibbs phenomena, Brigham (1974)], and can cause undesired end effects. In this case, the end effects are a coherent waveform [Fig. 2-14a] which could cause a strong apparent signal during interpretation. This is merely an artifact of the truncation. A Hanning window function (a cosine taper) was applied to the last 64 words on both ends of the 1024 word record [Fig. 2-14b].

At this point the data are transformed from the time domain into the frequency domain by the Fourier Transform

$$H(f) = \int_{-\infty}^{\infty} h(t) \exp(-i2\pi ft) dt$$

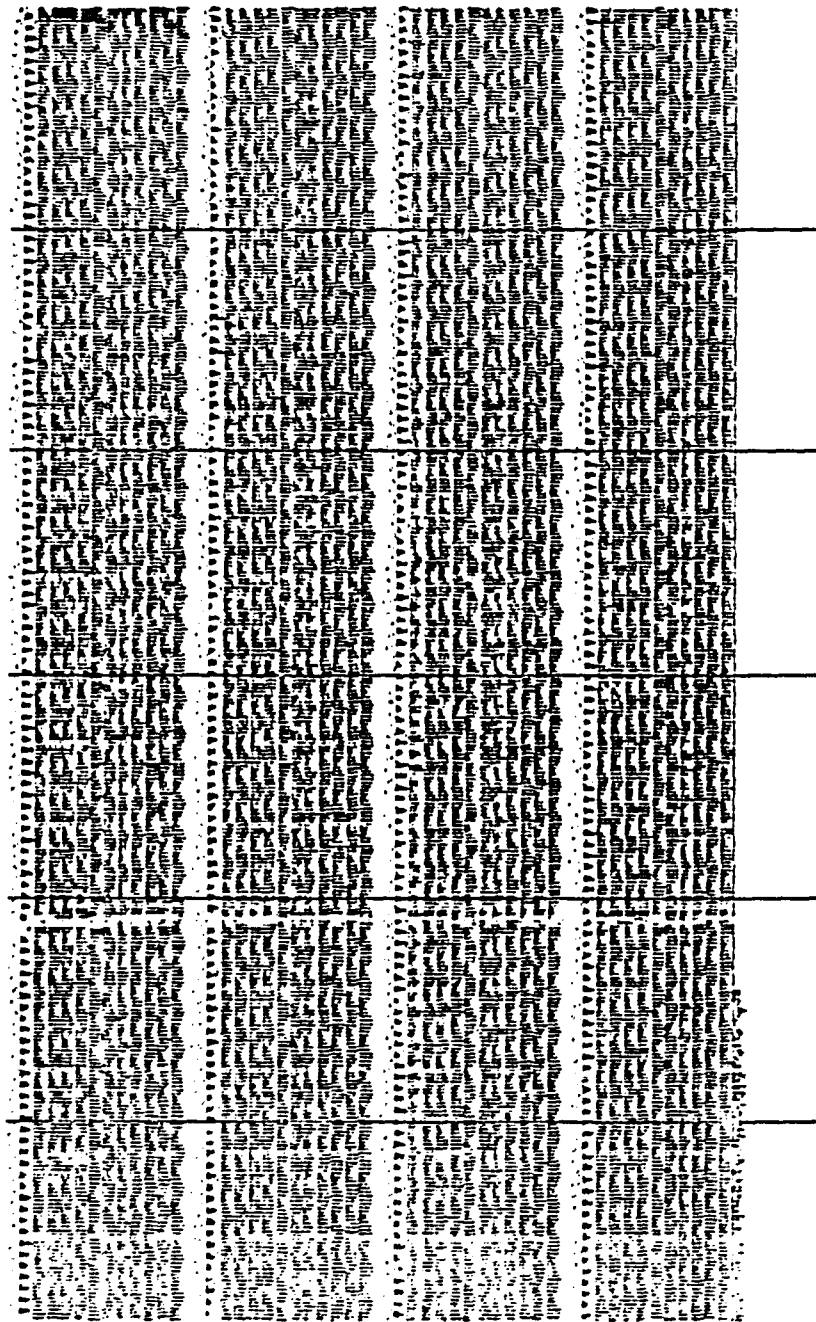


Figure 2-13: Demultiplexed data in the time domain before filtering. No waveforms except for the first channel can be observed. Time increases down and to the right.

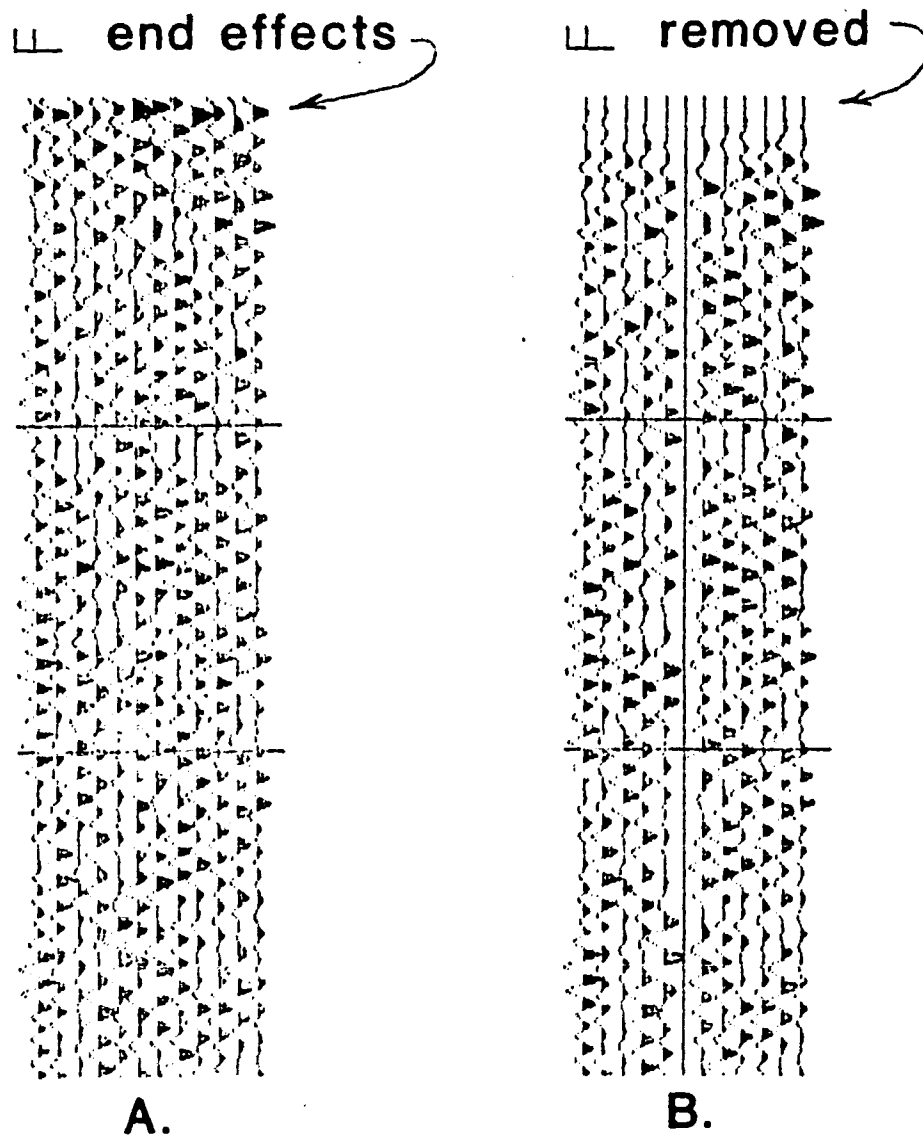


Figure 2-14: Illustration of a taper function removing the end effects of a field record.

The data are transformed using a Fast Fourier Transform (FFT) technique, and then normalized trace-by-trace. The transformed data are decomposed into a sum of sinusoids of different frequencies and amplitudes, the analysis revealing a strong contribution at 60 Hz [Fig. 2-15] except for the first channel. The electric field of nearby power lines is believed responsible for this induced high frequency signal. Also obvious in Fig. 2-15 is the trace's length of 86.8 Hz, the Nyquist frequency of our sampling function.

The next processing step is to filter the data. While most digital filtering is done in the time domain, filtering for our data was carried out in the frequency domain due to the length of the records. This filtering technique is carried out digitally by convolving the data with a filter function, $f(t)$,

$$h(t) = x(t)*f(t)$$

where $x(t)$ is the input, and $h(t)$ is the output. By use of the convolution theorem, the filtered output can be obtained by simple multiplication

$$X(f)F(f) \Leftrightarrow x(t)*f(t)$$

in the frequency domain. The data are then transformed back into the time domain for presentation.

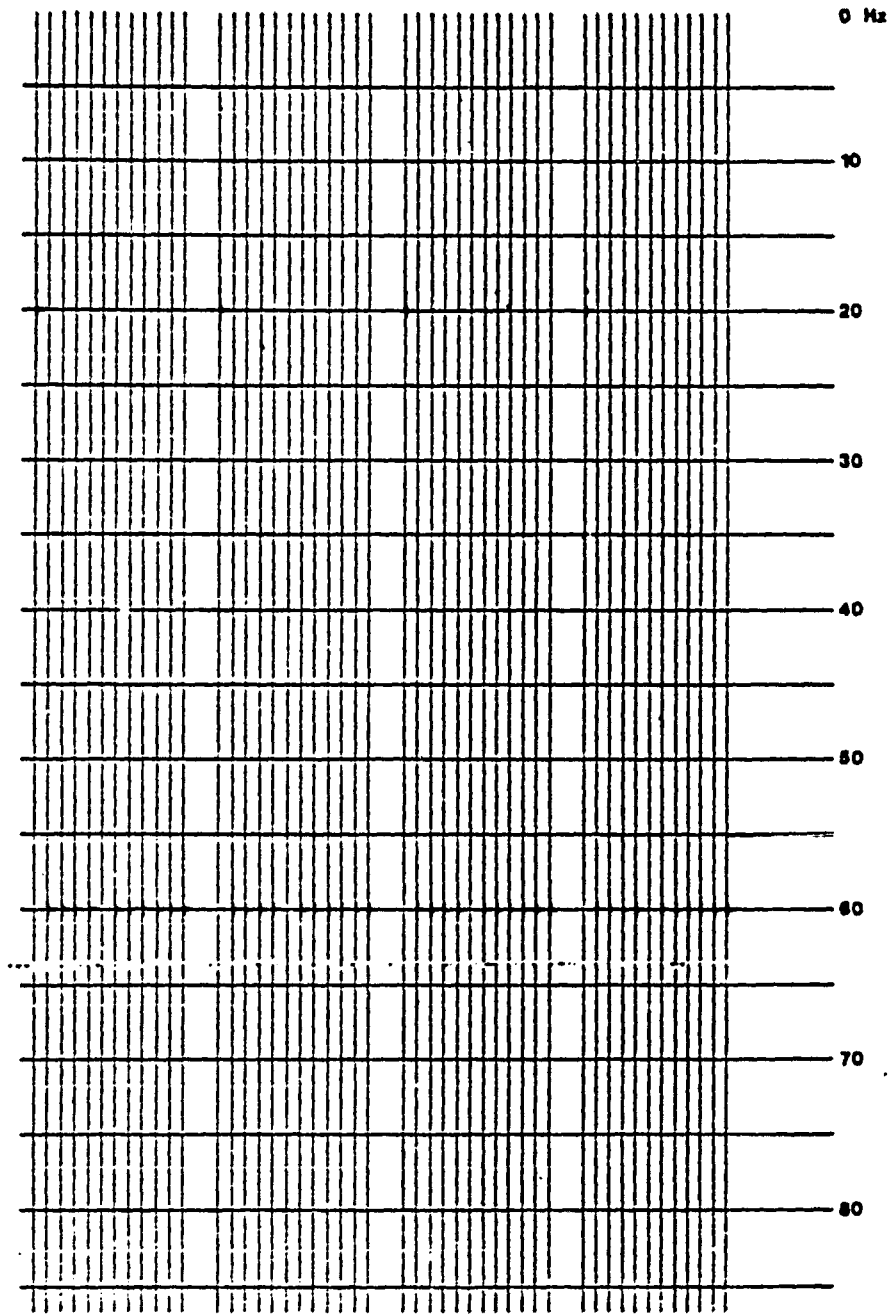


Figure 2-15: Fourier Transform into the frequency domain of the demultiplexed data. Notice the noise at 60 Hz except for the first channel quarry geophone.

The data are filtered using a low pass from 0 Hz to 45,55 Hz [Fig. 2-16] to remove 60 Hz noise. These data are then transformed into the frequency domain to check if the 60 Hz signal was removed [Fig. 2-17].

Another low pass filter further reduced the signals to the 0 Hz to 14,16 Hz frequency range. It can be seen that the trace amplitude increases due to the removal of higher frequency aliased data [Fig. 2-18], but that the dominant moveout appears reversed. A final trapezoidal band-pass filter from 6,8 Hz to 14,16 Hz gives the desired frequency range in that unwanted signals due to geophone response and spatially aliased frequencies are filtered out [Fig. 2-19]. However, the data do not improve due to reversed moveout of low frequency signals approaching from the opposite direction of the source blast. The reversed moveout are coherent signals of rather large amplitudes that can be followed across traces. Their existence is difficult to explain, but two possibilities are: 1) lake waves hitting the shore, 2) cultural noise that could not be discerned from the noise survey.

The sixth channel has been removed from the record sections since it is dominated by spurious signals caused by a faulty connection in the adapter plug to the amplifier.

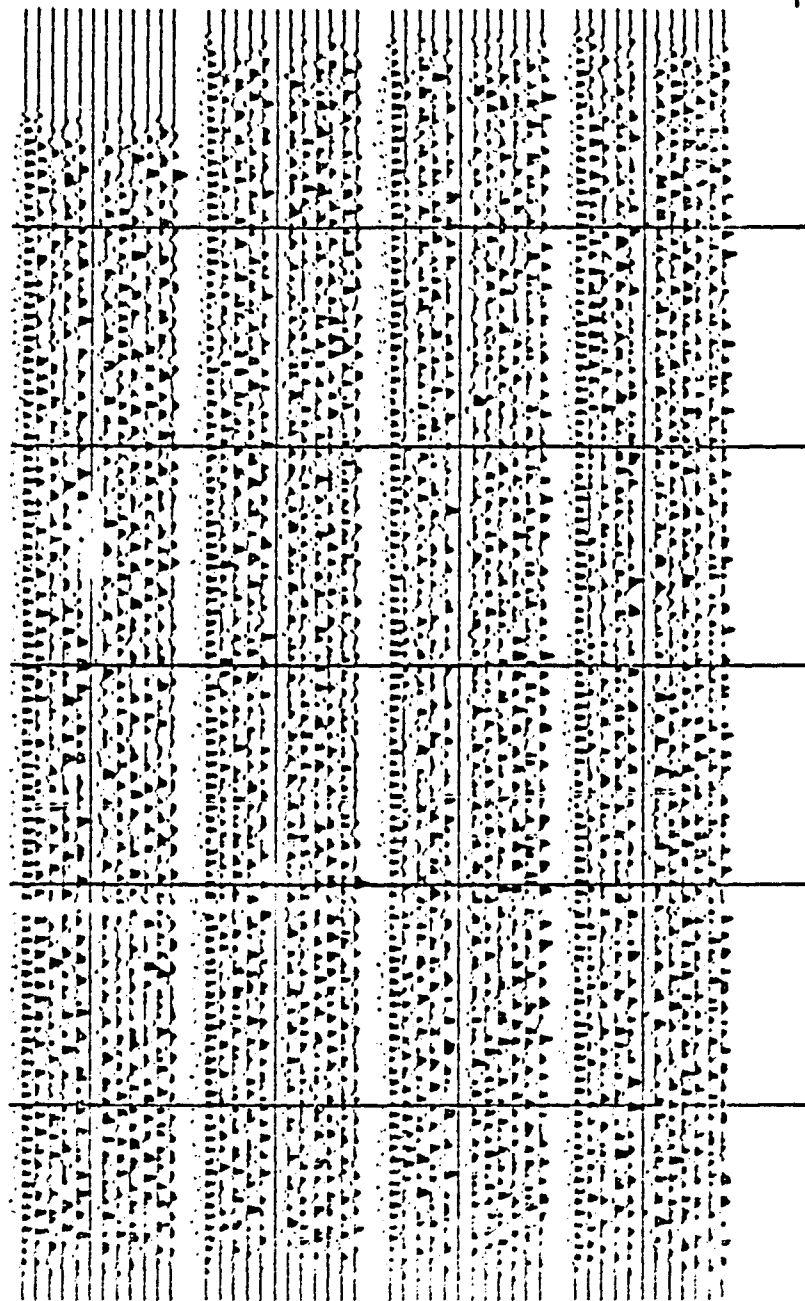


Figure 2-16: Data filtered from 0 Hz to 45,55 Hz in the time domain. The 60 Hz noise has been removed and waveforms can now be observed. Time increases down and to the right.

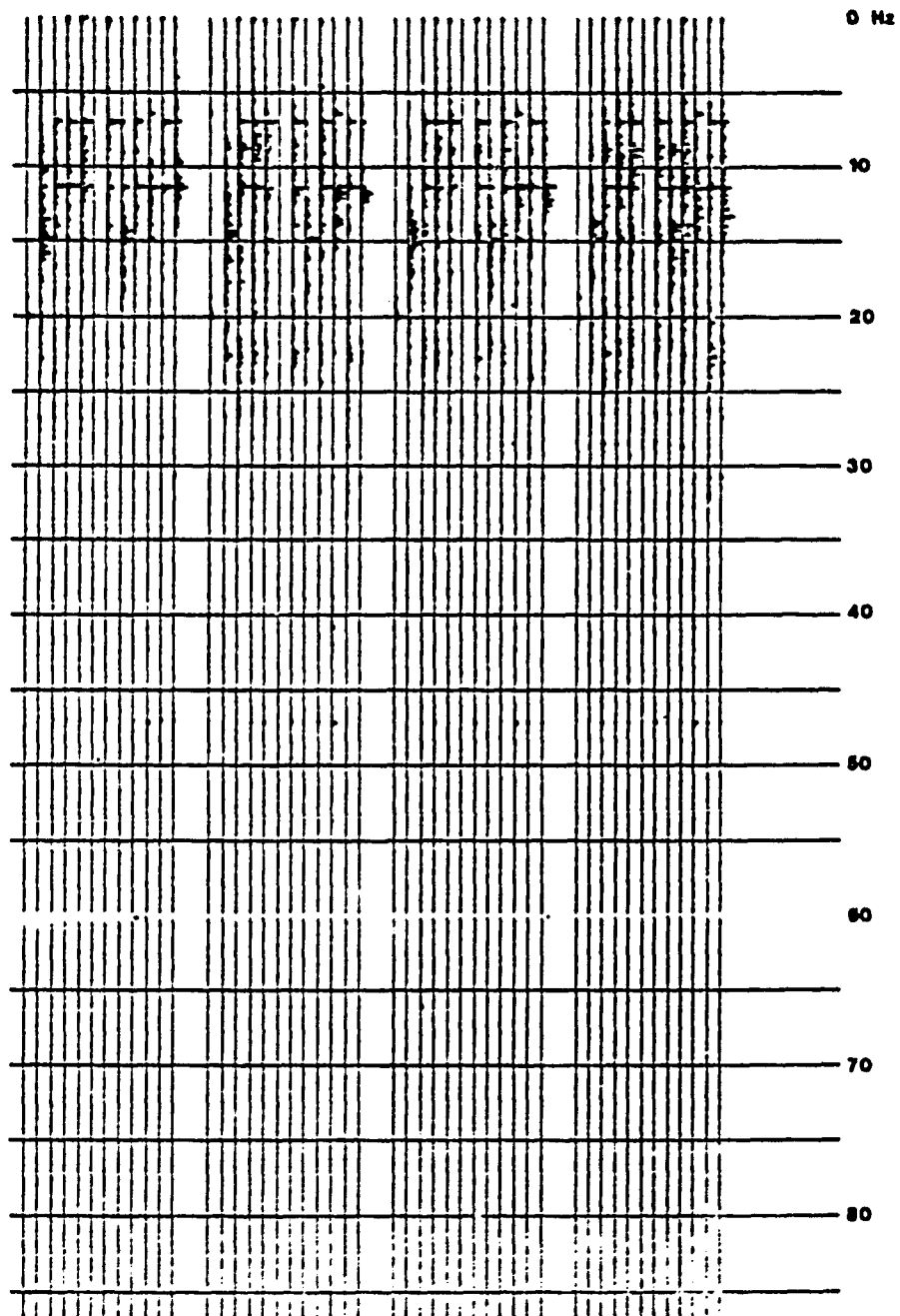


Figure 2-17: Fourier Transform into the frequency domain of the filtered data. With the removal of 60 Hz noise, the dominant frequencies appear below 20 Hz.

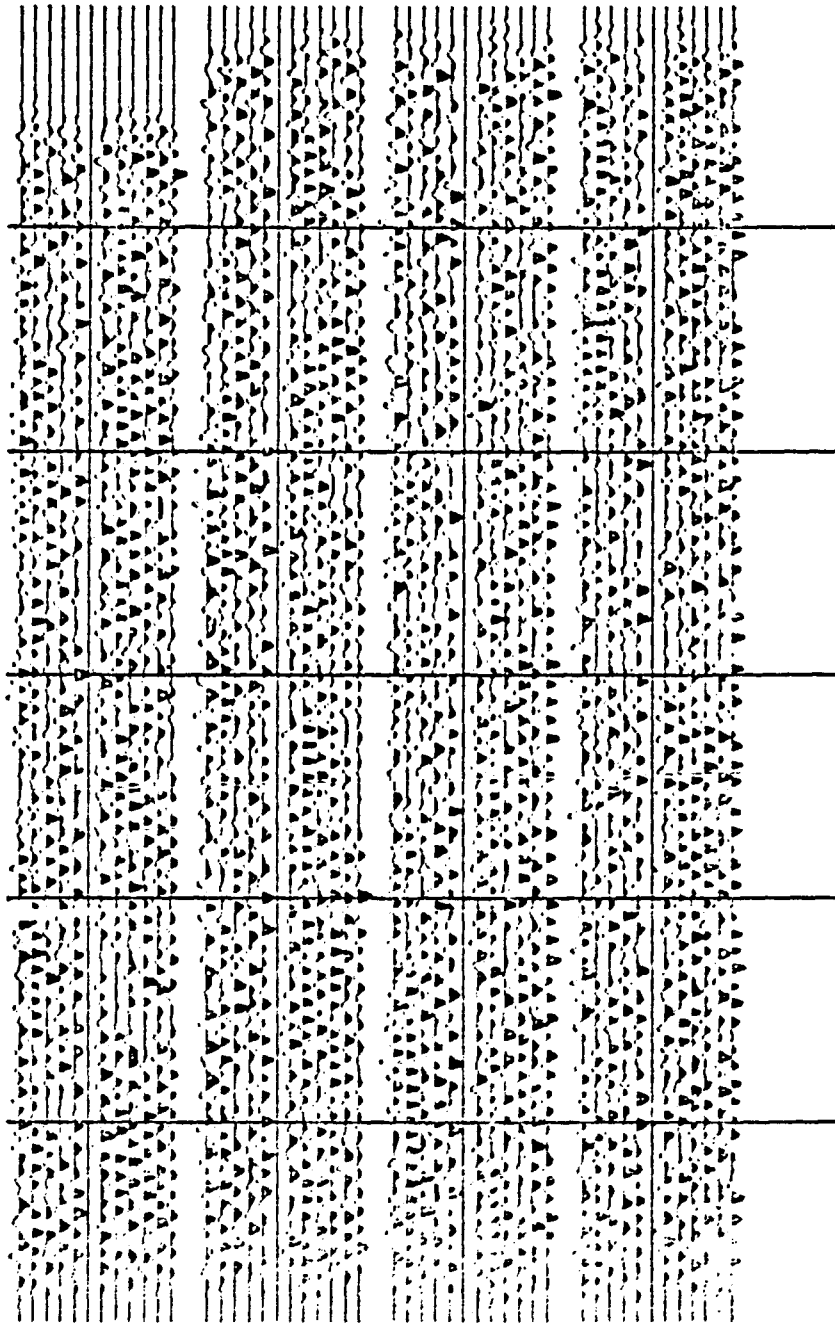


Figure 2-18: Data filtered from 0 Hz to 14,16 Hz in the time domain. Wave amplitudes have increased due to the removal of high frequency noise. Time increases down and to the right.

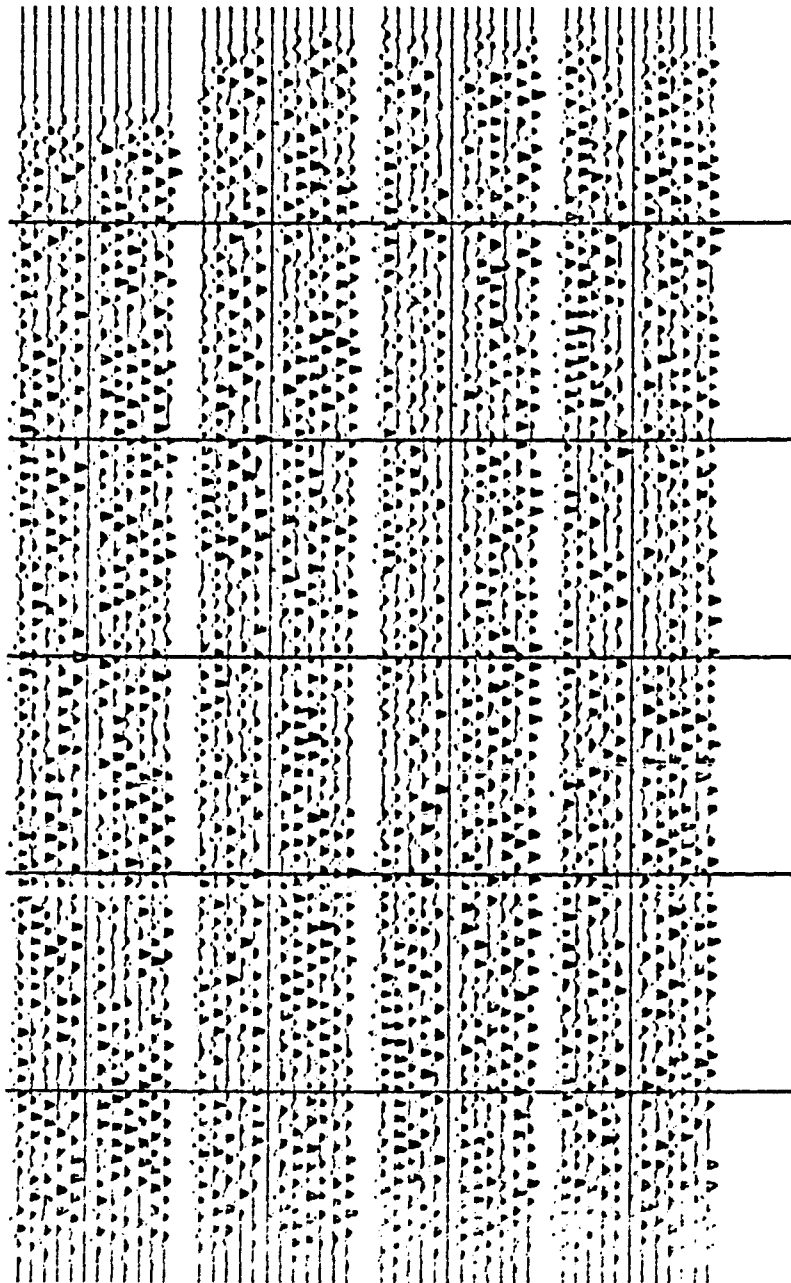


Figure 2-19: Data filtered from 6,8 Hz to 14,16 Hz in the time domain. This trapezoidal band-pass filter gives the desired frequency range. Time increases down and to the right.

The final steps in processing reconstruct the data into sections of 2048 words. The data are then shifted forward or backward, in time, so that the beginning of the record section is set to the exact time the source blast occurred. By constructing record sections in this manner, signal behavior can be observed from source blast time to after the signals are received. Appendix 1 contains the final processed data of the recorded blasts.

In the time window of expected P-wave arrivals, no outstanding normal moveouts can be detected (FIW figure, Appendix 1). This is due to a low S/N ratio. Not even filter processing enhances a very poor signal.

No static corrections were made for elevation variations between source and receiver, or for weathered layers. The recording site's elevation (152 m) does not vary much (<61 m) from the source elevations, since the source and receiver lie along strike in the Great Valley. Corrections for weathered layers were not necessary since the quarry blast is within bedrock and the geophones were within a few meters of or directly on bedrock.

3. INVERSE THEORY

3.1 Inversion Technique

Travel time curves are used for velocity-depth (V-Z) inversion. In the past, only refraction profiles were directly inverted for crustal structure using the Herglotz-Wiechert integral. New digital data collection techniques, superior to that used in earlier refraction surveys, allows more detailed analysis of both refractions and wide-angle reflections. The data are inverted directly for velocity-depth structure in a completely objective inversion technique.

This inversion technique, known as plane wave decomposition or slant stacking, has been used to transform digitally recorded $T(X)$ data into a $t(p)$ curve [Clayton and McMechan, 1981, Phinney et al., 1981, McMechan and Ottolini, 1980]. For ideal data, the $t(p)$ curve can be directly inverted for V-Z structure. The major advantage is that the inversions are computational transformations, automatically producing $t(p)$ and V-Z curves. This objectivity removes the errors due to human assumptions [Phinney et al., 1981, Stoffa et al., 1981, Bessonova et al., 1974].

The $t(p)$ curve is simply related to the $T(X)$ curve by

$$T = t + pX$$

where T is the travel time, t the intercept time, p the ray parameter (horizontal wave slowness), and X the offset distance. From this basic definition other relationships between these parameters follow:

$$t = \int X dp,$$

$$X = -dt/dp, \text{ and}$$

$$p = dT/dX$$

The inversion is an integration, as done in the time domain, over all points in the $T(X)$ data along slope p and intercept time t

$$\psi(p, t) = \int_{x_1}^{x_2} S^{1/2} \phi(X, t + pX) dX$$

where $S^{1/2}$ is a prestack scaling function for the recovery of true amplitudes, and x_1, x_2 represent finite endpoints of the array [Brocher and Phinney, 1981]. This integration is also known as an inverse Radon Transform. The integration, using the relationships defined above, computes a $t(p)$ curve by summing the maximum amplitude contribution along a given slope p and time intercept t in increments of dp and dt [McMechan and Ottolini, 1980] [Fig. 3-1]. The maximum amplitude contribution occurs only in the region of tangency in the $T(X)$ curve [Fig.

3-1). As would be expected, the quality of the $t(p)$ inversion is dependent on the $T(X)$ data quality.

In non-mathematical terms, the inversion separates refractions and wide-angle reflections in travel time space, combining them to form a single, well-defined trajectory in the $t(p)$ space. The $t(p)$ curve is a continuous, curving trajectory where t monotonically decreases with increasing p [Fig. 3-2]. Since the inversion is a summation along slope p , larger offsets will better define $t(p)$ data, refractions are transformed into points, and reflections remain curved.

The relation between $t(p)$ curves and $V-Z$ structure, known as t -sum inversion, can be mathematically expressed as a summation over all layers

$$Z_1 = [t(p)/2 - \sum_j Z_j q_j] / q$$

where Z_1 is the vertical thickness of the layer,

$$q = (a^2 - p^2)^{1/2}$$

is the vertical wave slowness, and $a = 1/V$ is the wave slowness. For inversion, a surface velocity must be specified in order to perform an iterative downward continuation (Clayton and McMechan, 1981, McMechan and Wiggins, 1972). This inversion sums only the refractions and wide-angle reflections in $t(p)$ and assumes horizontal

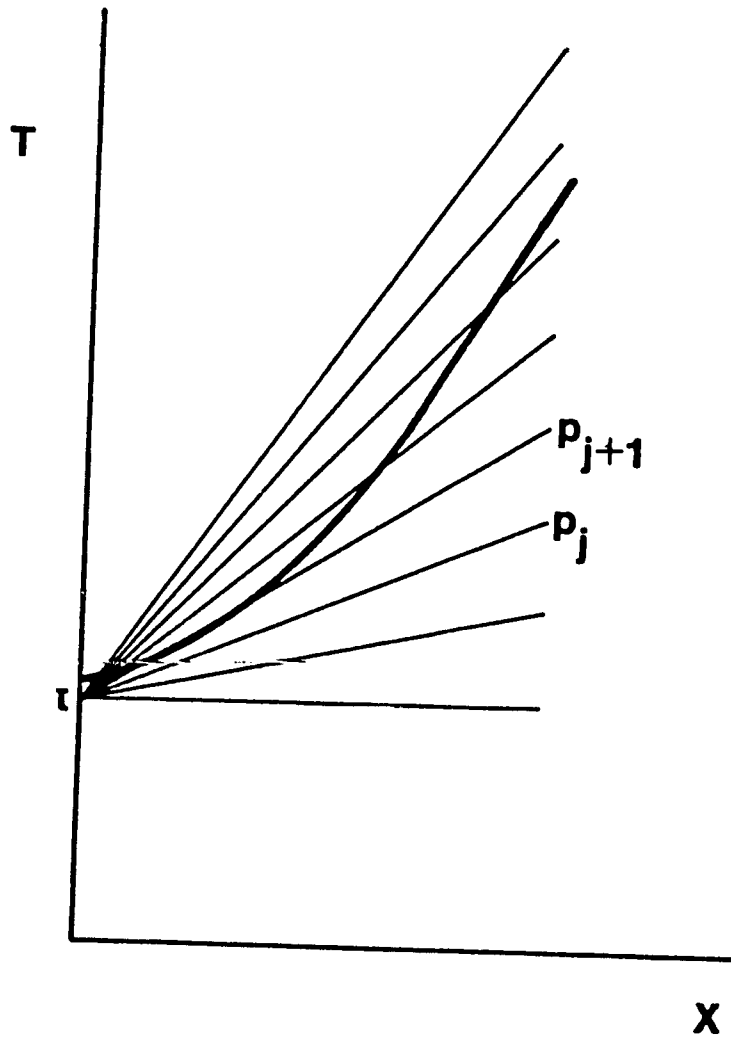


Figure 3-1: Slant stacking over a reflected wave in increments of dp . dt is also varied.

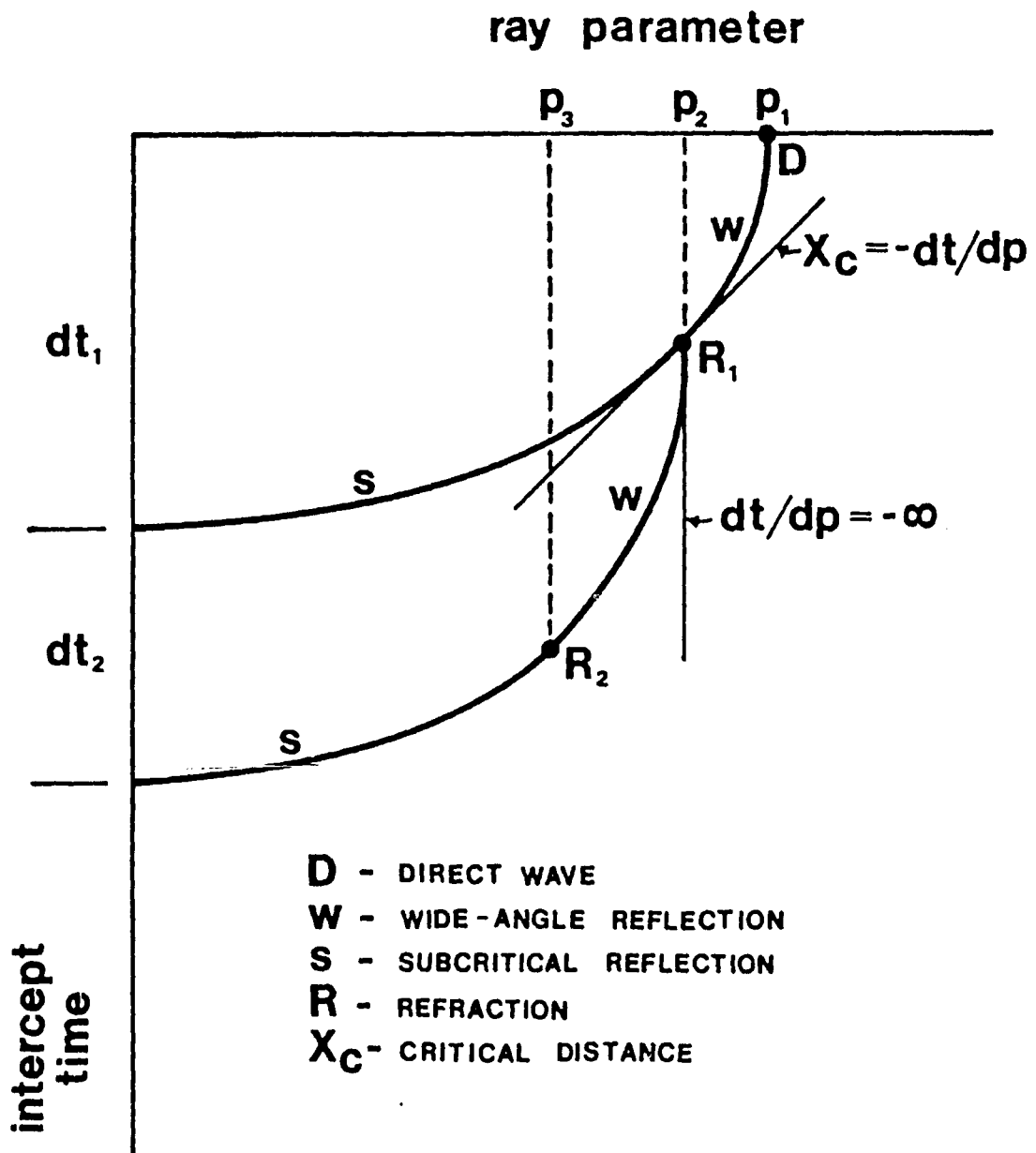


Figure 3-2: Interpretation of a two-layered crust in a $t(p)$ section. X_c is the critical distance for the first refraction, and the slope of the curve approaches minus infinity as it reaches its refraction point.

layering for calculating V-Z structure (Stoffa et al., 1981). Assuming good quality data and the existence of subcritical reflections, separate interval thicknesses and velocities can be determined by hand using the equation $Z_1 = dt/2p$. This t-sum inversion can also be expressed as a weighted Herdlotz-Wiechert integral determined by a Hilbert Transform

$$Z(p) = 1/2\pi \int_0^{t(p)} \frac{2}{[a(t) - p]^2 - 1/2} dt$$

where a is the inverse function to $t(p) = 1/V$ (Kennett, 1981).

Non-ideal conditions cause a scattering of data in both slant stacking and t-sum inversion. Bounds are placed to envelope the scatter in the data in the $t(p)$ plot (Fig. 3-5). For well-defined reflections in $T(X)$, the bounds are narrow. For confused reflection responses, the bounds are broad (Kennett, 1981). The broader the bounds, the more difficult it is to invert for the correct depth. It must be assumed that the best solution lies within the restricting bounds.

Inversion, like data processing, is subject to spatial and temporal aliasing. To reduce the effects of spatial aliasing, the stations must be spaced closely enough. To reduce temporal aliasing, the energy must be spread evenly throughout the recorded broadband frequency

spectrum. It must also be assumed that the velocity structure is laterally homogenous. This study meets all three requirements.

Truncation in the p domain can cause undesired end effects. These are removed by increasing the density of sampled p 's by decreasing dp .

Slant stacking can also minimize the effects of signal attenuation. The data can be improved by semblance or time windowing which admits only data having coherent phase signals across the traces at the time the data is expected to contribute to the slant sum.

Noise is also attenuated in $t(p)$ inversion because summation occurs only along coherent traces. The inversion compacts the data to a fixed size, unlike $T(X)$ data, thereby suppressing uncorrelated noise or placing noise outside the $t(p)$ curves [Phinney et al., 1981, Stoffa et al., 1981].

Because of the limited range of offsets in a common receiver array, $t(p)$ can only be determined when the isolated linear subarrays are at the critical and post-critical ranges. At the isolated subarrays, the data is slant stacked over the offset and midpoint distances [Phinney et al., 1981]. Inversion of $t(p)$ limited offset data can then provide approximate velocity-depth structures by best-fitting an ellipse to

the data points.

The $t(p)$ curve has several important characteristics when principal arrivals are inverted. The most obvious one is the variation of amplitude with p . The amplitude variation should be considered separately for different principal arrivals: 1) refractions, 2) wide-angle reflections, and 3) subcritical reflections. Refracted arrivals plot into single points due to the nature of the inversion. The direct arrival is a special case of a refracted arrival and plots as a point on the p -axis at t equal to zero. The largest amplitude on a $t(p)$ curve occurs at the critical distance where both refracted and reflected arrivals are summed. Wide-angle reflections plot as ellipses, their amplitude is large near the critical distance but decreases with increasing distance (distance on a $t(p)$ curve is measured as the negative slope $X = -dt/dp$). These ellipses terminate at each layer's critical refraction point. Subcritically reflected amplitudes depend on their reflection coefficients and are the continuation of the wide-angle reflection ellipse that intersects at the t -axis. If these reflections exist, layering is well-defined. If they do not exist, a continuous velocity function is inferred. Figure 3-2 defines the areas of different wave arrivals.

One of the most important aspects of $t(p)$ inversion is the ability to recognize low velocity zones. These zones can be identified by subcritical reflections from the top of the layer, or most easily by a discontinuity in t at p corresponding to a ray which turns at the top of the layer. The width of the t gap is the extent of the LVZ thickness [Fig. 3-3]. However, when gaps appear in both t and p , a LVZ can only be inferred.

Finally, synthetic models of $t(p)$ and $T(X)$ can be produced directly from velocity-depth structures by inverse slant stacking. The $t(p)$ model is mathematically derived by

$$t(p) = 2 \int_0^z \frac{2}{[a^2(Z) - p^2]^{1/2}} dz$$

where a is the wave slowness $1/V$, and Z is the depth. The $T(X)$ model is simply defined as the integration of the Hilbert Transform

$$\Phi(X, T) = 1/(2\pi) \int_{x_1}^{x_2} \psi(p, T - pX) dp$$

where ψ is a function of (p, t) , and is known as a Radon Transform. This integration uses the relationships

$$T(p) = 2 \int_0^z \frac{2}{a^2(Z)[a^2(Z) - p^2]^{-1/2}} dz,$$

$$X(p) = 2 \int_0^z \frac{2}{p[a^2(Z) - p^2]^{-1/2}} dz$$

for calculating $T(X)$ curves. As can be seen, both the

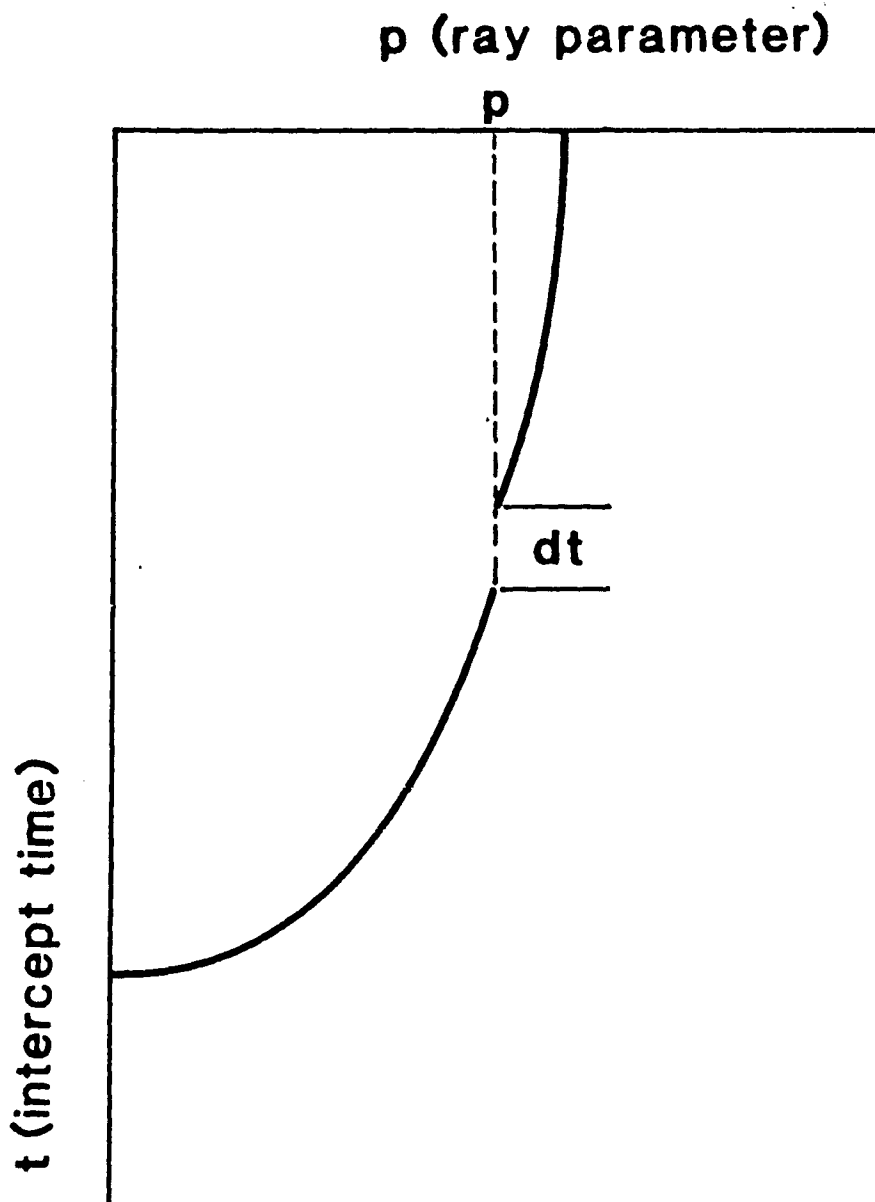


Figure 3-3: Behavior of reflected wave in a $t(p)$ section when a LVZ is encountered. The LVZ thickness is determined by $dt/2p$.

inverse and forward modelling are completely objective, relying on simple mathematical relationships.

3.2 Theoretical Modelling

Three theoretical models of the crust in $T(X)$ and $t(p)$ sections illustrate the advantage of inverting for crustal velocity structures from $t(p)$ sections. These forward models are computer calculated by specifying the number of horizontal layers, and each layer's velocity, density, and thickness. The range of ray parameters and angular frequencies must also be specified. These parameters are slant stacked in the $p-w$ (ray parameter-angular frequency) domain, the data then being filtered to the desired frequency range, and finally transformed into the $t(p)$ domain. The data from the $t(p)$ domain is then inverse slant stacked into the $T(X)$ domain using the mathematical relationships defined in the previous section.

This technique uses the Thompson-Haskell matrix method for calculating reflection coefficients for the desired frequency range [Phinney et al., 1981], thereby allowing the study of amplitude variation in the $T(X)$ and $t(p)$ sections. All models may be found in Appendix 2.

Model 1: a two layer, 35 km thick crust. The velocity (V), density (R), and thickness (Z) parameters of each layer are $V_1 = 6.1$ km/s, $R_1 = 2.6$ g/cc, $Z_1 = 20$

$V_1 = 6.7$ km/s, $R = 2.7$ g/cc, $Z = 15$ km. The mantle parameters are $V_2 = 8.1$ km/s, $R = 3.3$ g/cc, and an arbitrary thickness of 100 km. This crustal model represents an upper granitic layer separated from an intermediate layer by the Conrad discontinuity.

In the 6 km/s reduced travel time section, the 2 distinct reflections result from the acoustic impedance between crustal layers and the crust-mantle interface. The maximum amplitude with distance is found between 80-110 km, the critical distance range for Moho reflections.

The 2 distinct reflections appear as elliptical curves in the $t(p)$ section terminating at both axes. The $t(p)$ section is a fixed, compact size as compared to the $T(X)$ section which tends towards infinity along the X-axis. The curves outside the major ellipses, due to multiple reflections or aliased noise, are an artifact of forward modelling and appear in all three models.

The $t(p)$ section is easy to invert into its original horizontal layer parameters. The velocities of each layer is measured by the equation $V = 1/p$ at refraction points where $dt/dp = -\infty$ [Fig. 3-2]. The velocities calculated from this model are $V_1 = 6.1$ km/s and $V_2 = 6.7$ km/s. The refraction points also define the critical distance for the upper layer by the equation $X_c = -dt/dp$.

However, since no reflections below the Moho define the second layer's refraction point, X^c is determined as the point of maximum amplitude on the lower ellipse [Fig. 3-2]. The critical distance for layers 1 and 2 are approximately 43 and 89 km, respectively. The thicknesses of the layers, as determined by each ellipse and the equation $Z = dt/2p$, are 19.7 km for layer 1 and 14.9 km for layer 2. These calculations fit the entered parameters.

Model 2: a three layer, 40 km thick crust. The parameters of each layer are $V_1 = 5.9$ km/s, $R_1 = 2.55$ g/cc, $Z_1 = 10$ km, $V_2 = 6.1$ km/s, $R_2 = 2.6$ g/cc, $Z_2 = 20$ km and $V_3 = 6.7$ km/s, $R_3 = 2.75$ g/cc, $Z_3 = 10$ km. The mantle parameters are the same as Model 1. The interpretation is similar to the first model with an additional layer. This crustal model represents a sedimentary layer that overlies a granitic layer, separated from the intermediate layer by the Conrad discontinuity.

The reduced travel time section contains 3 distinct reflections resulting from acoustic impedances, but noise is present due to multiple reflections within the crust. The maximum amplitude with distance is found between 90-110 km.

In the $t(p)$ section, 3 major elliptical curves

define the layers. The interpreted velocities for each layer are $V_1 = 5.9$ km/s, $V_2 = 6.1$ km/s, and $V_3 = 6.7$ km/s. The critical distances for each layer are approximately 20 km for the first layer, 65 km for the second layer, and 104 km for the Moho reflection. The calculated thicknesses are $Z_1 = 9.9$ km, $Z_2 = 19.4$ km and $Z_3 = 10$ km. The calculations again fit the entered parameters well.

Model 3: a 35 km thick crust. The upper layer has the parameters $V_1 = 6.1$ km/s, $R_1 = 2.6$ g/cc, $Z_1 = 25$ km. This layer is followed by a continuous velocity function where the velocity increases from 6.3 to 7.1 km/s and the density increases from 2.65 to 2.85 g/cc over a vertical distance of 10 km. When a forward model is computed from a continuous velocity function, the slant stacking is carried out in small increments. In this case, the increments occur at 2 km intervals. The mantle parameters are the same as Model 1. This model represents a complicated crustal structure where the velocity increases with increasing depth independent of rock type, and is more difficult to interpret.

In the reduced travel time section, only one main reflection is observed resulting from the Moho reflection where the largest acoustic impedance is encountered. Other reflections cannot be distinguished. The maximum

amplitude variation with distance is found between 80-100 km.

In the $t(p)$ section, one major curve contains all the wide-angle reflections. Weak elliptical curves for 6 crustal layers can be discerned within one major curve. The velocities for these 6 layers range from 6.1 to 7.1 km/s. Critical distances are hard to define, but for the Moho reflection X_c is approximately 90 km. By close examination, the approximate thicknesses of the layers are $Z_1 = 24.7$ km, $Z_2 = 2$ km, $Z_3 = 2$ km, $Z_4 = 2$ km, $Z_5 = 2.1$ km and $Z_6 = 1.8$ km. These calculations fit the model well.

In an ideal data set, a continuous velocity function can be discerned. In a real data set, a continuous velocity function is difficult to distinguish from a simple one layer model, and can only be inferred.

These synthetic models illustrate the advantage of $t(p)$ sections over the traditional $T(X)$ sections for crustal structure inversion. The $t(p)$ sections have a fixed size in that the curves intersect the axes. The $t(p)$ sections place noise due to aliasing or multiple reflections outside the major elliptical curves, thereby reducing confusion in interpretation. The $t(p)$ is also easily inverted for crustal velocity structure by simple hand calculations. This makes interpretation from $t(p)$

sections more desirable than from T(X) sections.

3.3 Data Inversion

Even the advanced computer filtering and slant stacking techniques described in previous sections could not isolate a very weak signal in the data. Therefore, the data were treated in a more subjective manner. The following steps were taken to construct a crustal model:

- 1) A broad time window was chosen to cover the expected range of P-wave arrivals. These arrivals ranged from a high velocity direct wave to a low velocity wave reflected at a deep interface. The chosen time window did not overlook any expected arrivals. Within the time window, only data having at least 6 out of 10 coherent phase signals traceable across the record were used.
- 2) These coherent phase signals were measured for two-way travel time, the time between the source blast and the first signal received on the first trace, and for normal moveout (NMO), the time difference between the first and last traces. There were several NMO's measured for each blast.
- 3) The horizontal wave slowness (p) was calculated for each moveout by the equation dT/dx , x being the total geophone spacing.

- 4) The intercept time (t) was calculated for each moveout by the relation $t = T - pX$, X being the offset distance.
- 5) Each NMO was plotted as a point onto the $t(p)$ section [Fig. 3-4]. These data points define an ellipse, and are inverted for crustal structure.

This $t(p)$ plot should be a well-defined curve. The quality of this $t(p)$ plot is directly dependent upon the $T(X)$ data. Since the $T(X)$ data are poor, the $t(p)$ plot's scattered points do not define a narrow ellipse. The bounds placed enveloping the scattered points give an estimate of the resolution of the data. The bounds placed on the data must be ellipses, the slope of the ellipse approaching infinity as t approaches zero, and zero as p approaches zero. The best-fit elliptical curve within these bounds is used for inversion [Fig. 3-5]. The elliptical curves used were computer calculated and best-fit by hand.

The crustal velocity structure is easily calculated from the best-fit curve in the $t(p)$ section. The near surface velocity is defined as $V = 1/p$ where the slope of the curve dt/dp approaches minus infinity and intersects the p -axis. The inferred velocity is 5.8 km/s. The thickness is determined by the equation $Z = dt/2p$, and is approximately 41.2 km thick. The data does not define

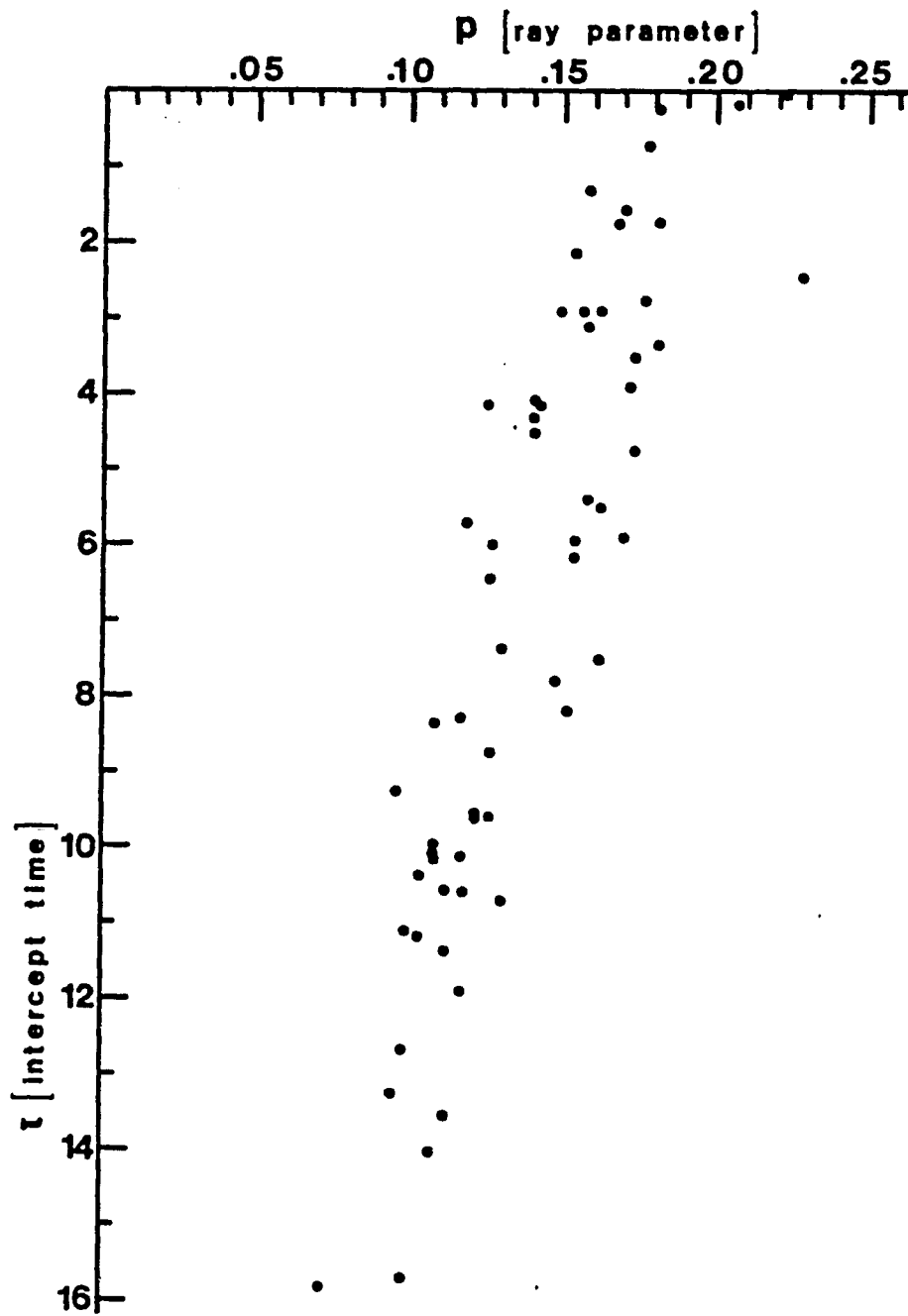


Figure 3-4: Data points from all blasts plotted on a $t(p)$ section.

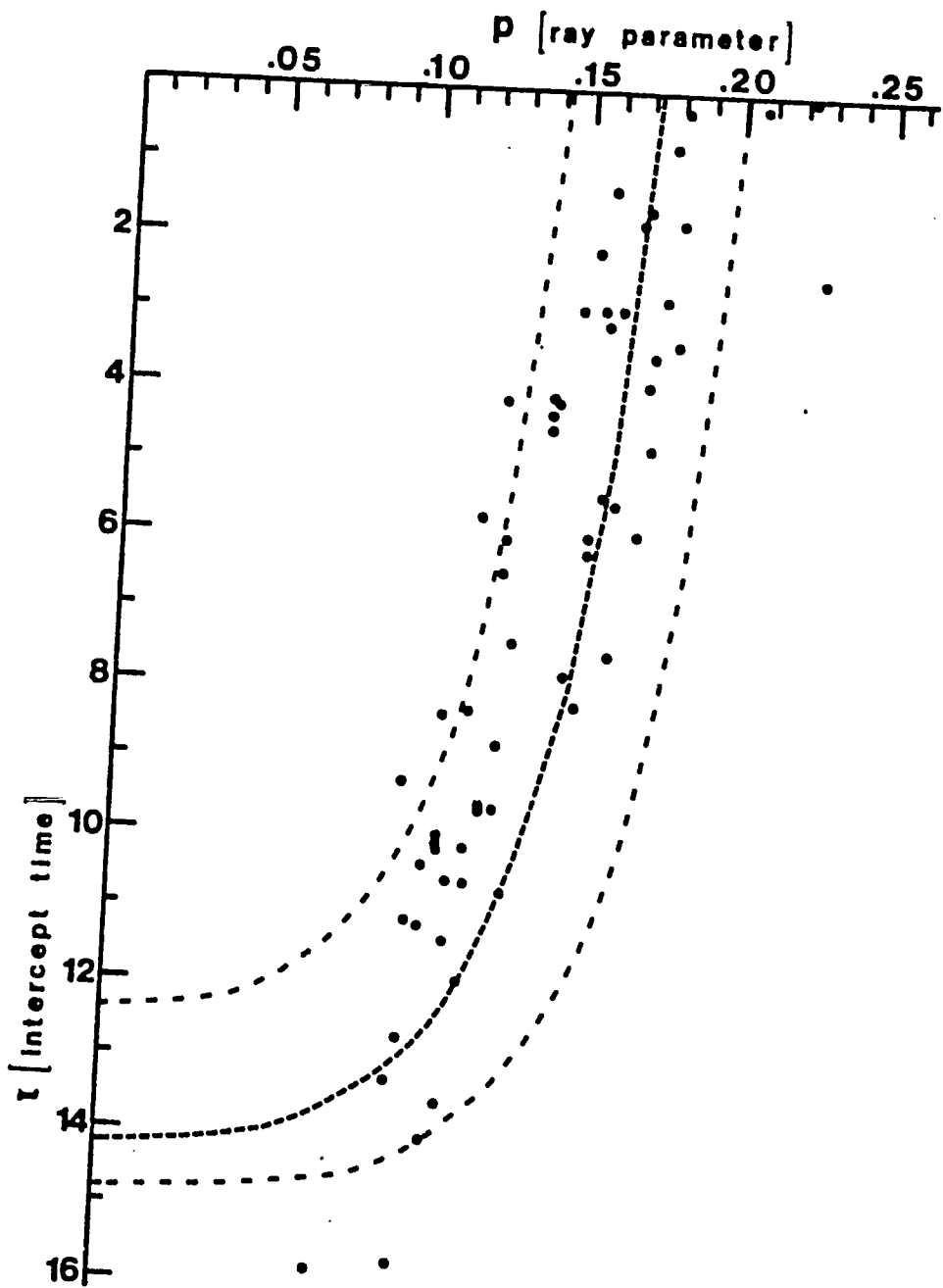


Figure 3-5: Data points with limiting bounds (light dash) and best-fit ellipse (heavy dash).

individual layering and velocities within the crust because of the poor data quality and lack of subcritical reflections. Since a simple one layer crust with an average velocity of 5.8 km/s is not based on geological reasoning, the data would infer that the crust in eastern PA.-northern N.J. has a continuous velocity where the velocity increases as a function of increasing depth. This inferred crustal interpretation could be compared to Theoretical Model 3.

Visual inspection of the $t(p)$ data could also suggest a two layer crustal structure. A cusp on the right hand side of the data may indicate that the first layer is about 29 km thick (velocity = 5.8 km/s), and the second layer is 17 km thick (velocity = 7.7 km/s).

The crustal velocity model presented in this study is consistent with previous studies in this area (Sienko, 1982, Langston and Isaacs, 1981, Taylor and Toksoz, 1979, Dorman and Ewing, 1962, Oliver et al., 1961, Katz, 1955). The crustal velocities determined in the other studies ranged from 6.04 km/s to 6.5 km/s with Langston and Isaacs (1981) and Sienko (1982) determining a 5.8 km/s velocity for near surface limestones. Crustal thickness values ranged from 34.4 km to 41 km. These thicknesses and velocities agree with the crustal model presented in this study. Table 3-1 lists the results of previous crustal studies in this area.

Table 3-1: Comparison of previous crustal structure studies to this study's results.

STUDY	MODEL	TECHNIQUE	AREA
Katz (1955)	1 layer 34.4 km V = 6.04 km/s	Refraction	PA-NY-NJ
Oliver et al. (1961)	3 layers 37 km V1 = 2.3 km/s V2 = 3.55 km/s V3 = 3.8 km/s	Rayleigh wave phase velocities	PA-NY
Dornan and Ewing (1962)	1 layer 38.6 km V = 3.64 km/s	Surface wave dispersion	PA-NY
Taylor and Toksoz (1979)	1 layer 37 km V = 6.5 km/s	P-wave travel time residuals	Northeastern U. S.
Langston and Isaacs (1981)	1 layer 41 km V = 6.04 km/s	P-SV wave conversion at the crust-mantle interface	PA
Sienko (1982)	2 layers 37 km V1 = 5.8 km/s V2 = 6.8 km/s	Wide-angle reflections and refractions	South-Central PA (N - S profile)
This Study (1982)	1 layer 41.2 km V = 5.8	Inversion of wide-angle reflections	Eastern PA-Northern NJ

4. DISCUSSION

4.1 Data Quality

The three most likely causes of poor reflection responses in the T(X) data are: 1) small size of the artificial source quarry blast, 2) effects of ripple-firing at the source on the energy level of the seismic signal, and 3) the attenuation of the seismic signal over its travel path.

The first cause is obvious. The recorded blast sizes in this study ranged from 1497 kg to 3651 kg. In Katz's (1955) study, the smallest recorded blast in Pennsylvania was 19,958 kg (22 tons). Mark Angelone, Penn State University, (personal communication) believes that a 9072 kg (10 ton) blast is necessary to receive a seismic signal over 100 km.

The effect of ripple-firing, the time delays between shots, is to impart periodicity on the seismic signal [Pollack, 1963]. The total delay time (Δt) results in fundamental and harmonic frequency peaks corresponding to $1/\Delta t$ [Pollack, 1963, Willis, 1963]. When $\Delta t < T$ (the seismic period), the effect on the frequency spectra are minimized [Frantti, 1963]. In this study, Δt ranged approximately from 0.24 s to 0.53 s, much greater than the desired seismic period (0.07 to 0.13 s). While a single blast would have its first

arrival wave energy concentrated near its front end, an increase in delay time causes an energy level decrease and attenuation of the seismic signal [Frantti, 1963].

Along its travel path, the seismic signal is altered by both attenuation [O'Brien, 1961] and the earth acting as a low pass frequency filter. The two factors determining the extent of attenuation are: 1) energy absorption due to the anelasticity of the crust; and 2) diffraction losses - partitioning of energy at each boundary [Claerbout, 1976, White, 1965, O'Brien, 1961].

Geometrical spreading plays only a minor role in attenuation because the offset distances necessary for wide-angle reflection studies are minimal when compared to refraction studies. Frictional losses through absorption also are relatively unimportant because of the lateral homogeneity of the crust in the eastern U.S. [Bolt, 1978], and especially within one crustal block. Therefore, the major cause of seismic signal attenuation is due to diffraction losses. The Great Valley is composed of a thick sequence of folded and faulted Cambro-Ordovician sedimentary rocks. The number of acoustic boundaries causes a multitude of energy partitions (i.e. scattering) resulting in the loss of seismic energy and the broadening of the seismic pulse. The effects of both ripple-firing and attenuation can be

overcome in part by recording larger blast sizes. The blast sizes necessary are not as available as in the past due to urbanization around the quarries, but they occur often enough to warrant further investigation.

Another factor affecting the data quality was the apparent reverse moveouts in the processed data. The moveout was a real effect and not an artifact of data analysis or improper filtering. The most likely cause of the reverse moveout was waves from the adjacent Paulinskill Lake hitting the shoreline. While the exact cause may be difficult to prove, larger blasts causing the reflected seismic signals to dominate the ground motion would overcome the effects of reverse moveout.

4.2 Modelling

In theoretical modelling, the effects of layering and continuous velocity functions within the crust is illustrated in $T(X)$ and $t(p)$ sections. This modelling also allows a study of the systematic change in amplitude variation of an ideal data set. The advantages of crustal interpretation from $t(p)$ sections is demonstrated in these models.

4.3 Results

This study met its major objective in determining the crustal velocity structure in eastern PA. and

northern N.J. However, due to the data quality, many objectives could not be met. The model presented in this study, a 41.2 km thick crust with a near surface velocity of 5.8 km/s, might suggest a continuous velocity function as in Theoretical Model 3. A simple one layer crust with an average velocity of 5.8 km/s is unreasonable and is not consistent with any previous crustal models of the study area. This would imply that crustal layering and the Conrad discontinuity either do not exist or can not be detected, and that velocity increases as a function of increasing depth in the study area.

This study was consistent with some of the previous work done in this area. James et al. (1968) suggested that the crust might thicken towards the Appalachian basin. Fletcher et al. (1978), by noting the association of the Great Valley with the northeast trending negative Bouguer gravity anomaly and the positive P-wave travel time residuals, suggested a crust of greater thickness than the adjacent areas. This study's thickness of 41.2 km seems to support these ideas. Taylor and Toksoz (1979) suggested that this region exhibits lower crustal velocity than the surrounding regions. The proposed 5.8 km/s near surface velocity supports this idea, but this may be dependent on the region's thick sedimentary cover.

If magnetic and gravity anomaly data define crustal blocks, then this study presents a model for this particular block. The velocity in this block is 5.8 km/s at the near surface and continuously increases with depth, independent of rock type. If separate crustal blocks do exist, future studies within blocks would lead to an overall understanding of crustal structure and seismicity in the northeastern U.S.

4.4 Suggestions for Future Work

- 1) Most importantly, discrimination must be made in the selection of quarry blasts before recording. Large shots with minimal ripple-fire must be chosen.
- 2) Recording sites must be carefully chosen so as to eliminate noise, such as reverse moveout, from the data.
- 3) A larger number of offsets will greatly enhance limited data.
- 4) Geophone spreads should be increased over that used in this study. This will increase the ability to measure normal moveout, and will lessen truncation effects during the computer reduction and inversion processes.

Note: The recording system used was a broad-band digital seismic system developed jointly by The Pennsylvania State University and Princeton University under U. S. Geological Survey Contract 14-08-001-18262.

REFERENCES

- Bessonova, E.N., V.M. Fishman, V.Z. Ryaboyi, and G.A. Sitnikova. The tau method for inversion of travel times - 1. Deep seismic sounding data. *Geophys. J. R. Astr. Soc.*, 1974, 36, 377-398.
- Bolt, B.A. *Earthquakes: A Primer*. San Francisco: W.H. Freeman and Co. 1978.
- Braile, L.W. and R.R. Smith. Guide to the interpretation of crustal refraction profiles. *Geophys. J. R. Astr. Soc.*, 1975, 40, 145-176.
- Brigham, E.O. *The Fast Fourier Transform*. Englewood Cliffs, N.J.: Prentice-Hall, Inc. 1974.
- Brocher, T.M., and R.A. Phinney. Inversion of slant stacks using finite-length record sections. *J. Geophys. Res.*, 1981, 86, 7065-7072.
- Carts, D.A. and G.A. Bollinger. A regional crustal velocity model for the southeastern United States. *Bull. Seis. Soc. Am.*, 1981, 71, 1829-1849.
- Claerbout, J.F. *Fundamentals of Geophysical Prospecting: With Applications to Petroleum Prospecting*. New York: McGraw-Hill, Inc. 1976.
- Clayton, R.W., and G.A. McMechan. Inversion of refraction data by wave field continuation. *Geophysics*, 1981, 46, 860-868.
- Colton, G.W. The Appalachian Basin -- its depositional sequences and their geologic relationships. In Fisher, G.W. et al. (Ed.), *Studies in Appalachian Geology: Central and Southern*, New York: Interscience Publishers, 1970.
- Cook, F.A., D.S. Albaugh, L.D. Brown, S. Kaufman, J.E. Oliver, and R.D. Hatcher, Jr. Thin-skinned tectonics in the crystalline southern Appalachians; COCORP seismic-reflection profiling of the Blue Ridge and Piedmont. *Geology*, 1979, 7, 563-567.
- Diment, W.H., O.H. Muller, and P.M. Lavin. Basement tectonics of New York and Pennsylvania as revealed by gravity and magnetic studies. Preprint of paper presented at the Caledonides in the U.S.A. Symposium, Sept. 6-9, Blacksburg, VA.

- Dorman, J., and M. Ewing. Numerical inversion of seismic surface wave dispersion data and crust-mantle structure in the New York - Pennsylvania area. *J. Geophys. Res.*, 1962, 67, 5277-5241.
- Drake, A.A. The Lynn Station - Paulins Kill Naube -- The frontal structure of the Musconetcong nappe system in eastern Pennsylvania and New Jersey. Prof. Paper 1023, U.S. Geological Survey, 1978.
- Fernandez, L.M., and J. Careaga. The thickness of the crust in central United States and La Paz, Bolivia, from the spectrum of longitudinal seismic waves. *Bull. Seis. Soc. Am.*, 1968, 58, 711-741.
- Fletcher, J.B., M.L. Sbar, and L.R. Sykes. Seismic trends and travel-time residuals in eastern North America and their tectonic implications. *Geol. Soc. Am. Bull.*, 1978, 89, 1656-1676.
- Frantti, G.E. Spectral energy density for quarry explosions. *Bull. Seis. Soc. Am.*, 1963, 53, 989-996.
- Garland, G.D. *Introduction to Geophysics (Mantle, Core and Crust)*. Philadelphia: W.B. Saunders Co. 1979.
- Gwinn, V.E. Thin-skinned tectonics in the Plateau and northwestern Valley and Ridge provinces of the central Appalachians. *Geol. Soc. Am. Bull.*, 1964, 75, 863-900.
- Gwinn, V.E. Kinematic patterns and estimates of lateral shortening, Valley and Ridge and Great Valley provinces, central Appalachians, south-central Pennsylvania. In Fisher, G.W., et al. (Ed.), *Studies in Appalachian Geology: Central and Southern*, New York: Interscience Publishers, 1970.
- Harris, L.D., and K.C. Bayer. Sequential development of the Appalachian orogen above a master decollement - A hypothesis. *Geology*, 1979, 7, 568-572.
- Harris, L.D., A.G. Harris, W. deWitt, Jr., and K.C. Bayer. Evaluation of southern eastern overthrust belt beneath Blue Ridge - Piedmont thrust. *Am. Assoc. Pet. Geol.*, 1981, 65, 2497-2505.
- James, D.E., T.J. Smith, and J.S. Steinhart. Crustal structure of the Middle Atlantic States. *J. Geophys. Res.*, 1968, 73, 1983-2007.

- Katz, S. Seismic study of crustal structure in Pennsylvania and New York. *Bull. Seis. Soc. Am.*, 1955, 45, 303-325.
- Kean, A.E., and L.T. Long. A seismic refraction line along the axis of the southern Piedmont and crustal thickness in the southeastern United States. *Bull. Seis. Soc. Am., Earthquake Notes*, 1980, 51, 3-15.
- Kennett, B.L.N. Slowness techniques in seismic interpretation. *J. Geophys. Res.*, 1981, 86, 11575-11584.
- King, E.R., and J. Zeitz. The New York - Alabama lineament: geophysical evidence for a major crustal break in the basement beneath the Appalachian basin. *Geology*, 1978, 6, 312-318.
- Kurita, T. Regional variations in the structure of the crust in the central United States from P-wave spectra. *Bull. Seis. Soc. Am.*, 1973, 63, 1663-1687.
- Landisman, M., S. Mueller, and B.J. Mitchell. Review of evidence for velocity inversions in the continental crust. In J.G. Heacock (Ed.), *The Structure and Physical Properties of the Earth's Crust*, : A.G.U. Geophys. Mon. 14, 1971.
- Langston, C.A., and C.M. Isaacs. A crustal thickness constraint for central Pennsylvania. *Bull. Seis. Soc. Am., Earthquake Notes*, 1981, 52, 13-22.
- McEvelly, T.V. Central United States crust-upper mantle structure from Love and Rayleigh wave phase velocity inversion. *Bull. Seis. Soc. Am.*, 1964, 54, 1997-2015.
- McMechan, G.A., and F. Ottolini. Direct observation of a p-t curve in a slant stacked wave field. *Bull. Seis. Soc. Am.*, 1980, 70, 775-789.
- McMechan, G.A., and R.A. Wiggins. Depth limits in body wave inversions. *Geophys. J. R. astr. Soc.*, 1972, 28, 459-473.
- Meissner, R. Exploring deep interfaces by seismic wide-angle measurements. *Geophys. Pros.*, 1967, 15, 598-617.
- Mitchell, B.J., and R.B. Herrmann. Shear velocity

- structure in the eastern United States from the inversion of surface-wave group and phase velocities. *Bull. Seis. Soc. Am.*, 1979, 69, 1133-1148.
- Mogi, K. Some discussion on aftershocks, foreshocks, and earthquake swarms: The fracture of a semi-infinite body caused by an inner stress origin and its relation to the earthquake phenomena, 3. *Bull. Earthquake Res. Inst. Tokyo Univ.*, 1963, 11, 615-658.
- Mueller, S. A new model of continental crust. In J.G. Heacock (Ed.), *The Earth's Crust: Its Nature and Physical Properties*, : A.G.U. Geophys. Mon. 20, 1977.
- Murrell, S.A.F. Rheology of the lithosphere - experimental indications. *Tectonophysics*, 1976, 36, 5-24.
- O'Brien, P.N. A discussion on the nature and magnitude of elastic absorption in seismic prospecting. *Geophys. Eras.*, 1961, 9, 261-275.
- Oliver, J., R. Kovach, and J. Dorman. Crustal structure of the New York - Pennsylvania area. *J. Geophys. Res.*, 1961, 66, 215-225.
- Phinney, R.A., K.R. Chowdhury, and L.N. Frazer. Transformation and analysis of record sections. *J. Geophys. Res.*, 1981, 86, 359-377.
- Pollack, H.N. Effect of delay time and number of delays on the spectra of ripple-fired shots. *Bull. Seis. Soc. Am., Earthquake Notes*, 1963, 34, 1-12.
- Prodehl, C. The structure of the crust-mantle boundary beneath North America and Europe as derived from explosion seismology. In J.G. Heacock (Ed.), *The Earth's Crust: Its Nature and Physical Properties*, : A.G.U. Geophys. Mon. 20, 1977.
- Rankin, D.W. Appalachian salients and recesses: Late Precambrian continental breakup and the opening of the Iapetus Ocean. *J. Geophys. Res.*, 1976, 81, 5605-5619.
- Root, S.I., and D.M. Hoskins. Lat 40° N fault zone, Pennsylvania: A new interpretation. *Geology*, 1977,

5, 719-723.

- Sbar, M.L., and L.R. Sykes. Contemporary compressive stress and seismicity in eastern North America: An example of intraplate tectonics. *Geol. Soc. Am. Bull.*, 1973, 84, 1861-1882.
- Sbar, M.L., and L.R. Sykes. Seismicity and lithospheric stress in New York and adjacent areas. *J. Geophys. Res.*, 1977, 82, 5771-5786.
- Sbar, M.L., J.M.W. Rynn, F.J. Gumper, and J.C. Lahr. An earthquake sequence and focal mechanism solution, Lake Hopatcong, northern New Jersey. *Bull. Seis. Soc. Am.*, 1970, 60, 1231-1243.
- Sbar, M.L., R.R. Jordan, C.D. Stephens, T.E. Pickett, K.D. Woodruff, and C.G. Sammis. The Delaware - New Jersey earthquake of February 28, 1973. *Bull. Seis. Soc. Am.*, 1975, 65, 85-92.
- Seeber, L. and J.G. Armbruster. The 1886 Charleston, South Carolina earthquake and the Appalachian detachment. *J. Geophys. Res.*, 1981, 86, 7874-7894.
- Sienko, D.A. Crustal structure of south-central Pennsylvania determined from wide-angle reflections and refractions. Master's thesis, Penn State University, 1982.
- Smithson, S.B., and S.K. Brown. A model for lower continental crust. *E. Pl. Sci. Let.*, 1977, 35, 134-144.
- Smithson, S.B., and P.N. Shive. Seismic velocity, reflections, and structure of the crystalline crust. In J.G. Heacock (Ed.), *The Earth's Crust: Its Nature and Physical Properties*, : A.G.U. Geophys. Mon. 20, 1977.
- Stewart, S.W. Crustal structure in Missouri by seismic refraction methods. *Bull. Seis. Soc. Am.*, 1968, 58, 291-323.
- Stoffa, P.L., P. Buhl, J.B. Diebold, and F. Wenzel. Direct mapping of seismic data to the domain of intercept time and ray parameter - A plane-wave decomposition. *Geophysics*, 1981, 46, 255-267.
- Taylor, S.R., and M.N. Toksoz. Three-dimensional crust

and upper-mantle structure of the northeastern United States. *J. Geophys. Res.*, 1979, 84, 7627-7644.

White, J.E. *Seismic Waves; Radiation, Transmission, and Attenuation*. New York: McGraw-Hill, Inc. 1965.

Willis, D.E. A note on the effect of ripple-firing on the spectra of quarry shots. *Bull. Seis. Soc. Am.*, 1963, 53, 79-85.

Yang, J., and Y.P. Aggarwal. Seismotectonics of the northeastern United States and adjacent Canada. *J. Geophys. Res.*, 1981, 86, 4981-4998.

Zoback, M.D., and M.L. Zoback. State of stress and intraplate earthquakes in the United States. *Science*, 1981, 213, 96-104.

I. Appendix 1: Final Processed Data

The figures are the reconstructed field records into lengths of 2048 words (11.7965 seconds). The beginning of the record represents the breakpulse of the blast. Time increases down and to the right.

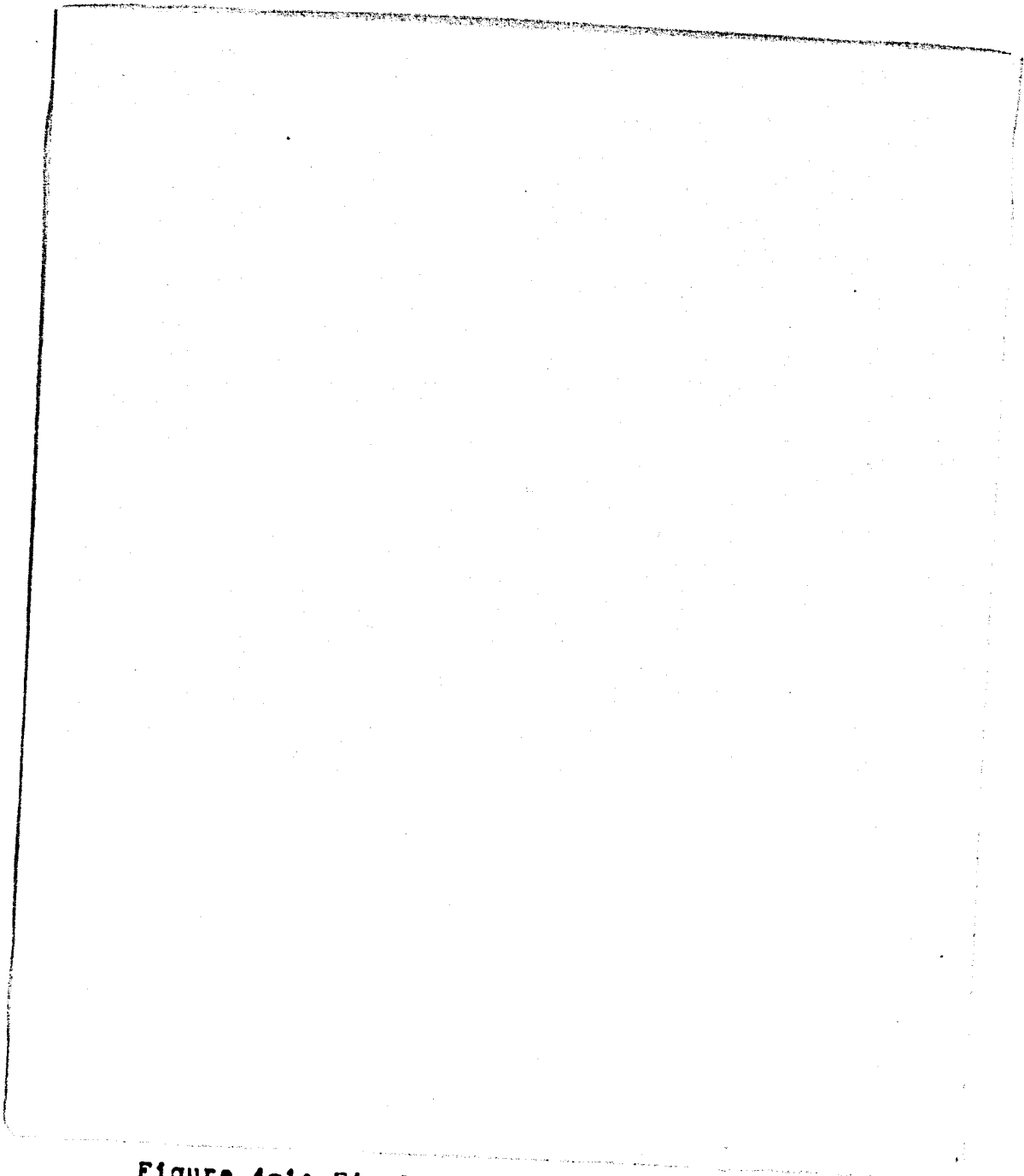
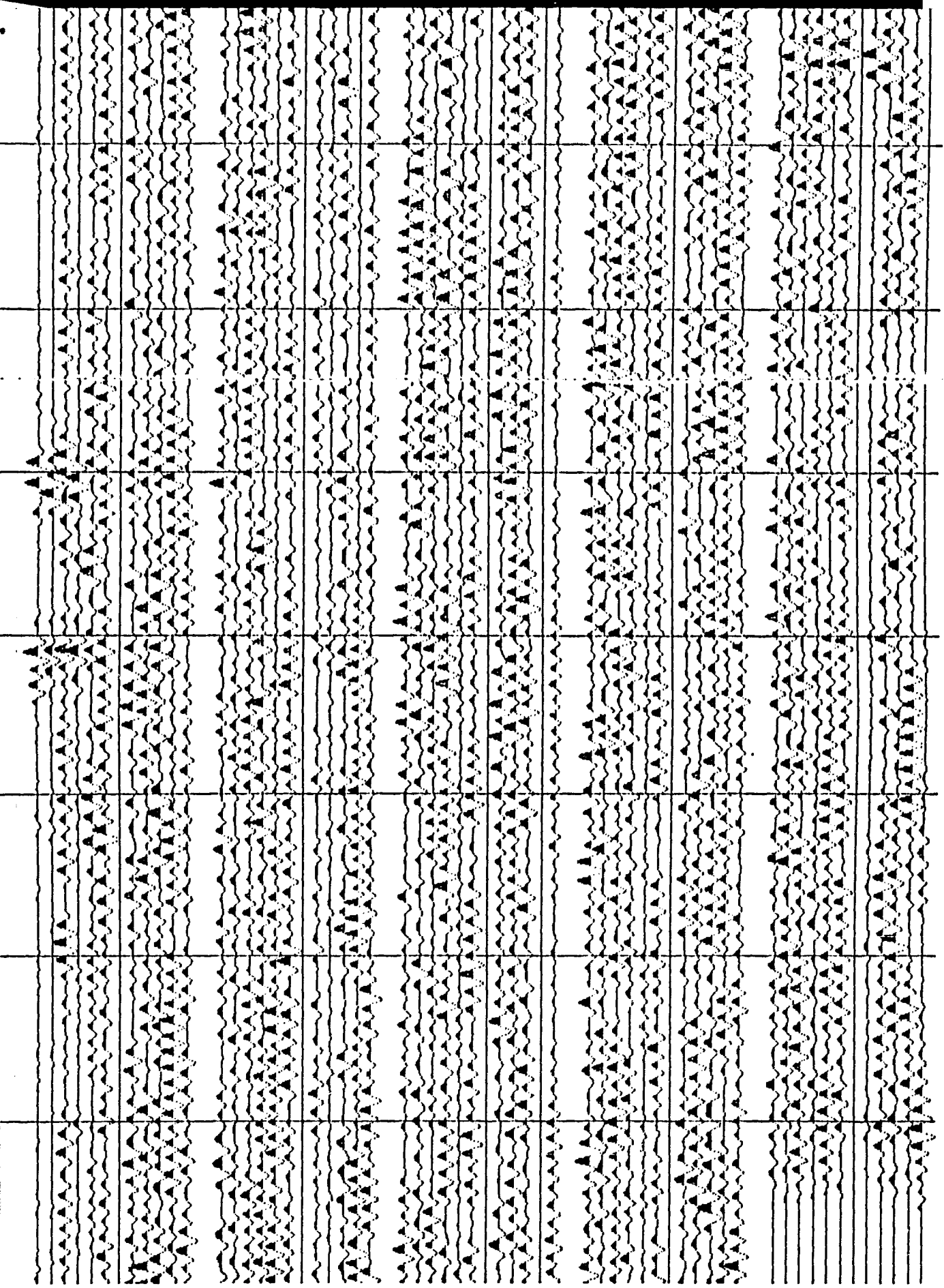
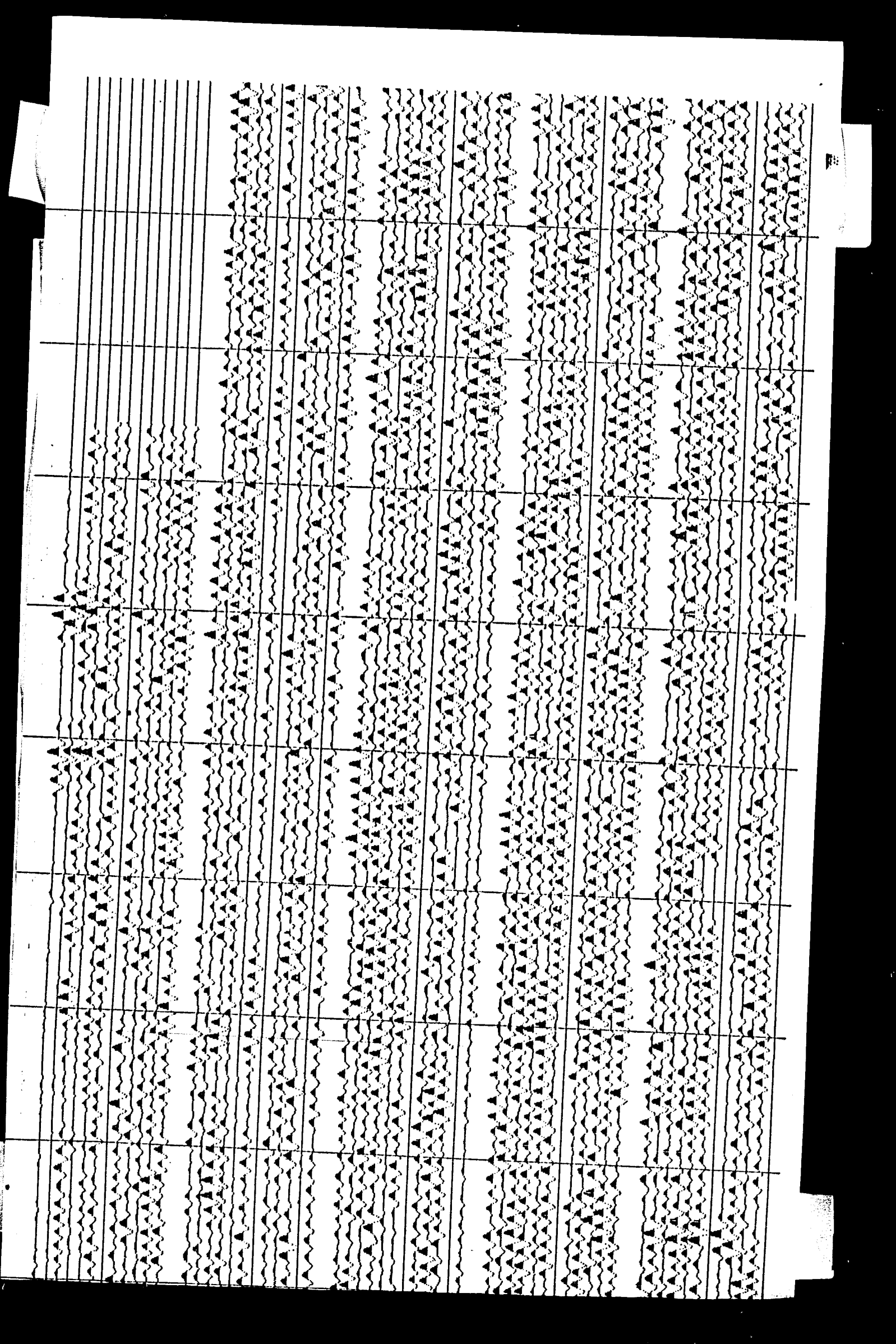


Figure 4-1: Final processed data of MLBR 1, 11/13/81. The records have been shifted forward 0.3168 seconds to breakpulse. The expected P-arrivals occur between 24.4566 to 30.3874 seconds.

MLBB, 11/13/81; F.R. 2-41, 1ST BLAST; RECPILT 6, 8, 14, 16; SHIFTED 55

F





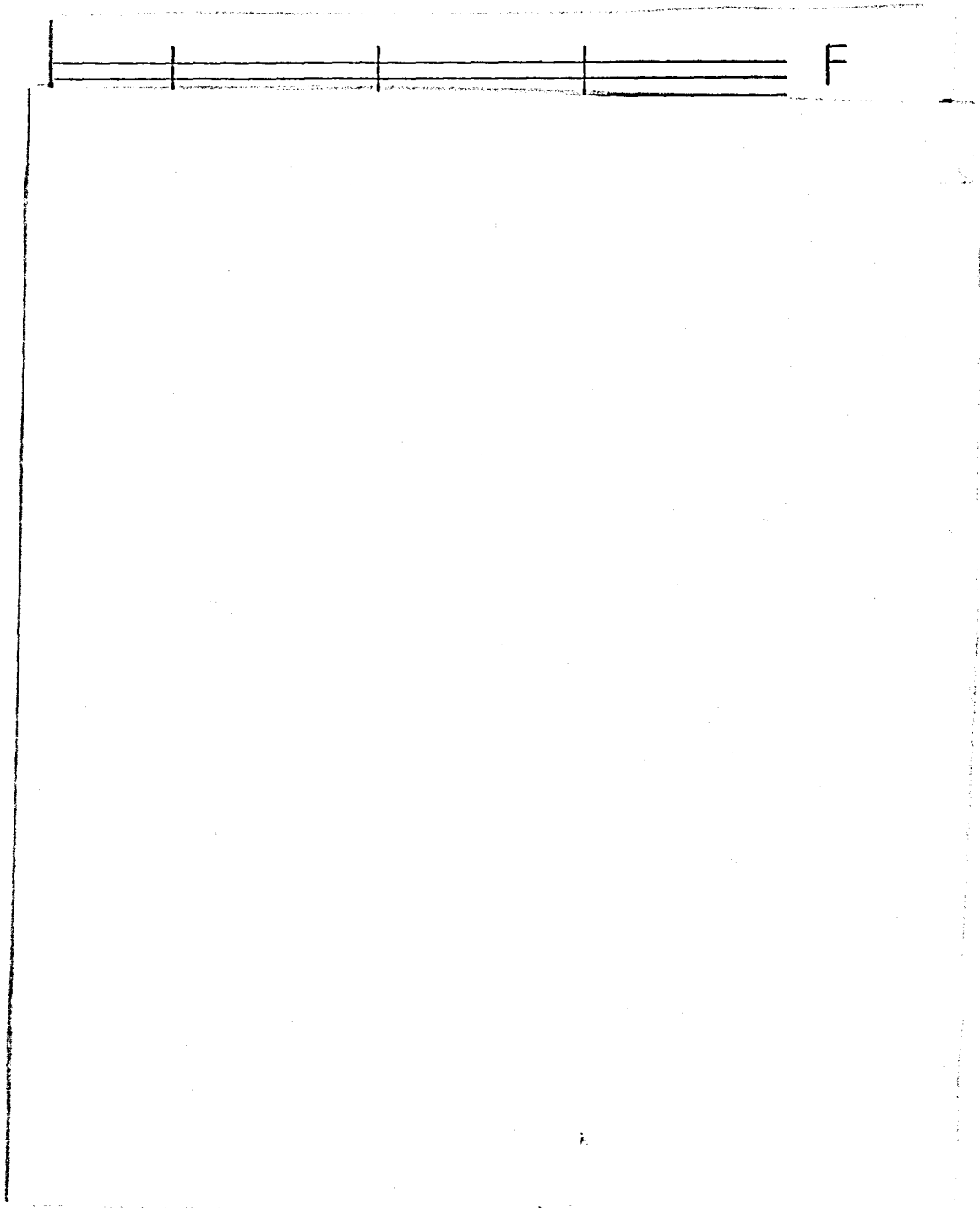
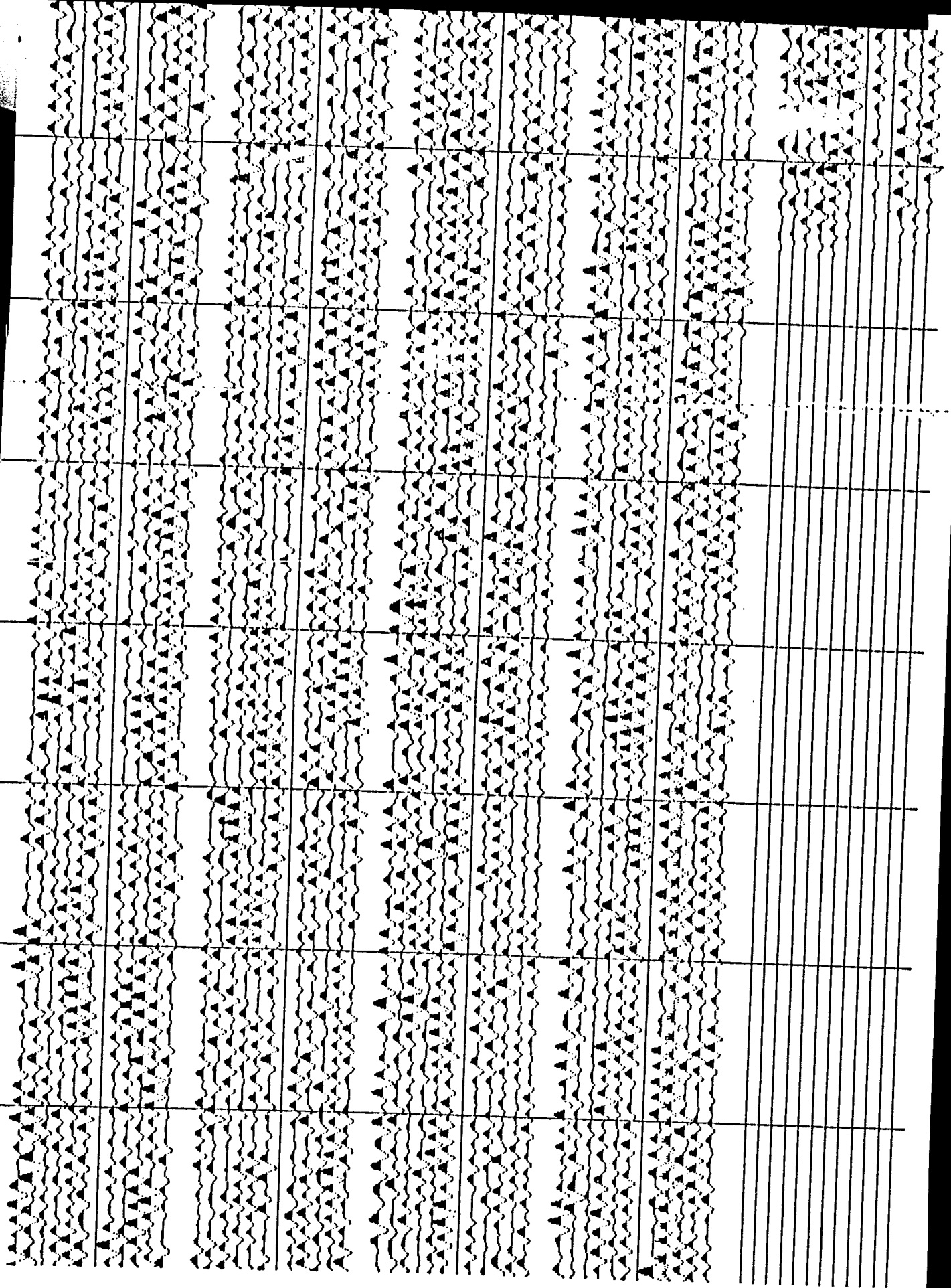
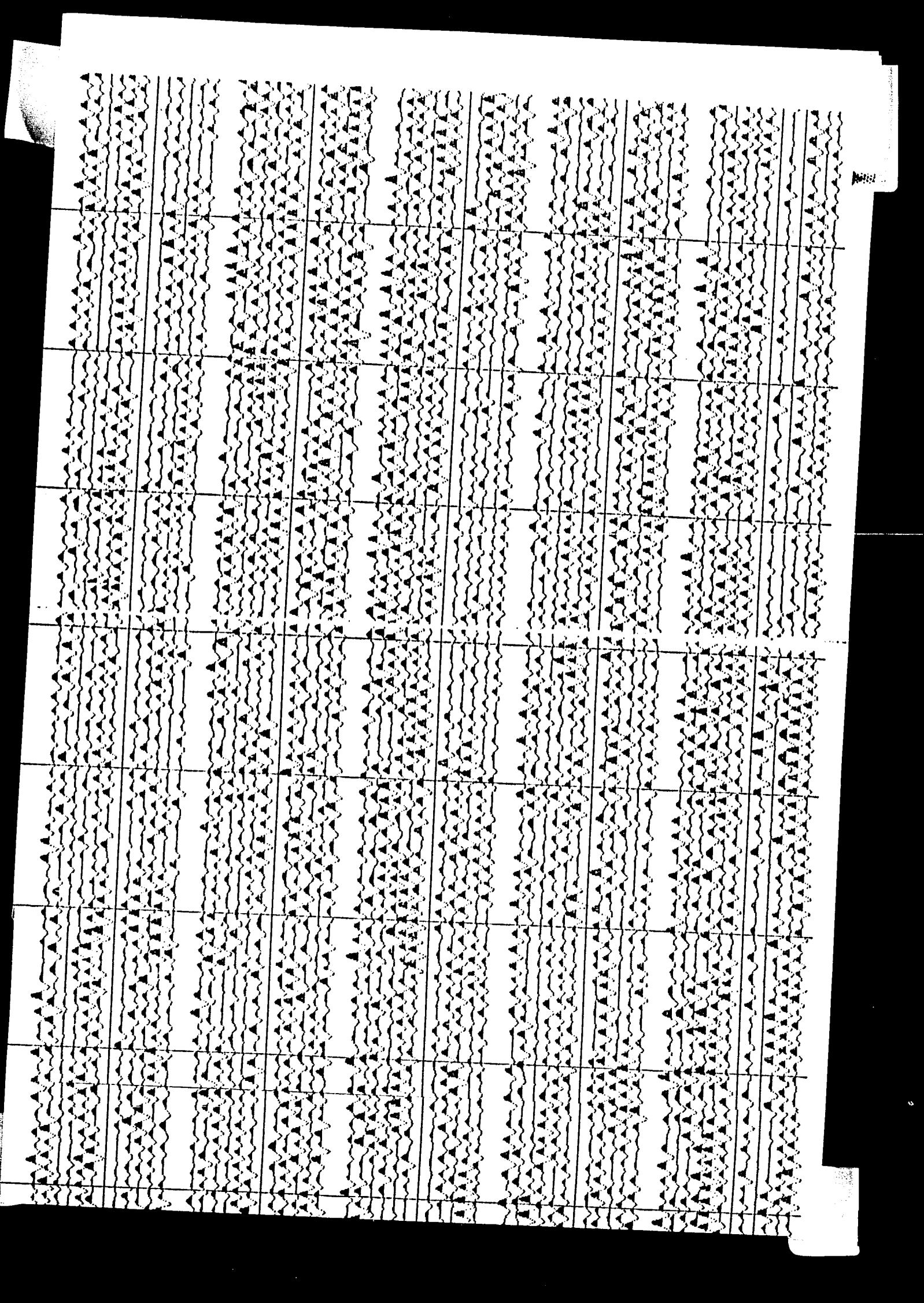


Figure 4-2: Final processed data of MLBB 2, 11/13/81. The records have been shifted forward 4.6656 seconds to breakpulse. The expected P-arrivals occur between 24.4566 to 30.3874 seconds.

L

MLBB, F.R. 45-100; 11/13/81; SECOND BLAST; RECFL176.8,14,16; SHIFTED





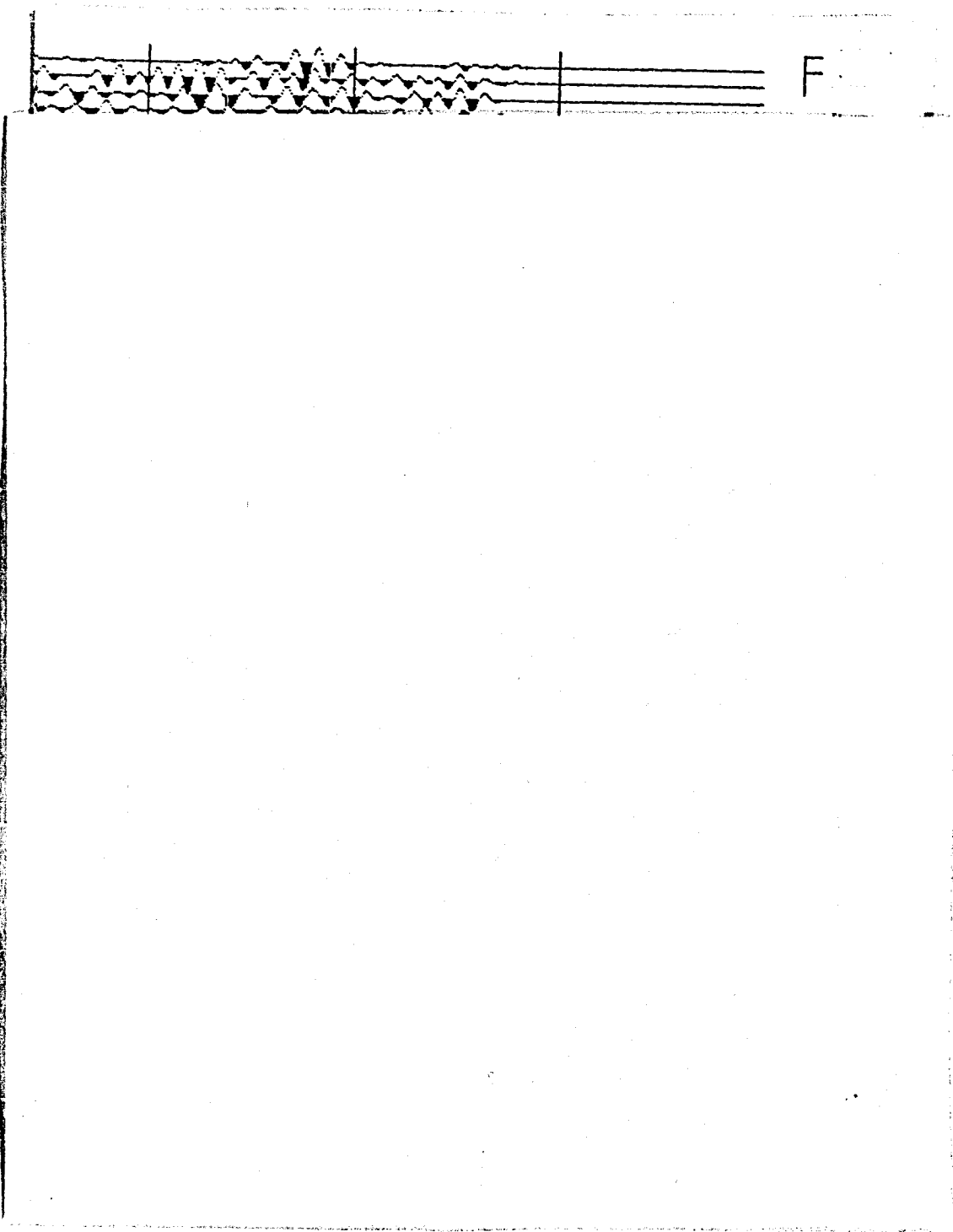
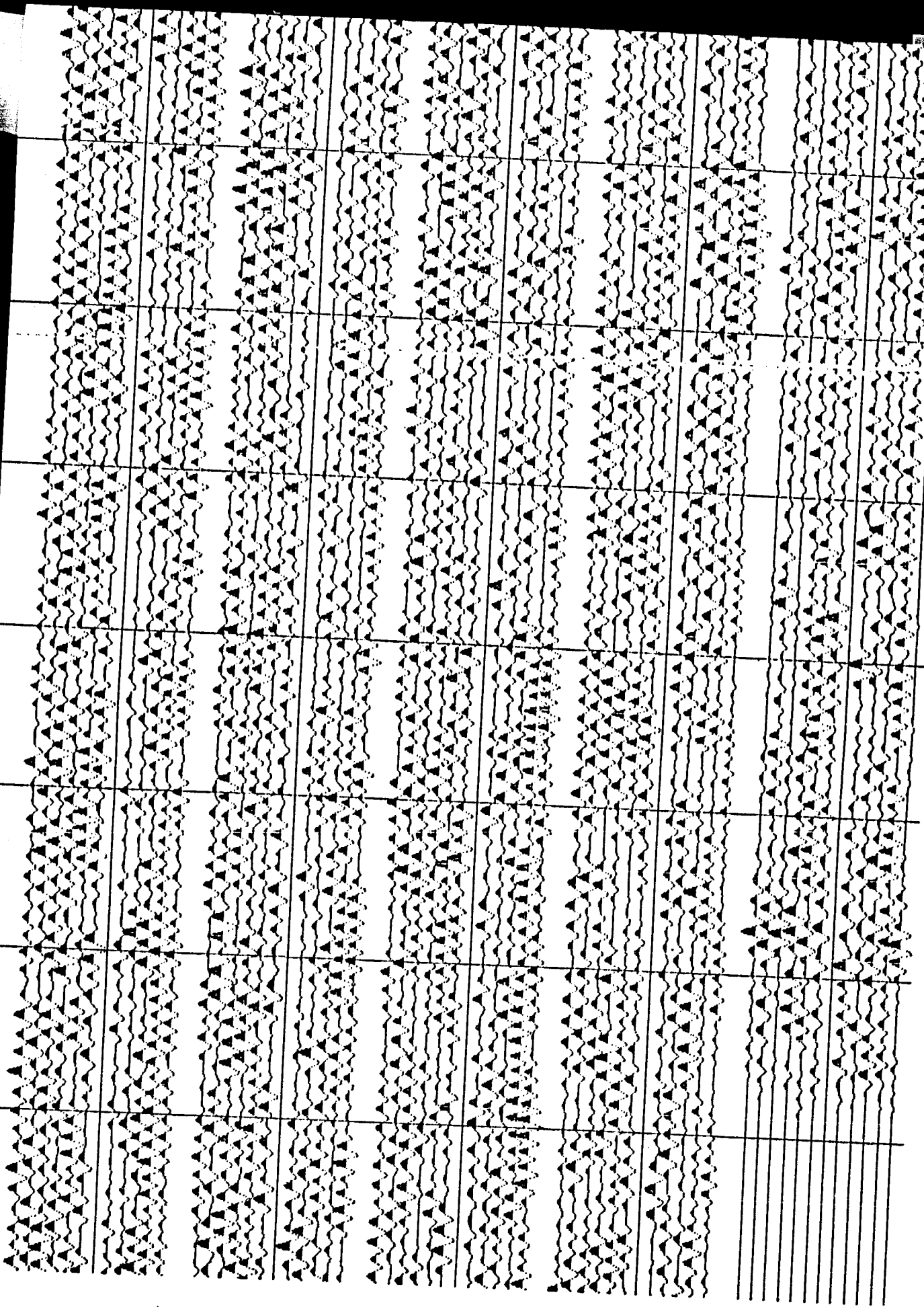
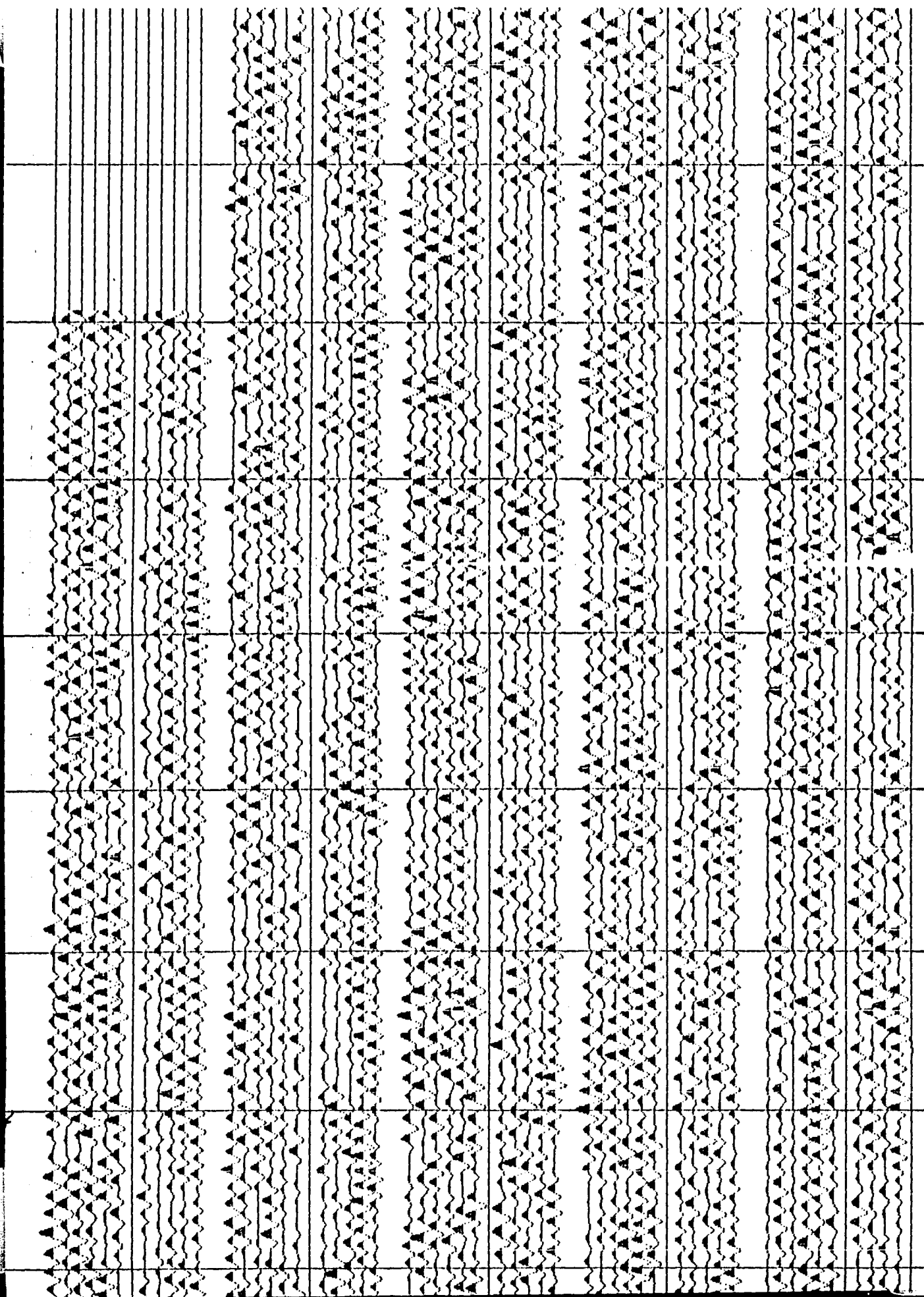


Figure 4-3: Final processed data of EIW, 11/19/81. The records have been shifted forward 0.7949 seconds to breakpulse. The expected P-arrivals occur between 12.2933 to 19.7844 seconds.

EIM 11/19/81, F.R. 2-41, SHIFTED +138 POINTS TO BREAKPULSE

L





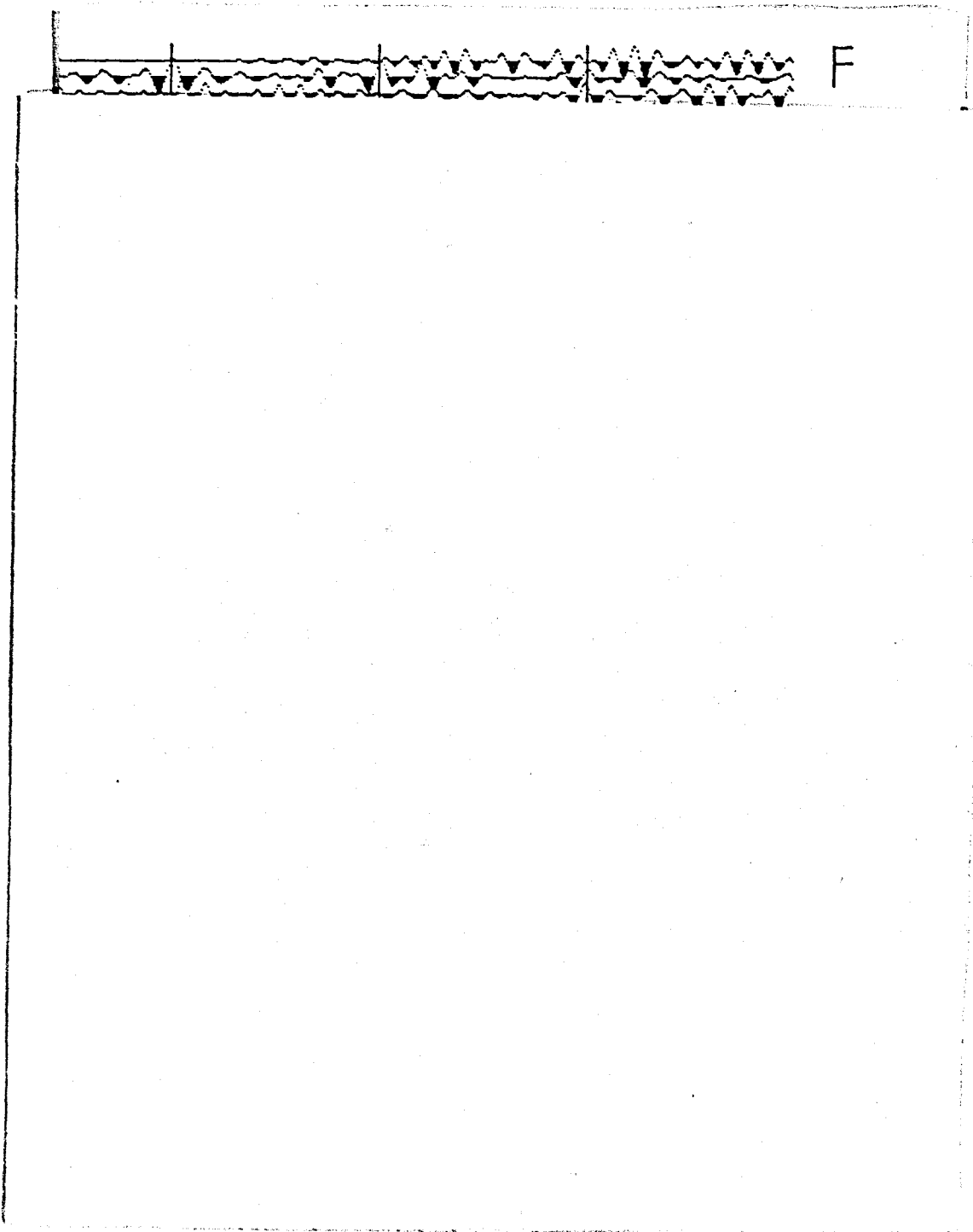
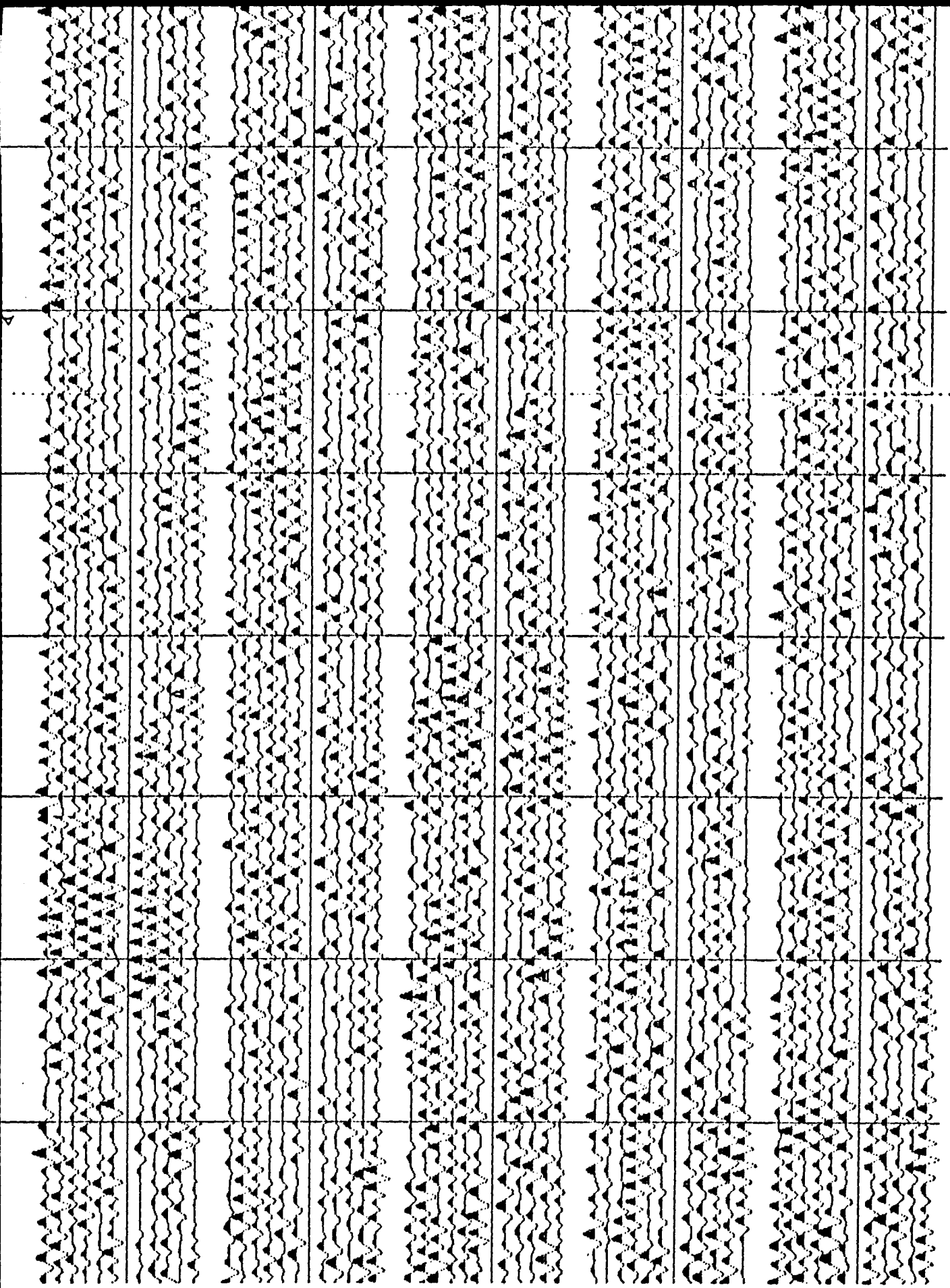
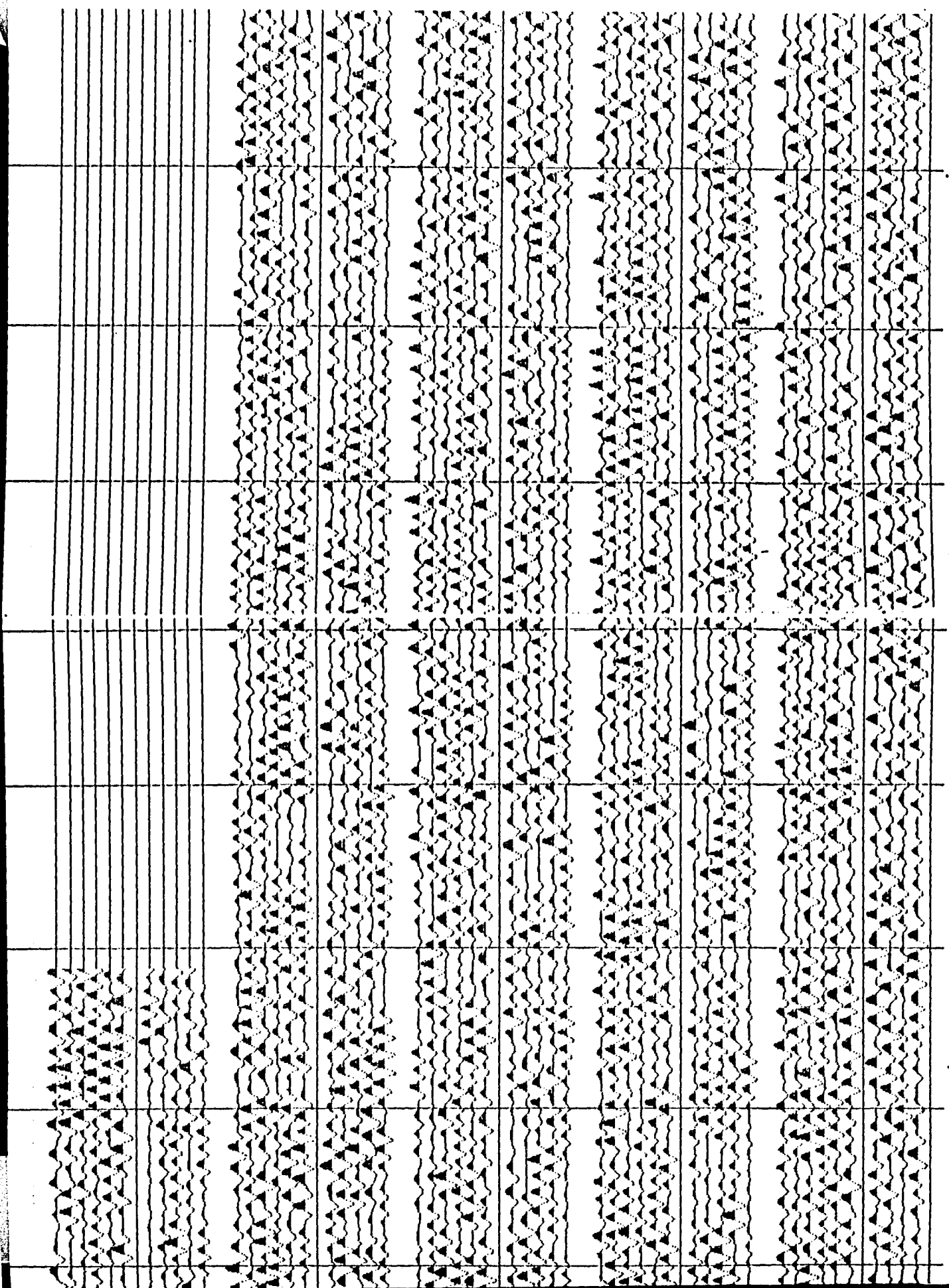


Figure 4-4: Final processed data of BPST, 12/9/81. The records have been shifted backward 2.2982 seconds to breakpulse. The expected P-arrivals occur between 19.7150 to 25.9641 seconds.



BPST 12/9/81, F.R. 182-221, SHIFTED -399 TO BREAKPULSE

L



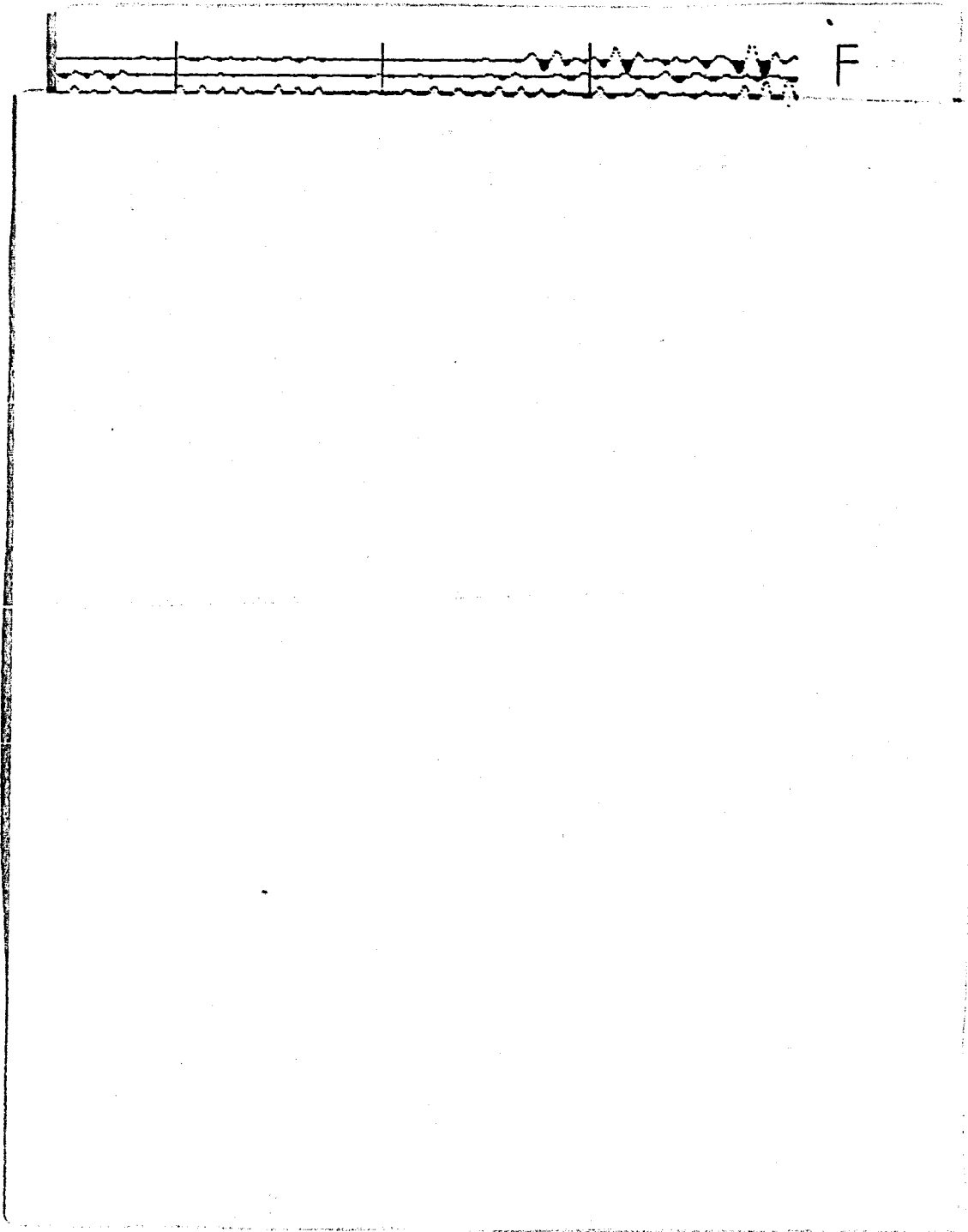


**Figure 4-5: Final processed data of MLBB 1,
12/11/81. The records have been shifted
backward 0.5472 seconds to breakpulse.
The expected P-arrivals occur between
24.4566 to 30.3874 seconds.**

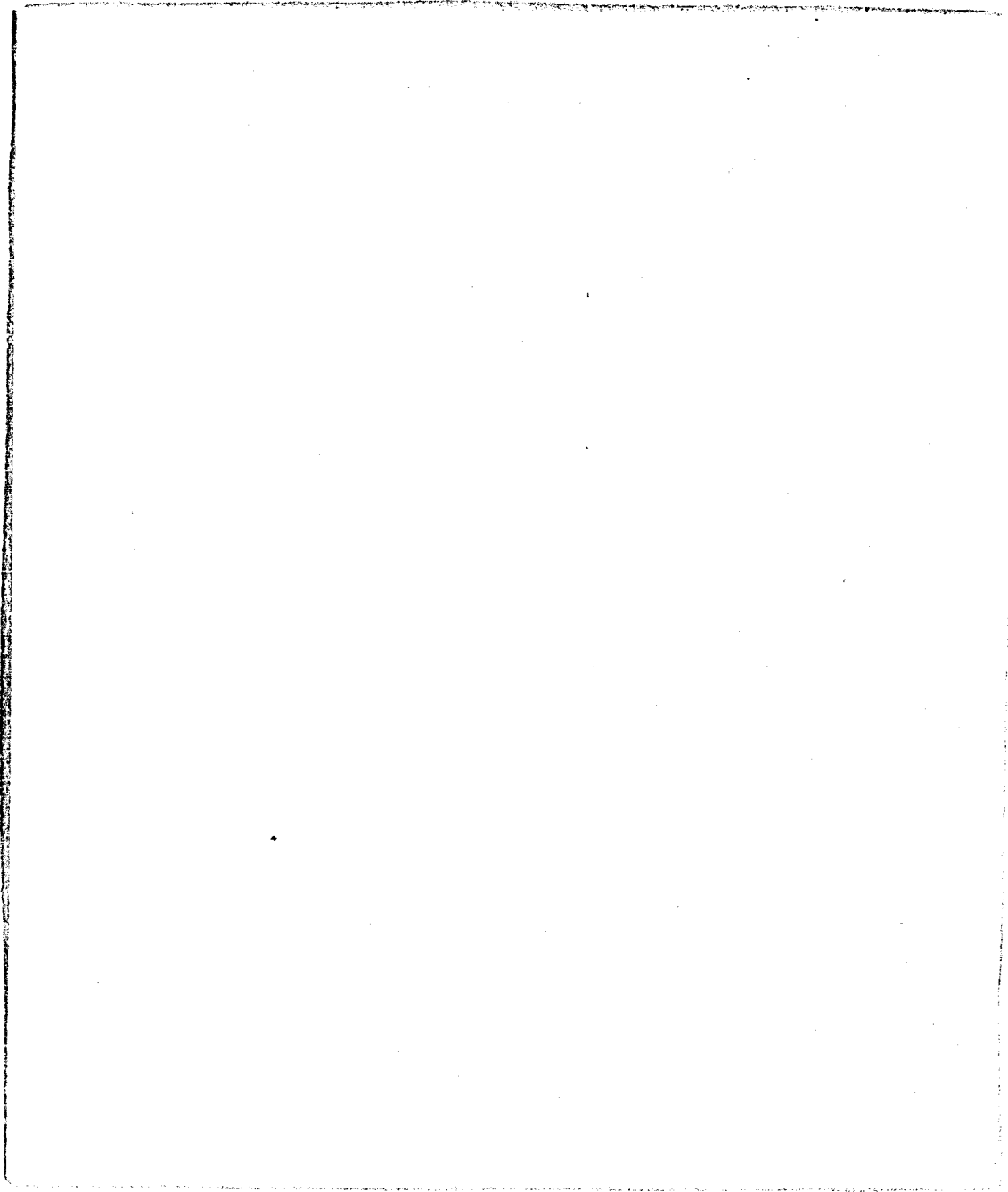
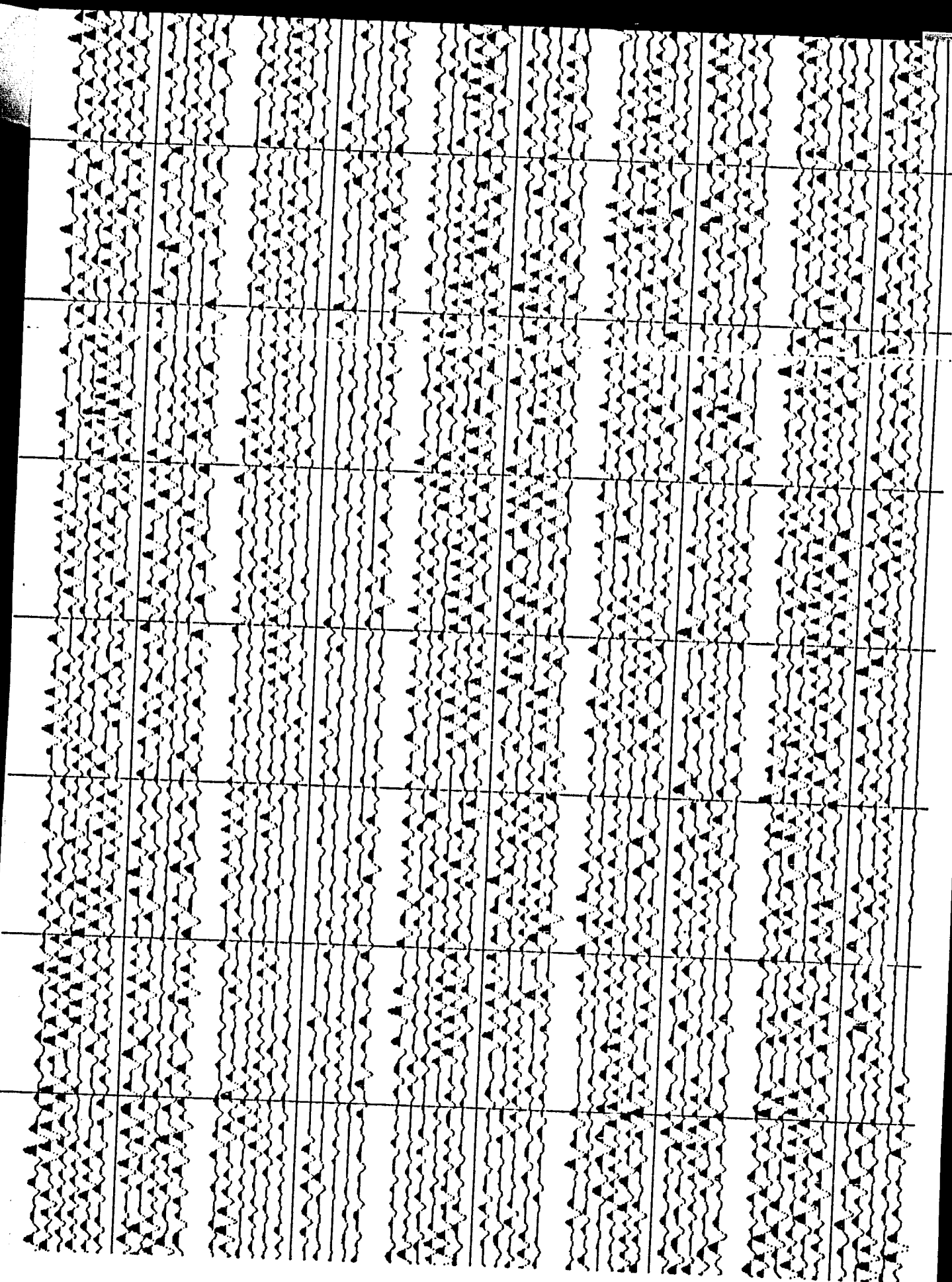
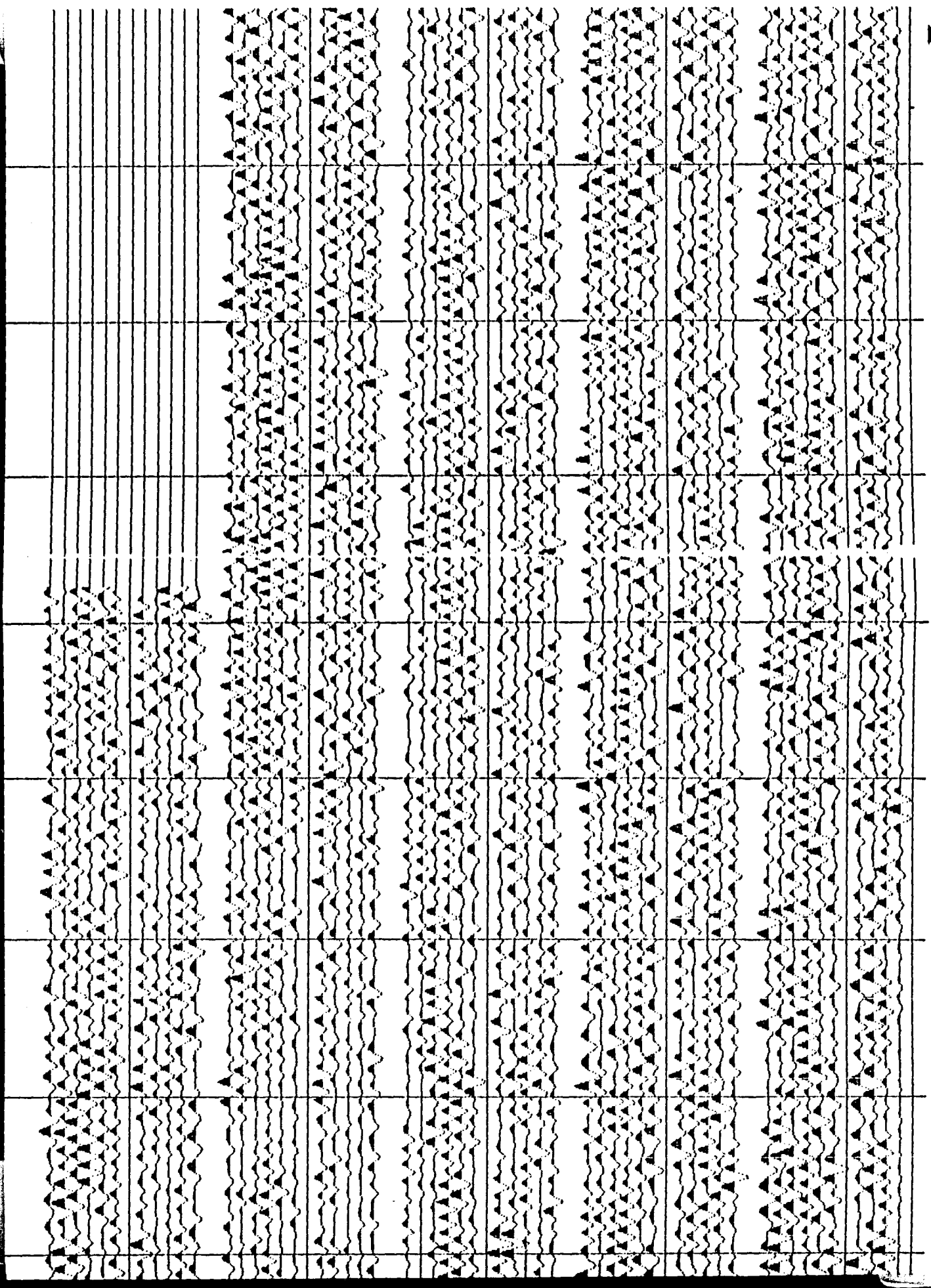


**Figure 4-5: Final processed data of MLRB 1,
12/11/81. The records have been shifted
backward 0.5472 seconds to breakpulse.
The expected P-arrivals occur between
24.4566 to 30.3874 seconds.**



MLBB 12/11/81, F.R. 178-212, SHIFTED -95 PTS TO BREAKPULSE

11



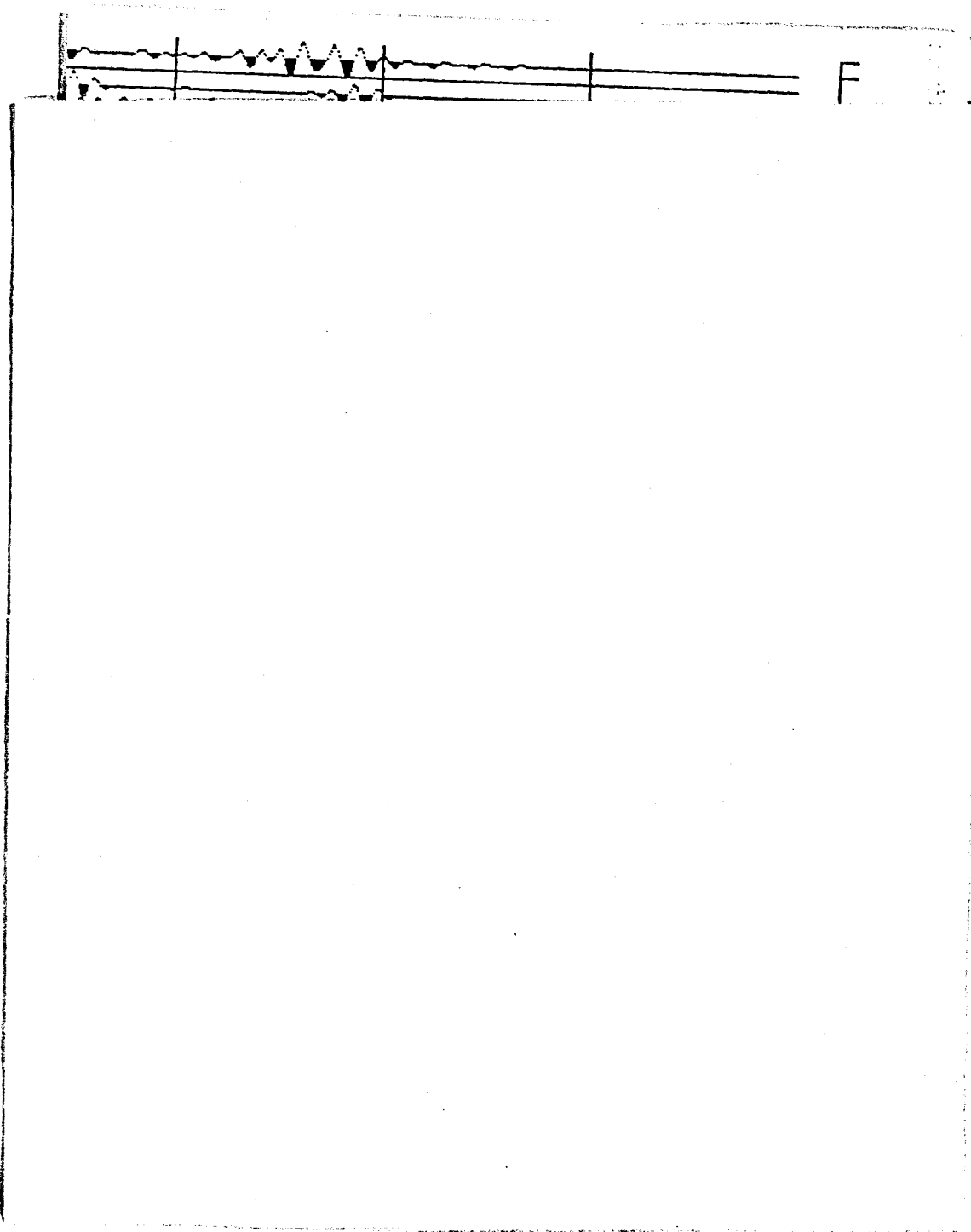
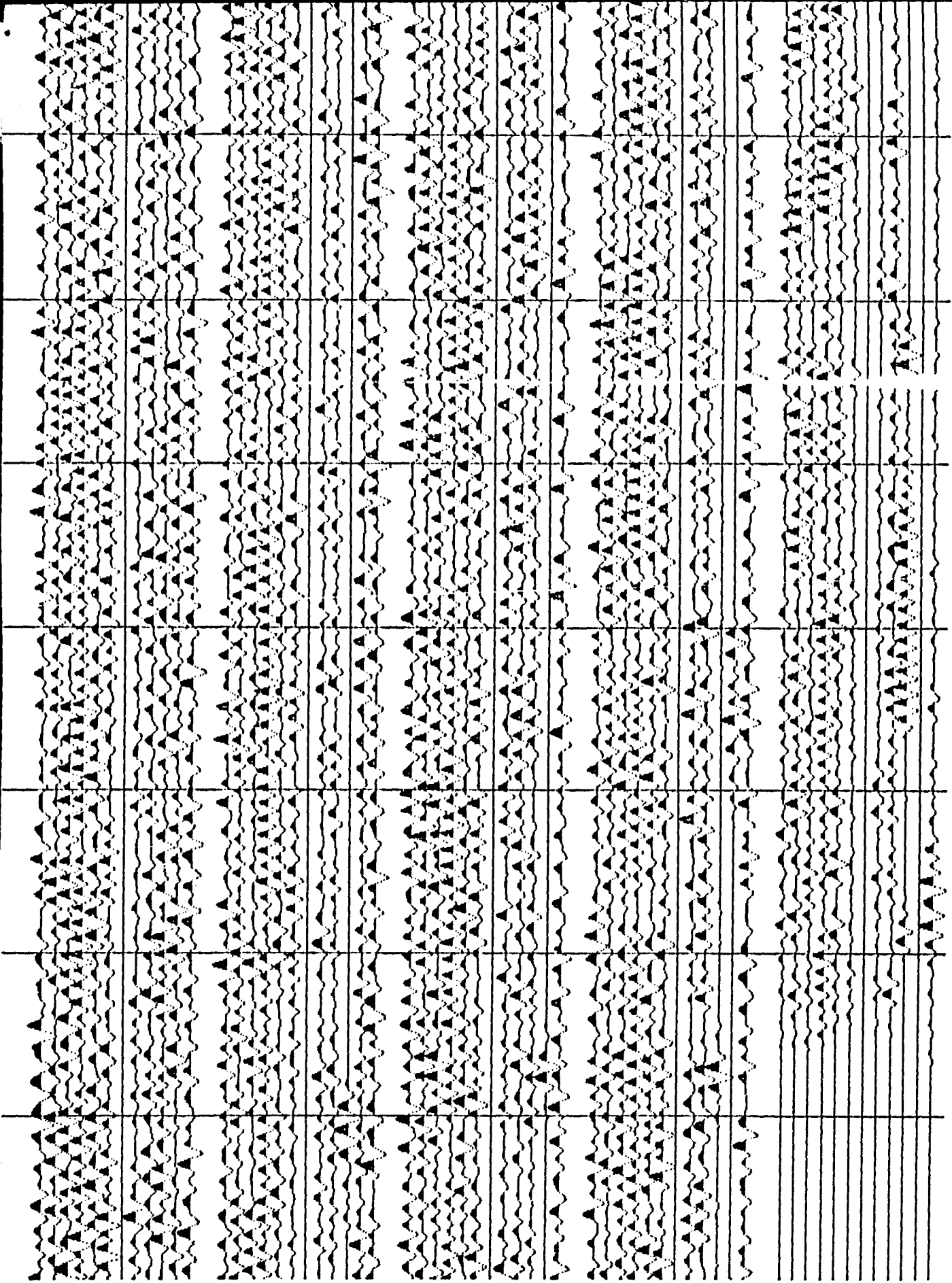
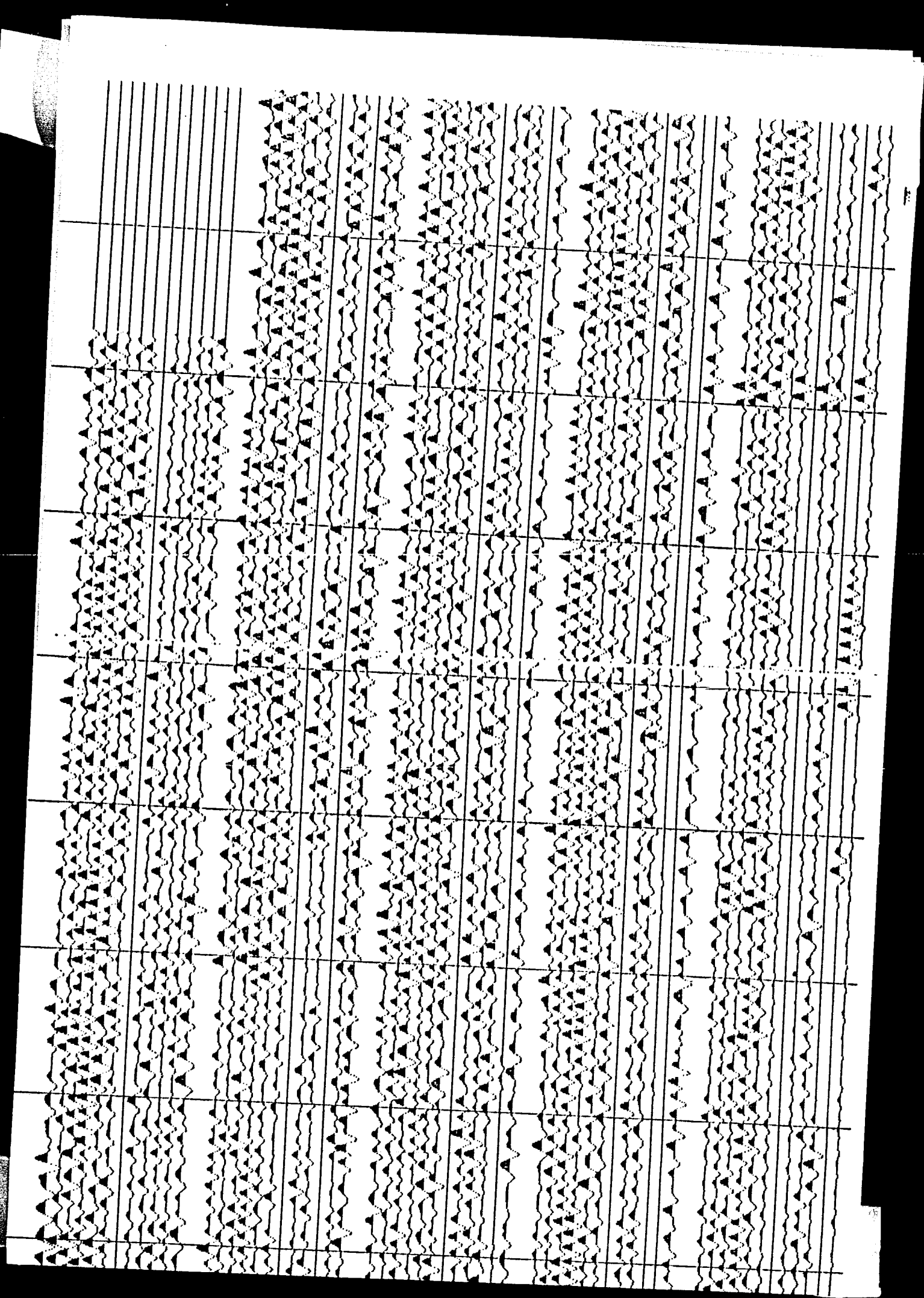


**Figure 4-6: Final processed data of MLRR 2,
12/11/81. The records have been shifted
forward 0.9389 seconds to breakpulse.
The expected P-arrivals occur between
24.4566 to 30.3874 seconds.**

MLBB 12/11/81, F.R. 222-261, SHIFTED 163 POINTS FORWARD TO BREAKPU



11



II. Appendix 2: Theoretical Models

These theoretical models in T(X) and t(p) sections represent possible crustal models and illustrate the difference between synthetic, ideal data and field record data.

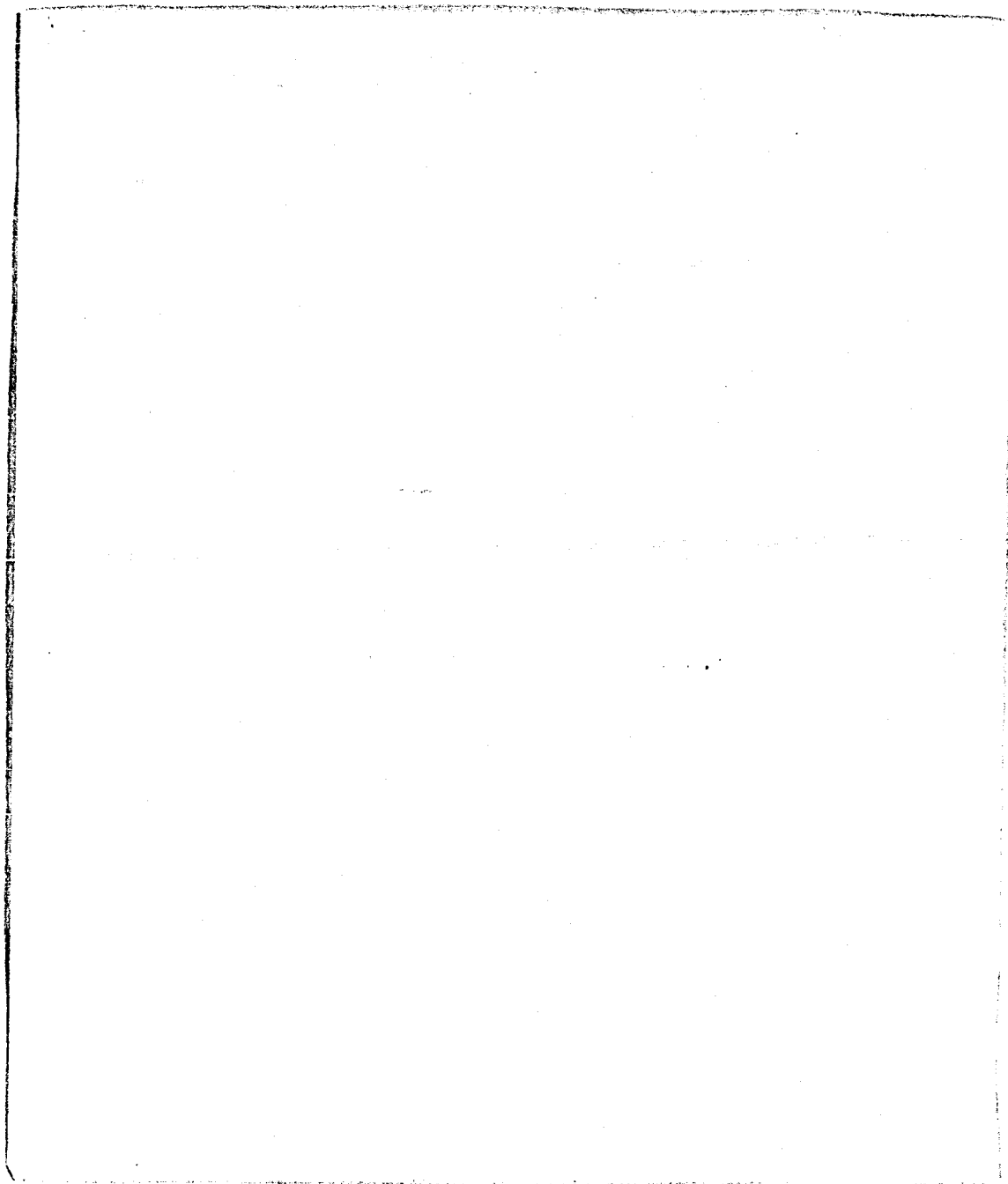
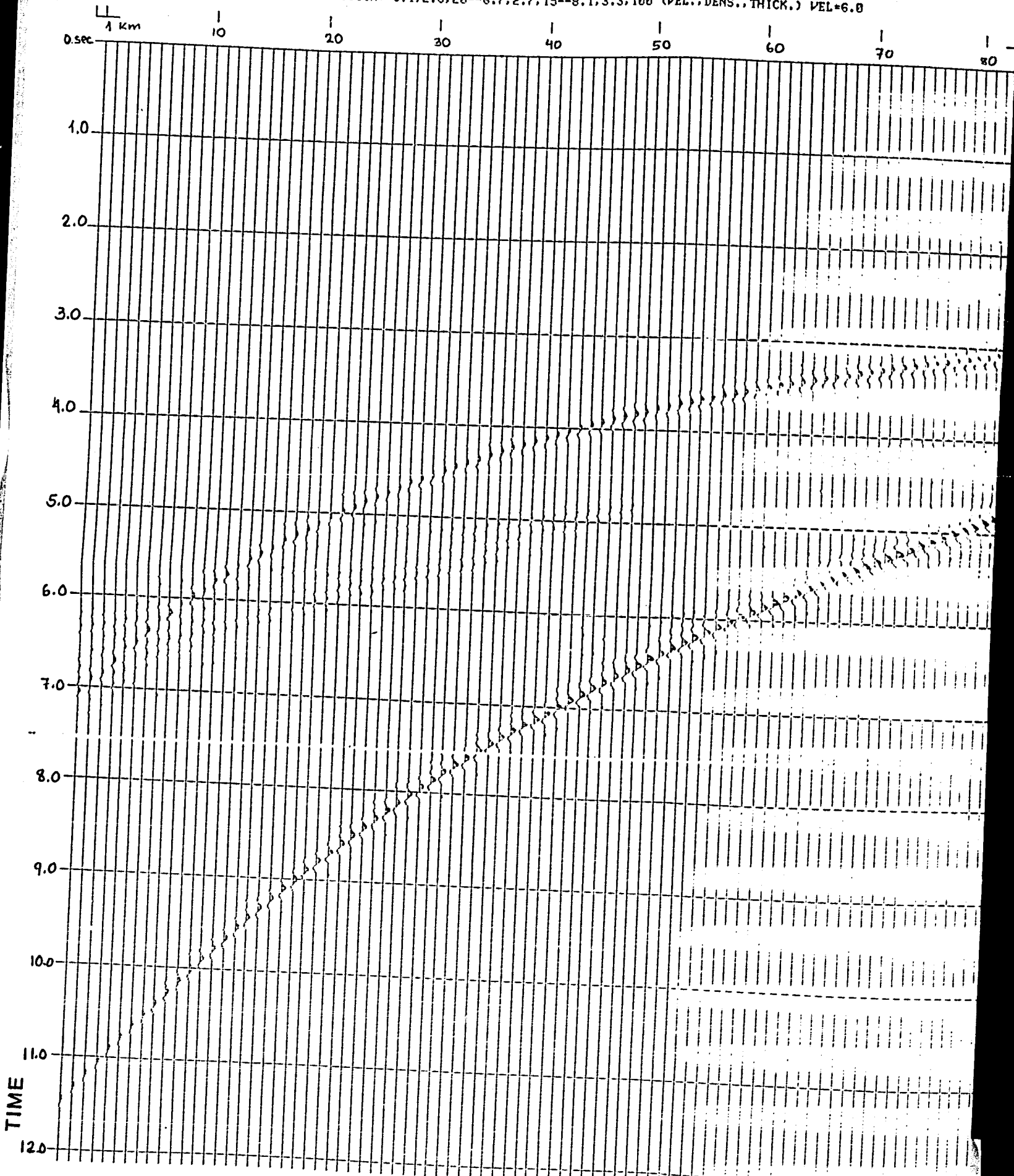


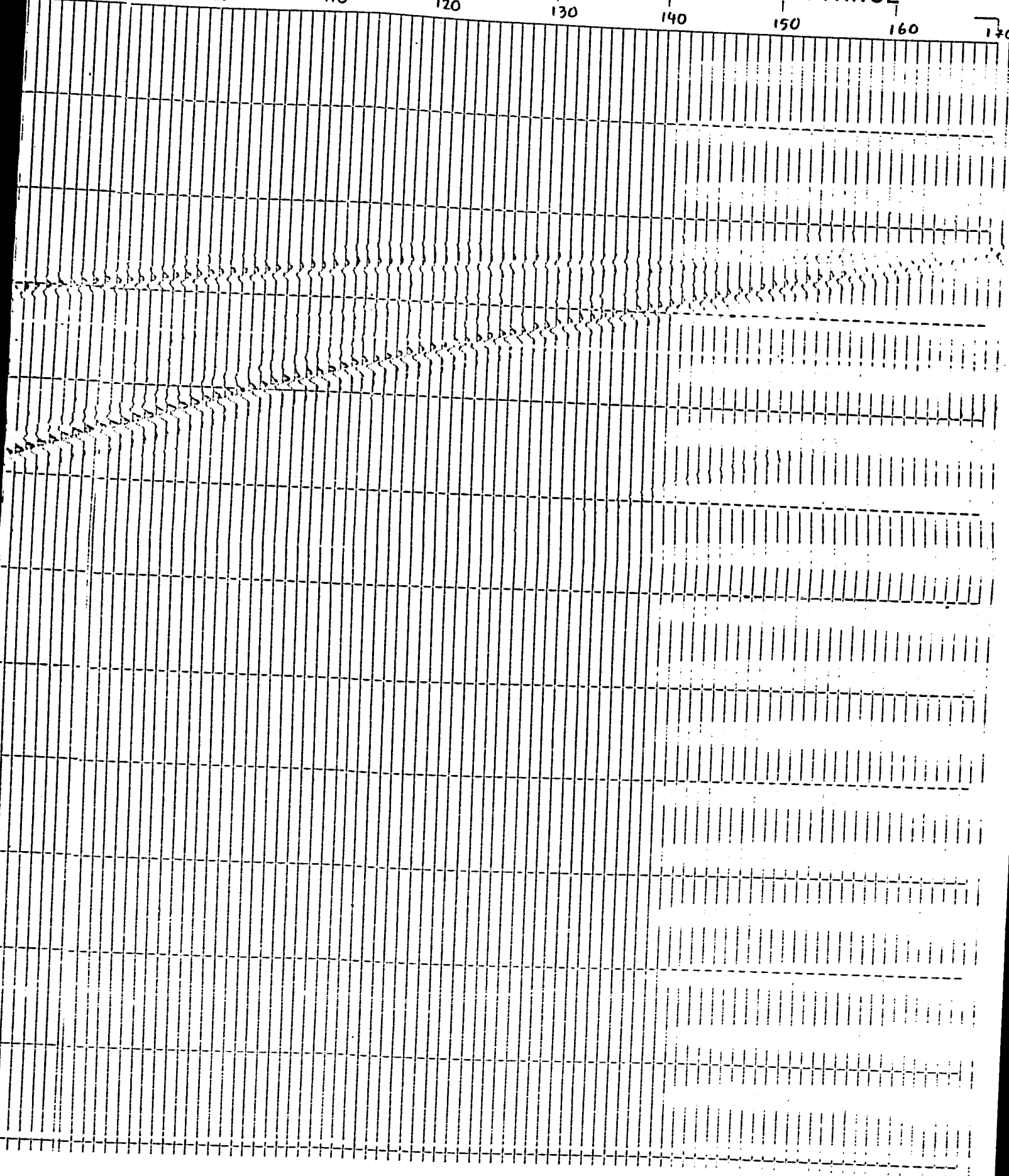
Figure 4-7: Model 1: T(X) section of two horizontal layers in a 35 km thick crust.

MODEL # 1: X-T SECTION: 6.1.2.6.20--6.7.2.7.15--8.1.3.3.100 (VEL., DENS., THICK.) VEL=6.0



90 100 110 120 130 140 150 160 170 km

DISTANCE



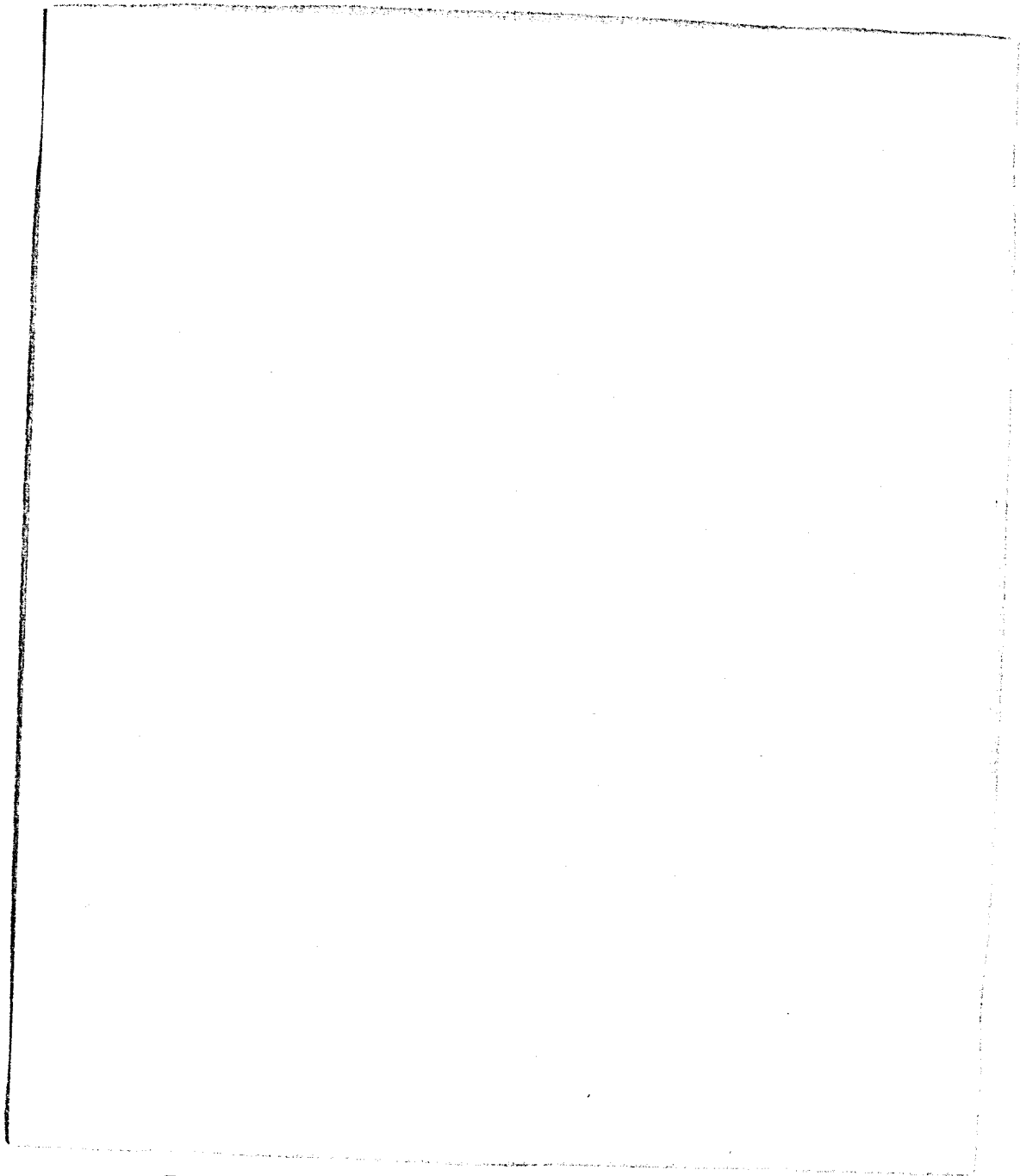
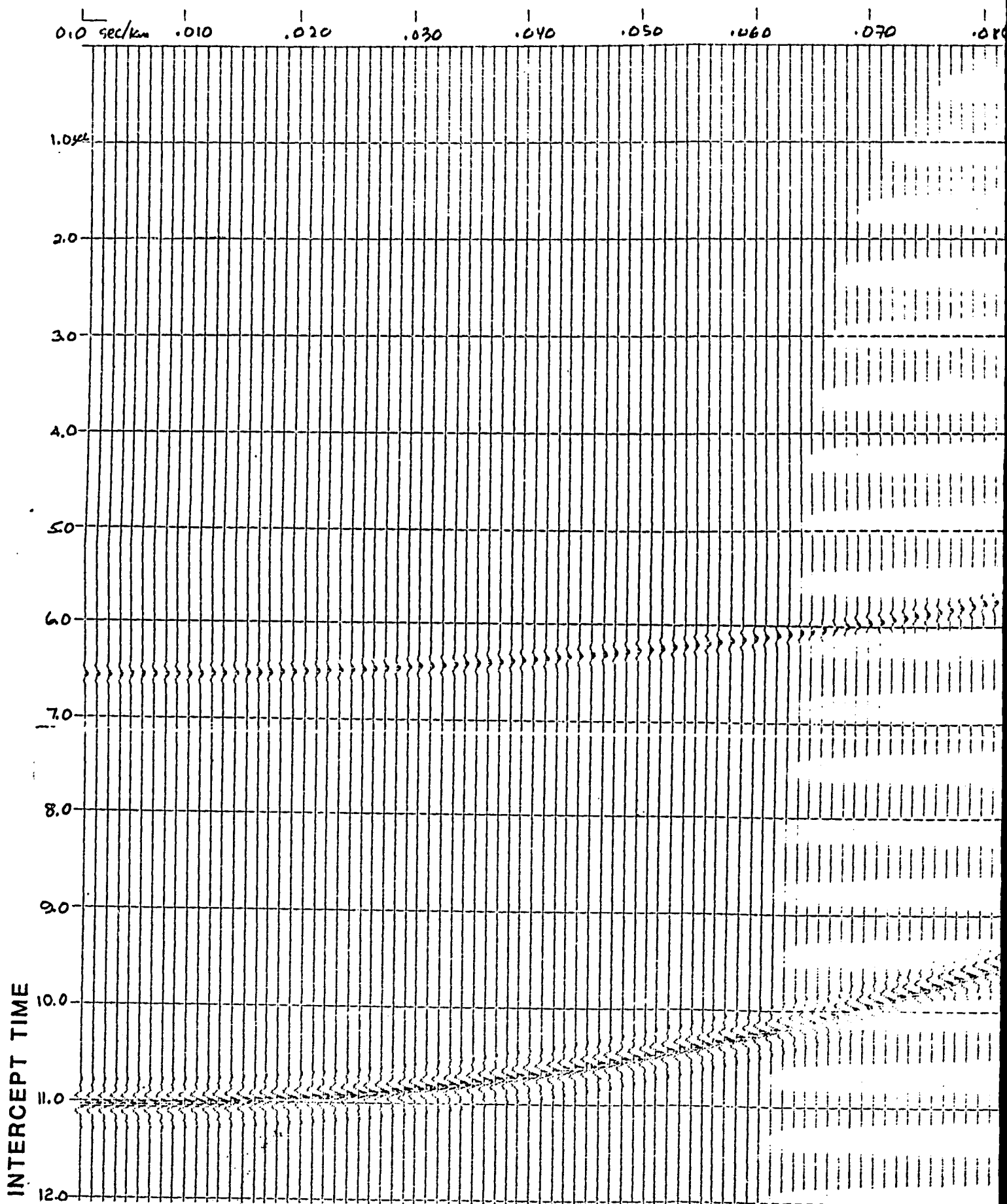
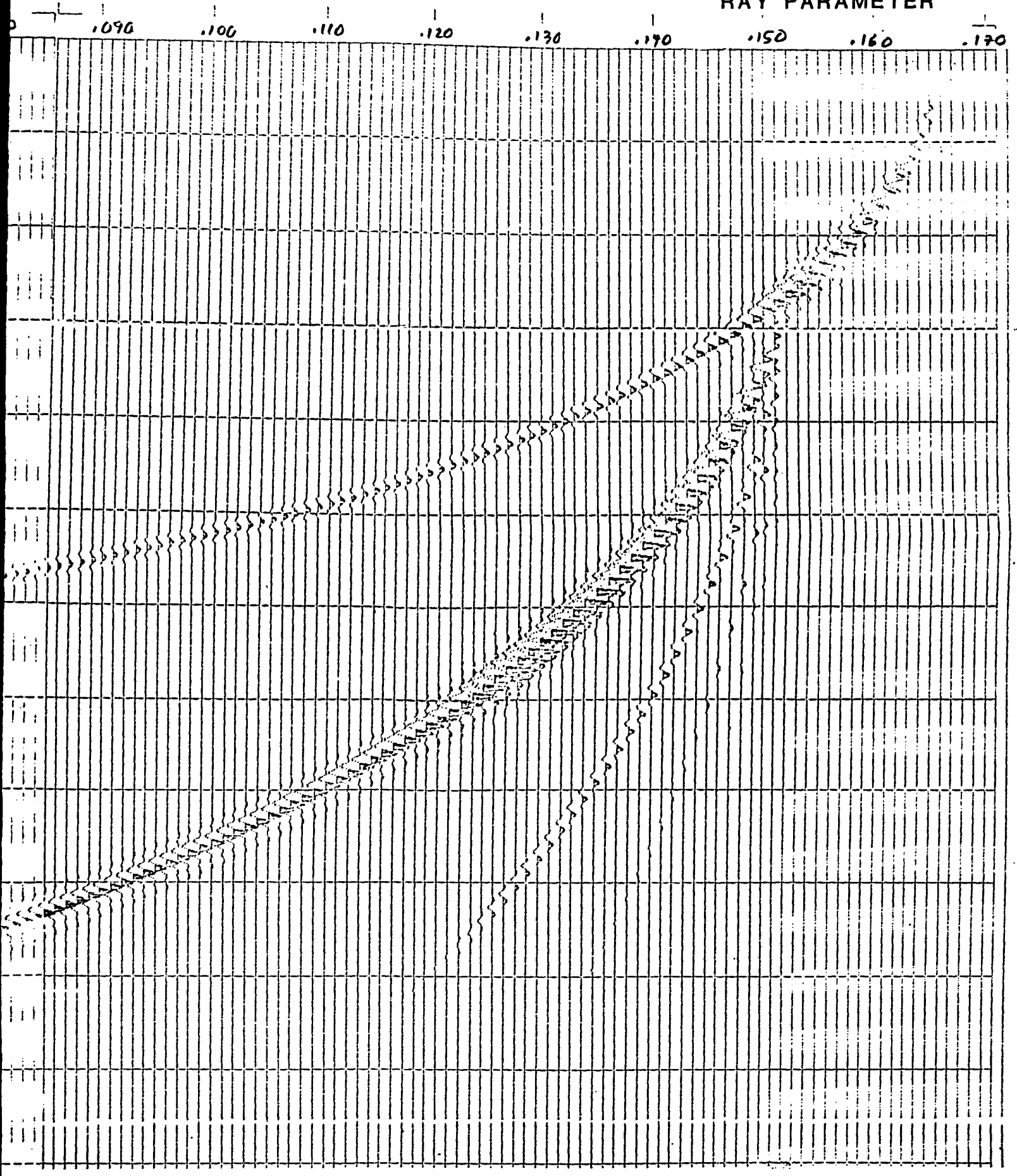


Figure 4-8: Model 1: $t(p)$ section of two horizontal layers in a 35 km thick crust.

MODEL = 1: PTAU SECTION: 6.1.2.6.28--6.7.2.7.15--8.1.3.3.100 (VEL., DENS., THICK.)



RAY PARAMETER



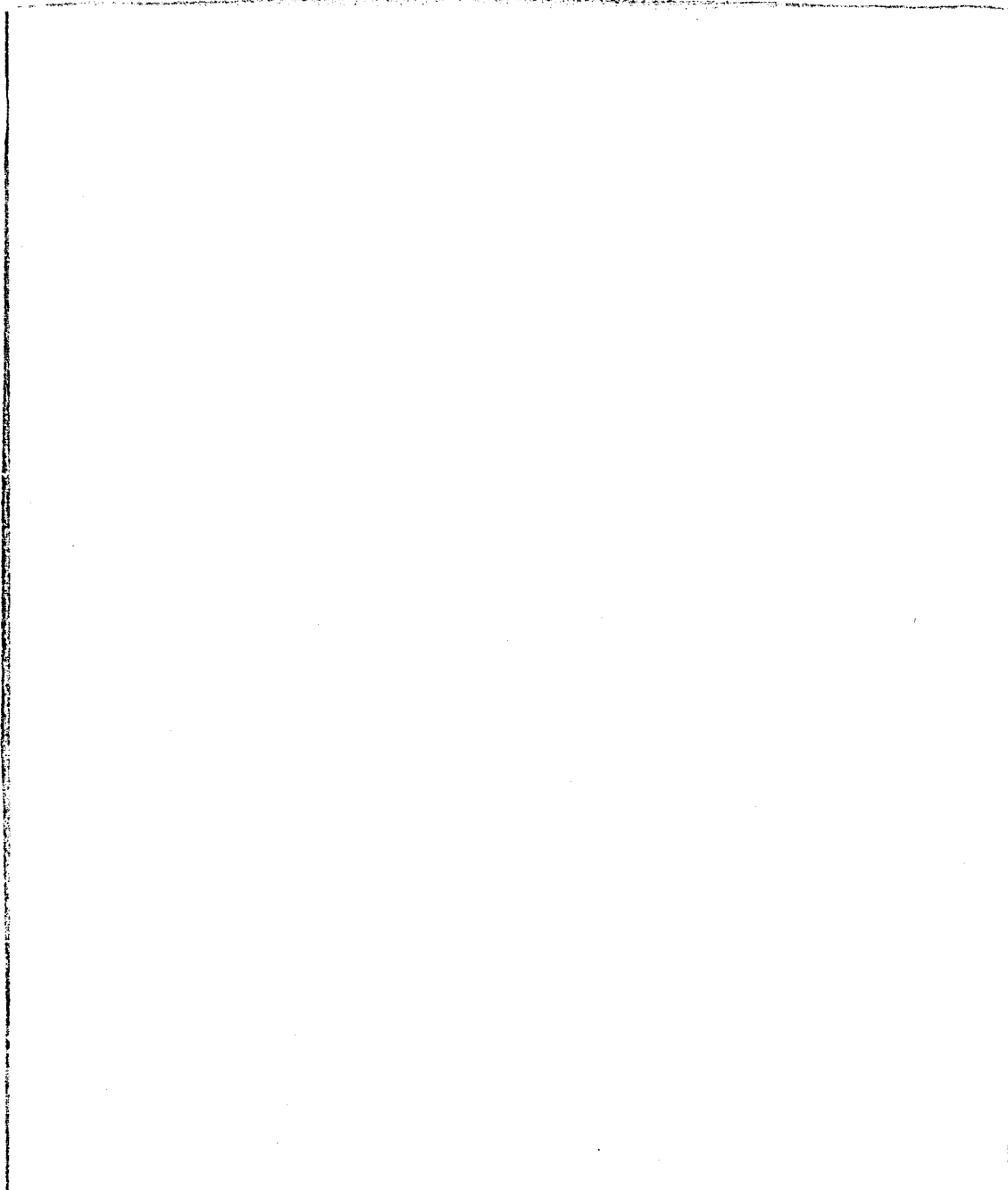
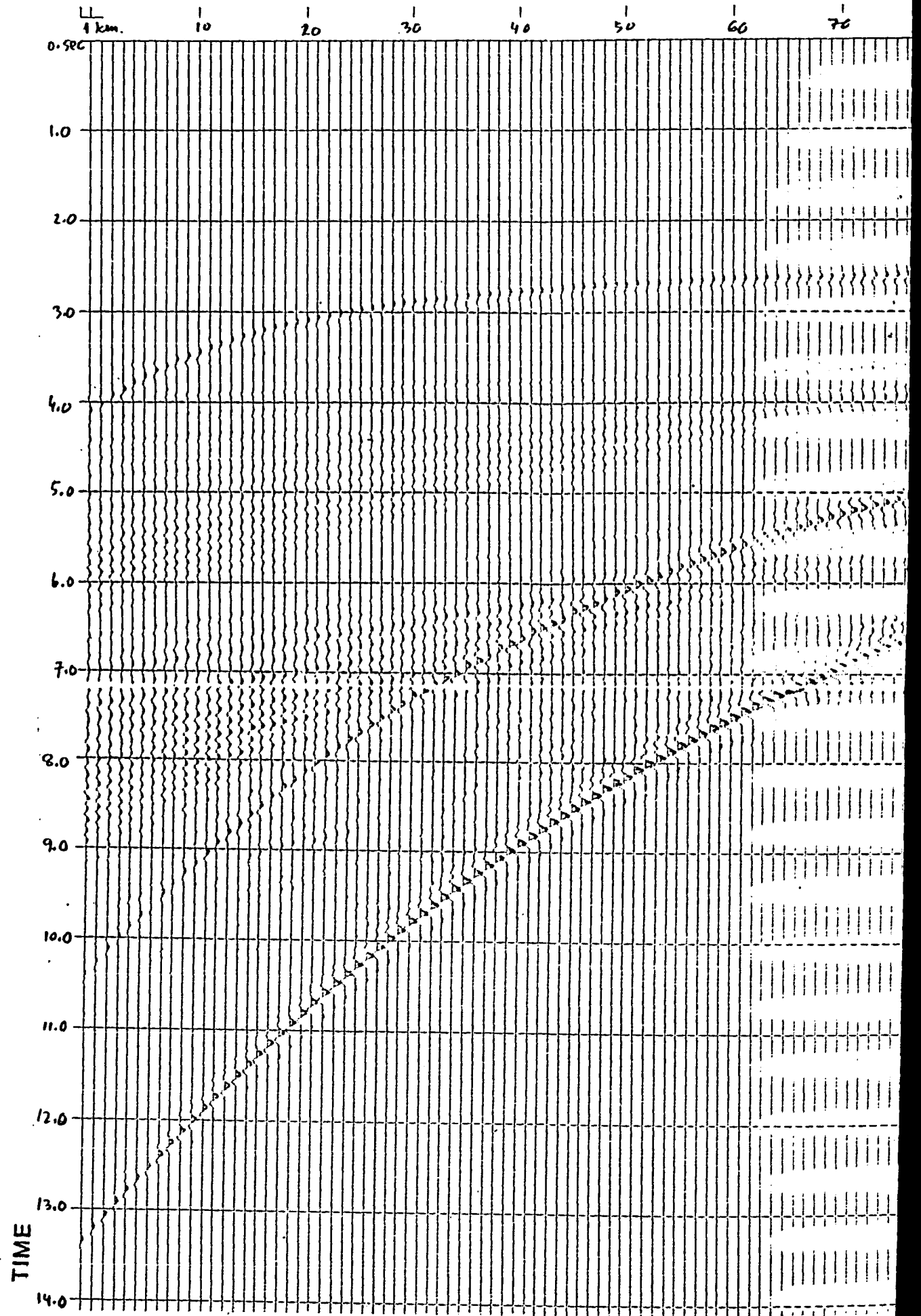


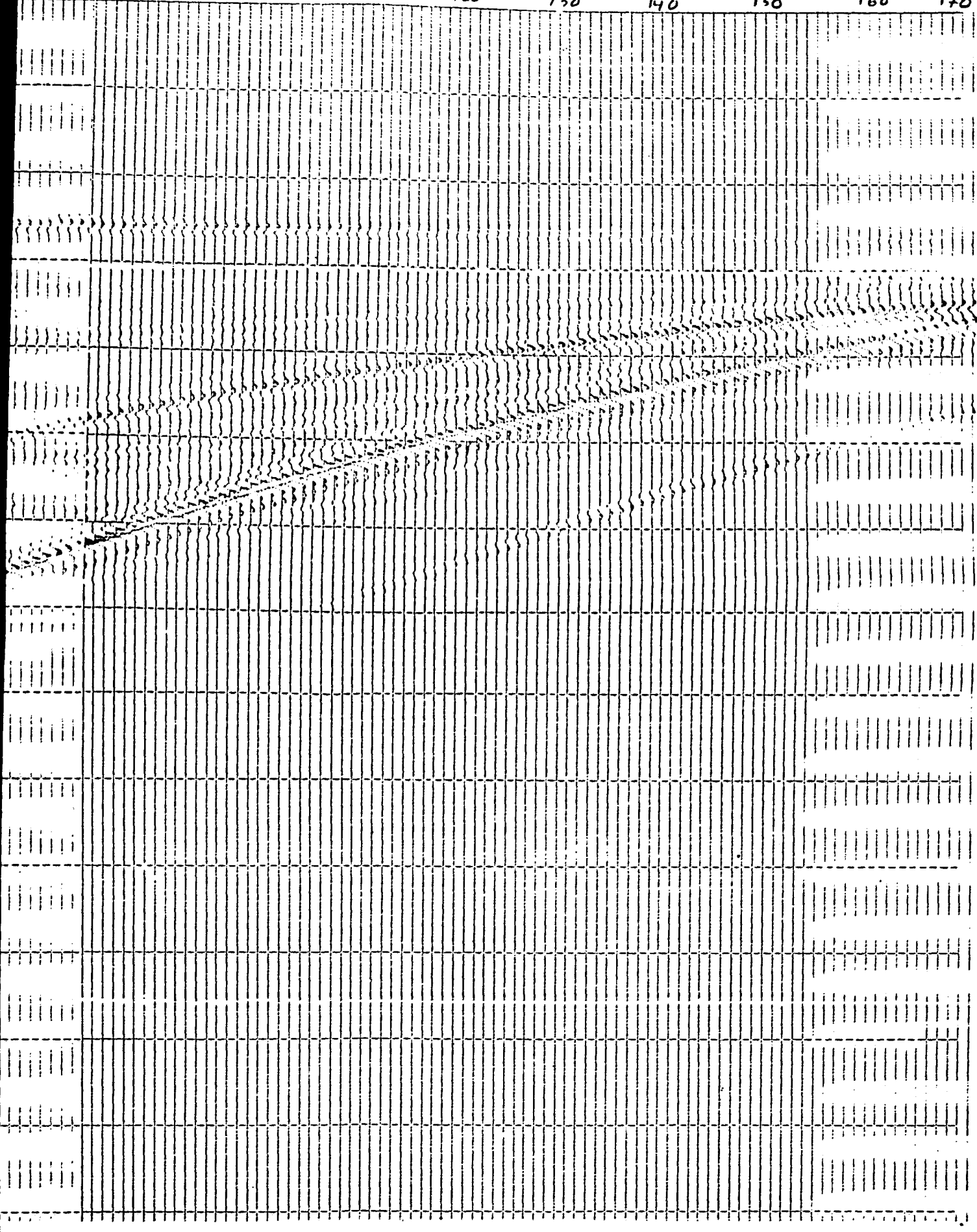
Figure 4-9: Model 2: T(X) section of three horizontal layers in a 40 km thick crust.

MODEL # 2: X-T SECTION: 5.9, 2.55, 10--6.1, 2.6, 20--6.7, 2.73, 10--8.1, 3.3, 100 (VEL., DENS., THICK.) x-2



DISTANCE

80 90 100 110 120 130 140 150 160 170



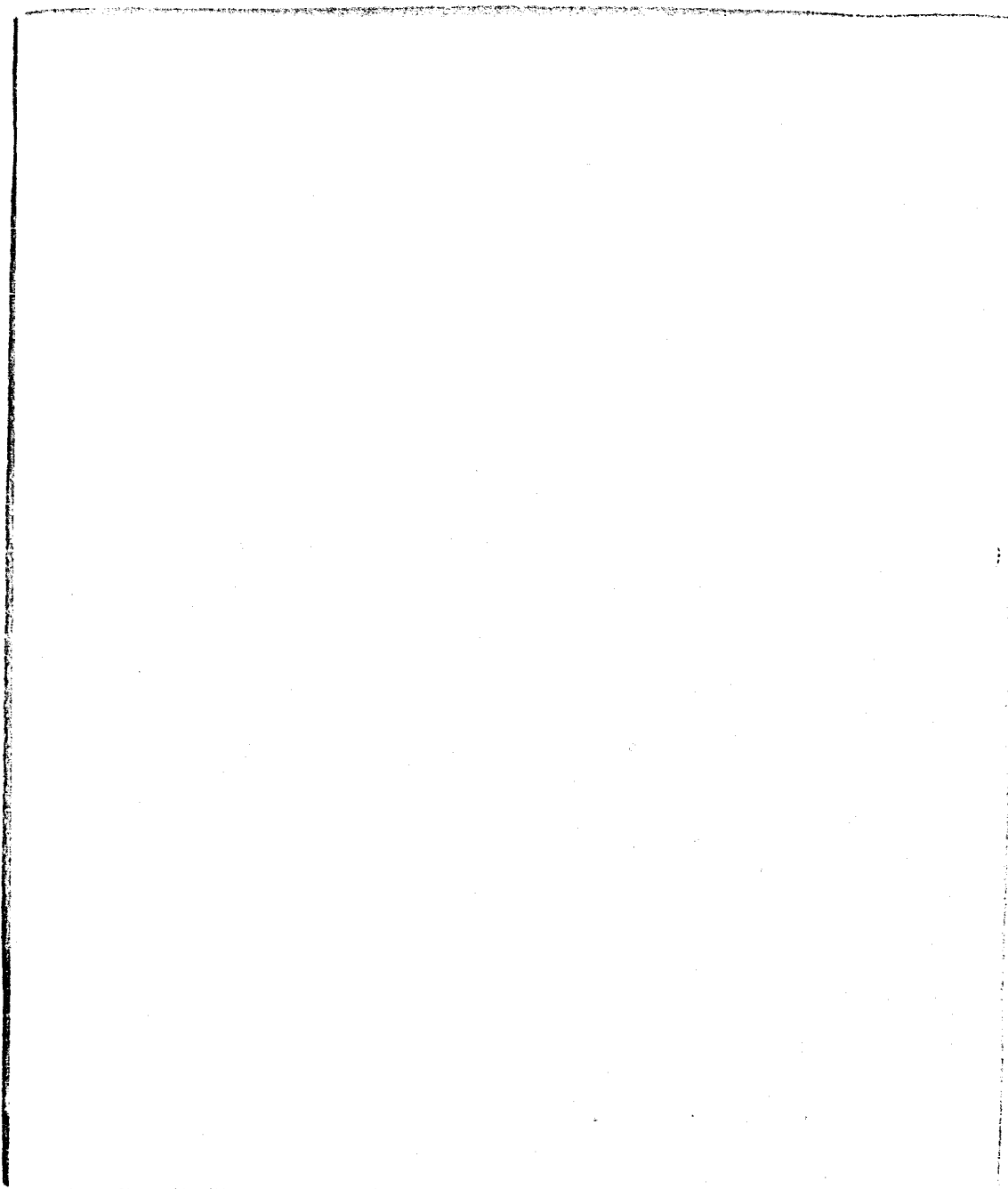
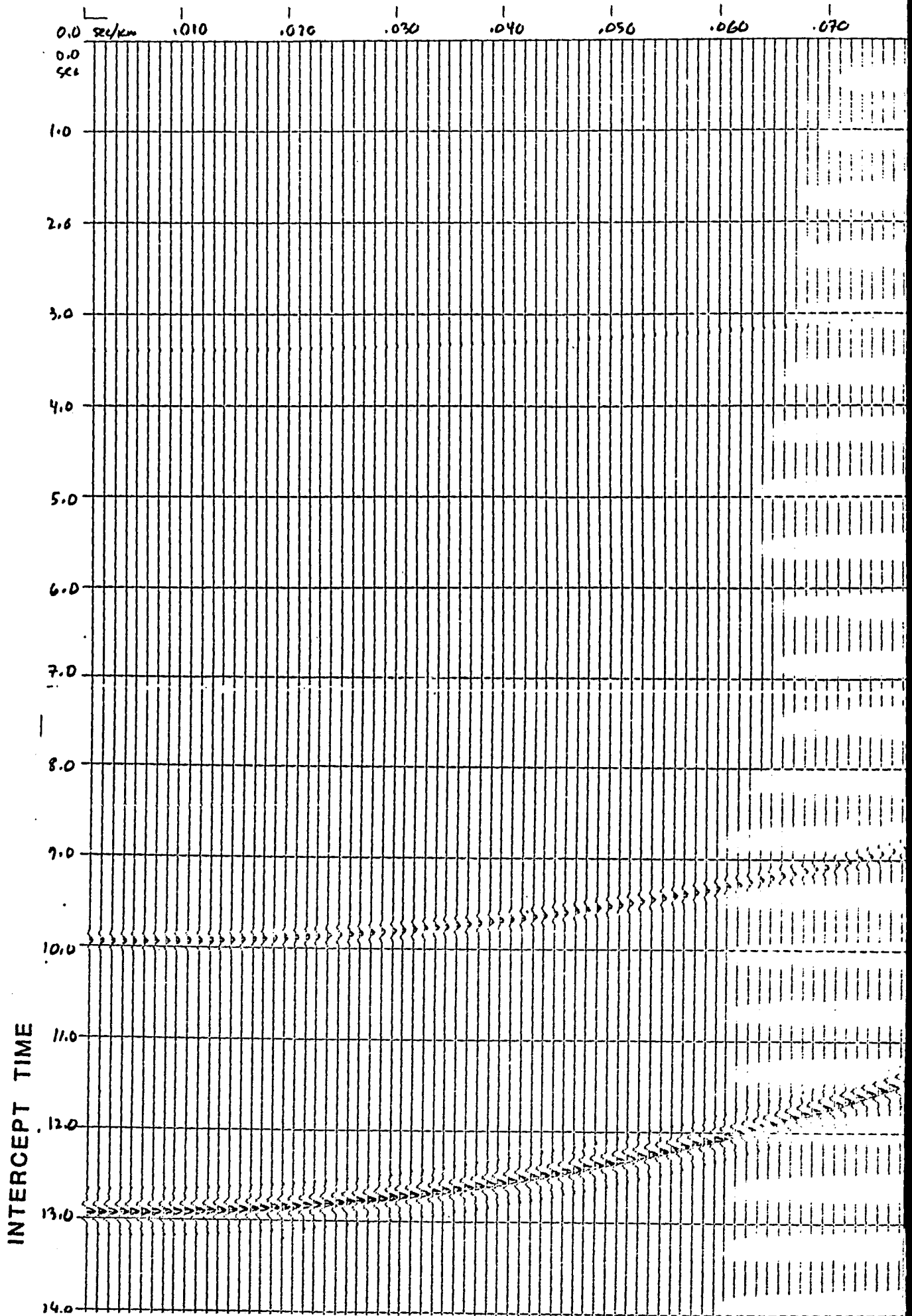


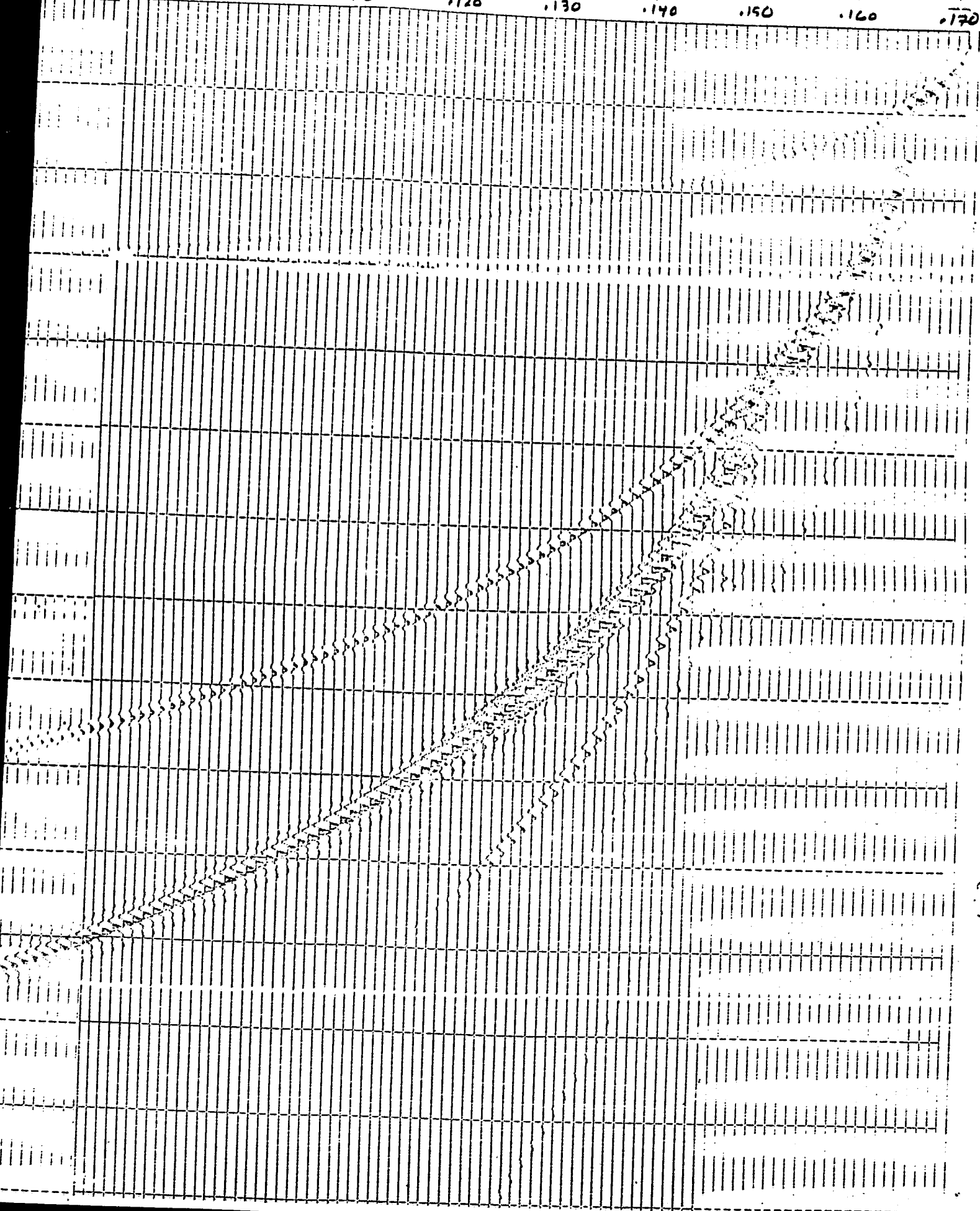
Figure 4-10: Model 2: $t(p)$ section of three horizontal layers in a 40 km thick crust.

MODEL * 2: PTAU SECTION: 5.9.2.55.10--6.1.2.6.20--6.7.2.75.10--8.1.3.3.109 (VEL..DENS..THICK.)



RAY PARAMETER

.080 .090 .100 .110 .120 .130 .140 .150 .160 .170



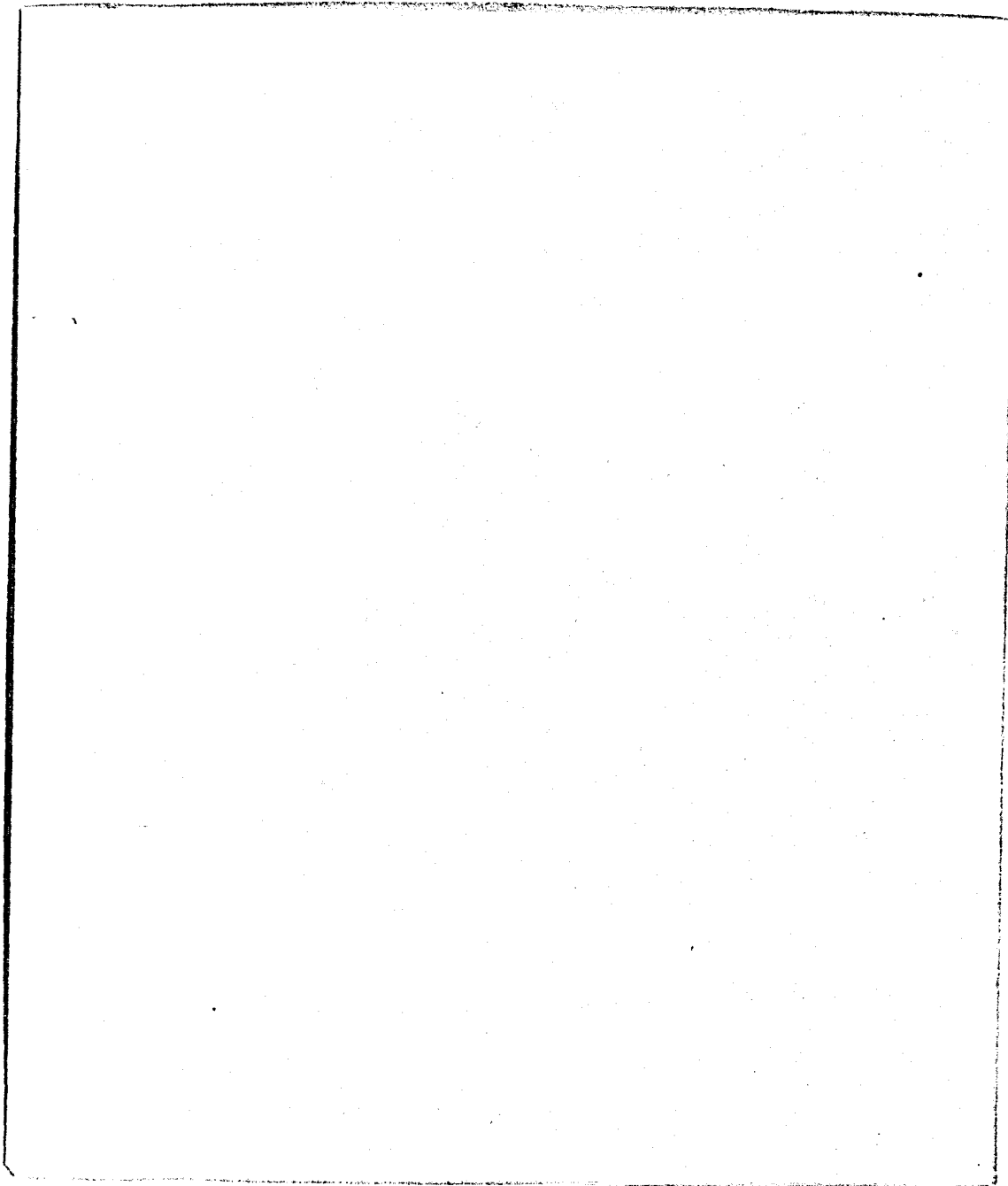
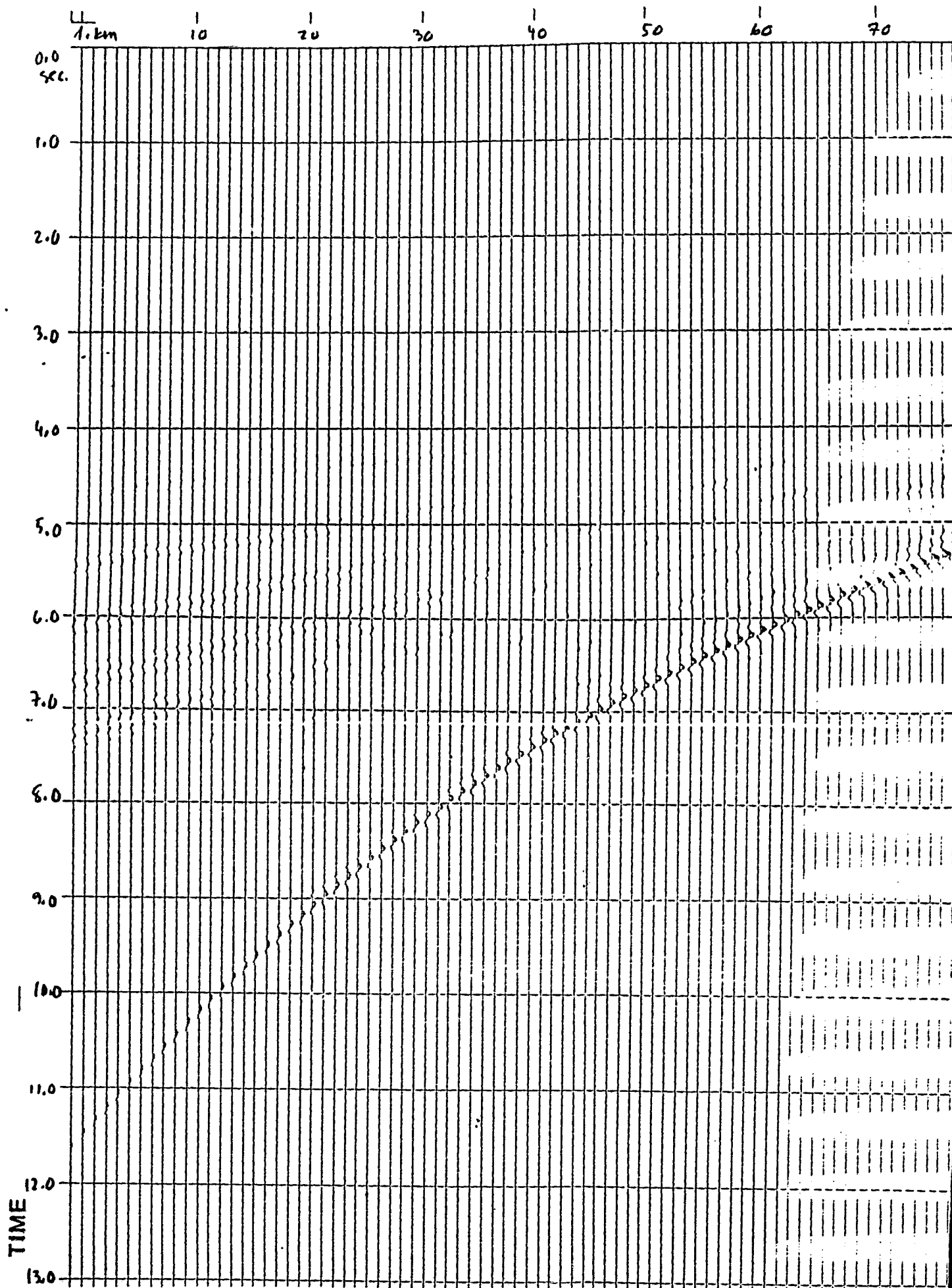


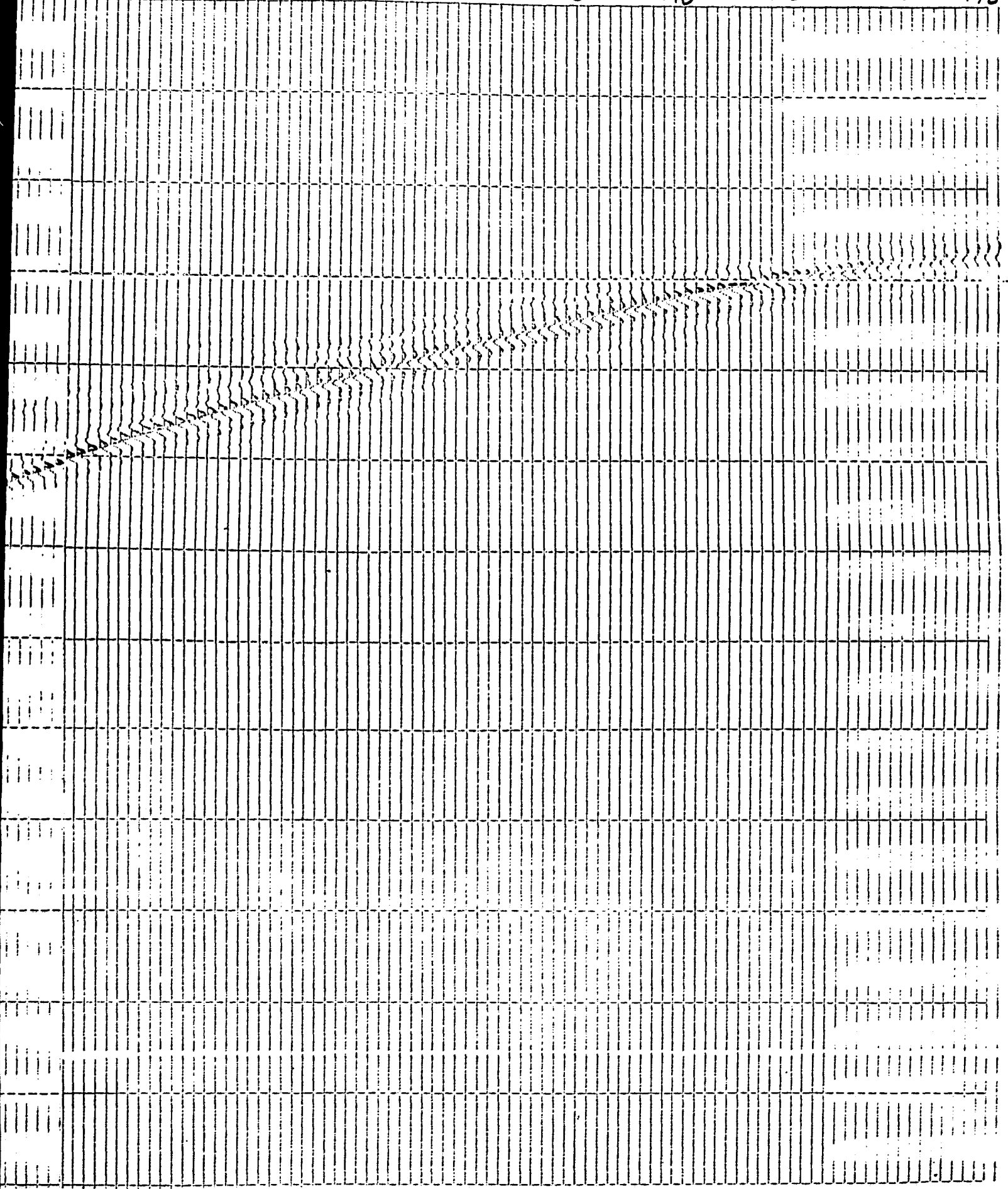
Figure 4-11: Model 3: T(X) section of a 10 km continuous velocity function overlain by a 25 km horizontal layer.

MODEL # 3: X-T SECTION: 6.1.2.6.25--6.3-7.1.2.65-2.85.020-8.1.3.3.100 (VEL., DENS., THICK) VEL.=6.0



DISTANCE

80 90 100 110 120 130 140 150 160 170



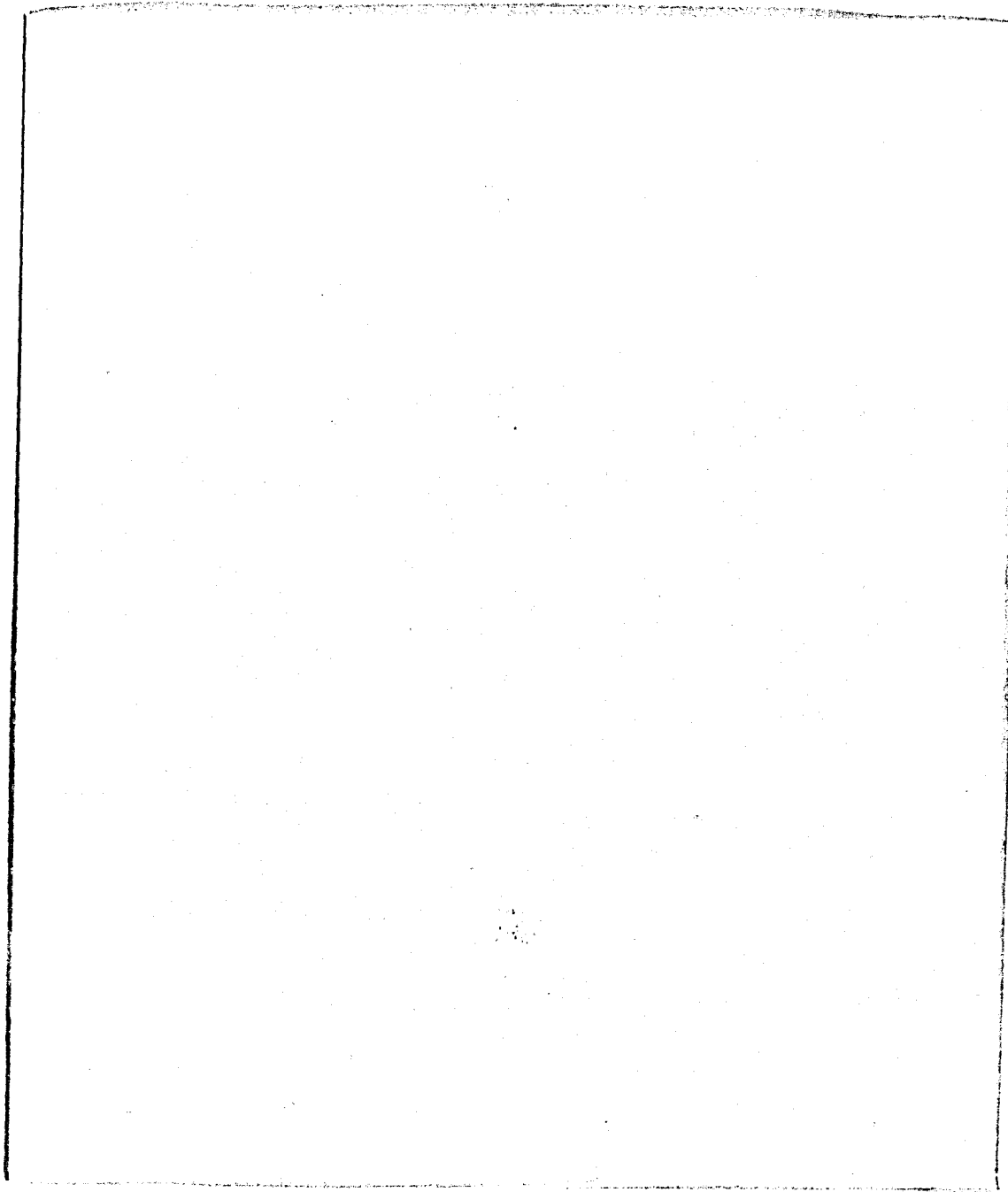
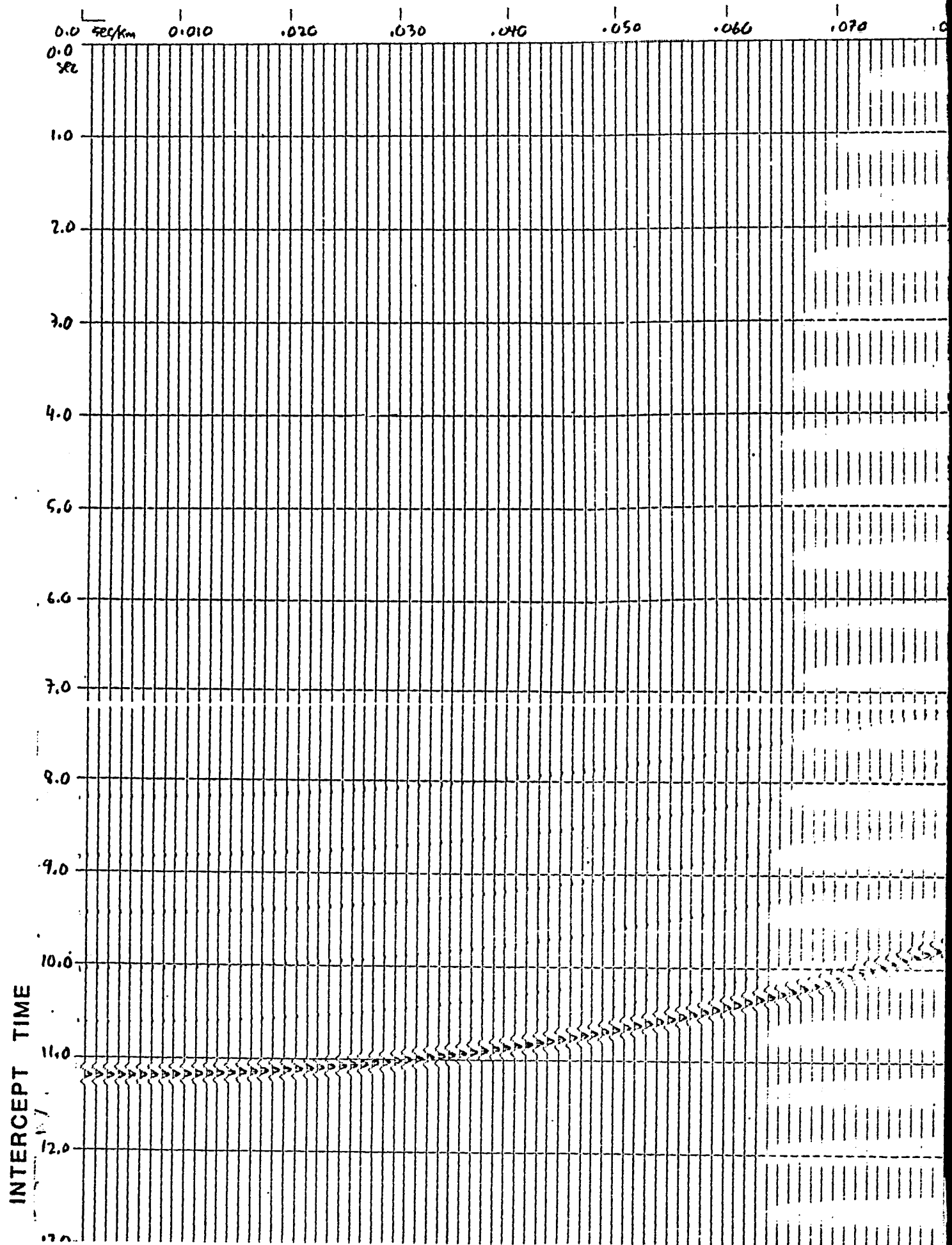


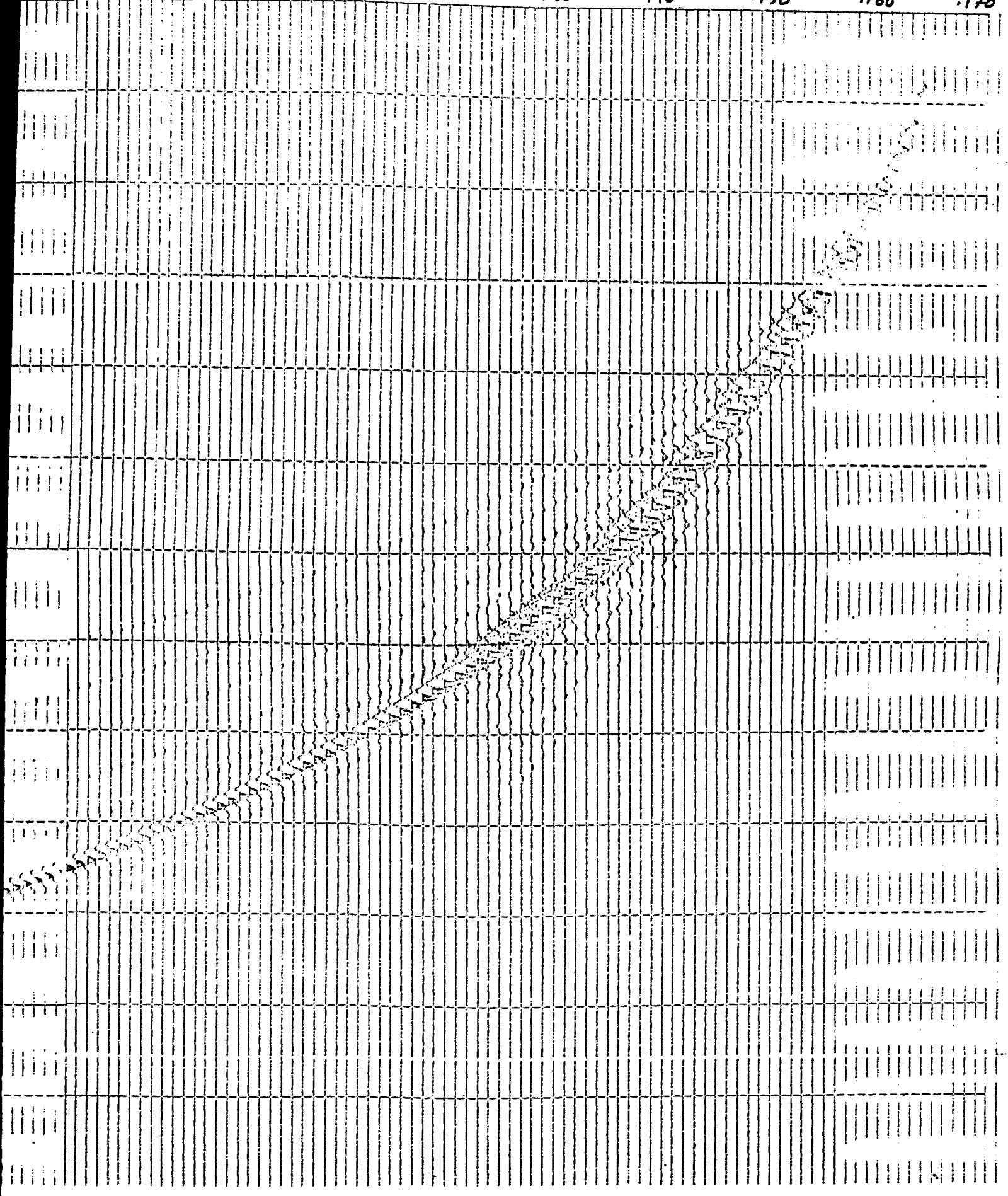
Figure 4-12: Model 3: t(p) section of a 10 km continuous velocity function overlain by a 25 km horizontal layer.

MODEL * 3: PTAU SECTION: 6.1.2.6.25--6.3-7.1.2.65-2.85.02--8.1.3.3.100 (VEL., DENS., THICK.)



RAY PARAMETER

80 .090 .100 .110 .120 .130 .140 .150 .160 .170



VITA

ROY JOHN REDMOND

Born: 30 January 1957, Newark, New Jersey
Parents: Leroy John and Dorothy Margaret Redmond

Education:

Blair Academy, 1975

B.A., Geology, Rutgers University, 1979

M.S., Geology, Lehigh University, 1982

Professional Societies:

Sigma Xi

Society of Exploration Geophysicists

American Association of Petroleum Geologists

Current Position:

Geophysicist

Chevron USA, Inc.

935 Gravier Street

New Orleans, LA. 70112